Origin of Properties in High Entropy Alloys

By

Andrew Cunliffe

Thesis submitted for the degree of Doctor of Philosophy

Department of Materials Science and Engineering

The University of Sheffield

September 2018

Abstract

The novel class of alloys known as high entropy alloys (HEAs) present two fundamental problems; 1) prediction of their properties and reaction to alloying adjustments, 2) prediction of compositions capable of forming the random solid solution with simple crystal structure that appears to be key to their behaviour.

Here DFT is applied to model the electronic structure of HEAs based on the CoCrFeNi pseudo base metal. This approach explains a number of properties such as preferred crystal structure and allows fundamental properties such as elastic moduli to be calculated accurately. The stability of HEAs is discussed and compared to that of bulk metallic glasses and a composition is produced which is capable of forming both a glassy and high entropy solid solution phase. A simple thermodynamic model is proposed to allow likely HEA solid solution forming compositions to be identified. This modelling approach using both DFT and thermodynamics is used to assess two potential high entropy alloys based on light metals.

The approach shows that the electronic structure of HEAs may be used to predict their properties and therefore their behaviour is due to a free electron structure, it also suggests that the most important consideration in their stability as solid solution alloys is a lack of strong covalent interactions, *ie* a close to zero entropy of mixing.

Acknowledgements

I would like to thank my wife Dr Zhen Xu for always refusing to accept that I was just too tired or too busy to complete this thesis. If ever there was proof, that; behind every worthwhile endeavour achieved by a man there is a good woman to thank, then this work and indeed our marriage is that evidence. If I *would* never have finished without Zhen's encouragement, then I *could* never have finished without the support of Professor Iain Todd. Without Iain's support during the writing phase, the project would have been in vain, I would like to take this opportunity to express my deep thanks to Iain for fighting my corner.

I would also like to thank Iain for being such a receptive sounding board for my ideas and for the many enjoyable, sometimes sober discussions, which we had about metallurgy. Thanks also to Dr Colin Freeman for help with DFT modelling, Professor Panos Tsakiropoulos for interesting discussions, Dr Cathy Shields, Dr Peng Zeng, Dr Le Ma and Dr Peter Korgul for electron microscopy training.

Finally my sincere thanks to all of the technical staff of the Materials Science and Engineering department and the Electronics and Electrical Engineering workshop for their help with training in experimental techniques, maintenance and design and fabrication of experimental equipment. Particular thanks to Mr Richard Kangley, Mr Dean Haylock and my friend Mr Paul Hawksworth.

In addition to the above I would like to thank Junheng Gao and YuHe for help with additional experimental work and the logistics of resubmission from the other side of the world.

Contents

Introduction to Thesis

The so-called high entropy alloys (HEAs) are a novel class of alloy, which consist of five or more elements in approximately equiatomic proportions. This is a departure from the conventional approach to alloy development that seeks to develop and enhance or compliment the properties *intrinsic* to a chosen base metal. For example (water cooled) copper is the material of choice for molten metal processing technologies such as continuous casting and induction skull melting; this is due to its excellent thermal conductivity, but in service the pure metal suffers from creep, grain growth and poor structural stability, therefore it is often alloyed with zirconium and boron. This gives precipitation strengthening and grain boundary pinning thus the alloy has sufficient strength for design engineers to make use of the excellent thermal properties. Often the alloying additions made, whilst improving a primary or secondary property, will cause a deterioration in a different property and so conventional alloying becomes an exercise in optimisation. In other words *compromise*.

The conventional approach has given rise to many alloys optimised for particular applications but generally there is an acceptance that the capabilities of an alloy system are limited by the properties of the base metal. As compositions become more heavily alloyed the likelihood of the formation of deleterious phases; either low melting point or brittle, is increased simply because the likelihood of incompatible elements being present in unsuitable ratios is increased. HEAs as multiprincipal component alloys are very definitely heavily alloyed. But they are generally reported to not form intermetallic, Laves or other topologically close packed (TCP) phases. It is this

observation which first gave rise to interest in HEAs. Further investigations discovered compositions with exceptional mechanical properties, excellent corrosion resistance and electro/magnetic properties.

Two fundamental problems which research into HEAs must overcome are now apparent:

1. High entropy alloys have multiple principal components and therefore are outside of the scope of conventional approaches to alloy development. There is no base metal with properties that may be improved or added to by making alloying additions. Therefore how might the properties of these alloys be predicted, when they cannot be extrapolated from those of a well characterised base metal or alloy family?
2. What is the reason for the unexpected stability of high entropy alloys as random solid solutions with simple crystal structures?

It is the aim of this thesis is to address these two questions.

The properties of materials are derived from their microstructure and the nature of their bonding (their electronic structure). Where alloys have a single base metal it is the electronic structure of the base metal which dominates the bonding in all alloys in the family, and the electronic structure is not a significant variable in alloy development, compared to microstructural influences. In HEAs the electronic structure is not due to a single metal nor is it consistent due to the huge alloying additions. But if it can be predicted and understood many properties of the alloy may be calculated from this fundamental property. The bonding, which is due to the electronic structure,

determines; elastic moduli, crystal structure, crystal anisotropy, Burger's vector and thermo electric power. These properties in turn influence other properties in concert with microstructure such as plasticity, thermal and electrical conductivity. In Chapter 5 of this thesis the electronic structure of HEAs will be modelled using density functional methods and the description of a pseudo base metal is proposed. The modelling results are used to predict fundamental properties, which are compared to experimentally measured values. But the pseudo base metal treatment is only appropriate where the alloy exists an a random solid solution and all of the components are donating electrons to metallic bonds, giving rise to an electronic structure unique to the alloy system. The thermodynamic and kinetic considerations which allow HEAs to form a simple random solid solution are worked through in chapter 6 and the alloys are compared to amorphous alloys as another family of kinetically metastable alloys with a high degree of compositional complexity.

In Chapter 7 the themes developed in chapter's 5 and 6 are applied *a priori* to the prediction of compositions which may be capable of forming an HEA type random solid solution. The compositions are then subject to the pseudo base metal DFT analysis and their properties are predicted. This chapter provides a testing ground for the approaches.

The methods outlined are shown to be capable of predicting the occurrence and properties of HEAs, particularly the properties which are insensitive to microstructure such as thermo electric power and elastic moduli. Further work will be required to develop the methods to improve accuracy and broaden their applicability

1. Literature Review

1.1 High Entropy Alloys

1.1.1 Opening comments on High Entropy Alloys

Due to the implied requirement for compromise, metal alloy development has long been considered by many to be mature; offering opportunities only for incremental and diminishing improvements in properties. This may be true for traditionally composed alloys designed to improve or compliment the properties intrinsic to an existing metal. Many researchers in materials science and engineering look to ceramics and polymers or nano-scale structures to provide a step-change in materials capabilities.

However metallic systems continue to surprise and delight, with new novel and hitherto unsuspected properties such as; the shape memory effect and super elasticity [1], amorphous alloys [2], and now the discovery of high entropy solid solution alloys (HEAs) [3,4].

High entropy alloys were first discovered, accidentally, in 2004 by Cantor et al [3], although it was not until later that Yeh [4] coined the term “high entropy alloy”. Cantor discovered that approximately equiatomic alloys of five to twelve metals and metalloids prepared by melting were capable of forming solid solutions with simple bcc or fcc crystal geometries. This discovery was remarkable because the alloys did not appear to obey the equilibrium phase rule:

$$F = 2 + C - P \qquad \textit{Equation 1.1}$$

where the degrees of freedom (F) are equal to two plus the number of components (C) minus the number of different phases (P) present. This rule can generally be applied to all equilibrium phase diagrams, for example the phase diagram for water figure 1.1 has one component and either one, two or three phases may be present but on the lines where two phases may exist only temperature *or* pressure may be chosen freely the other parameter is not independent. At the triple point where three phases may exist there are 2 +1-3 = 0 degrees of freedom.

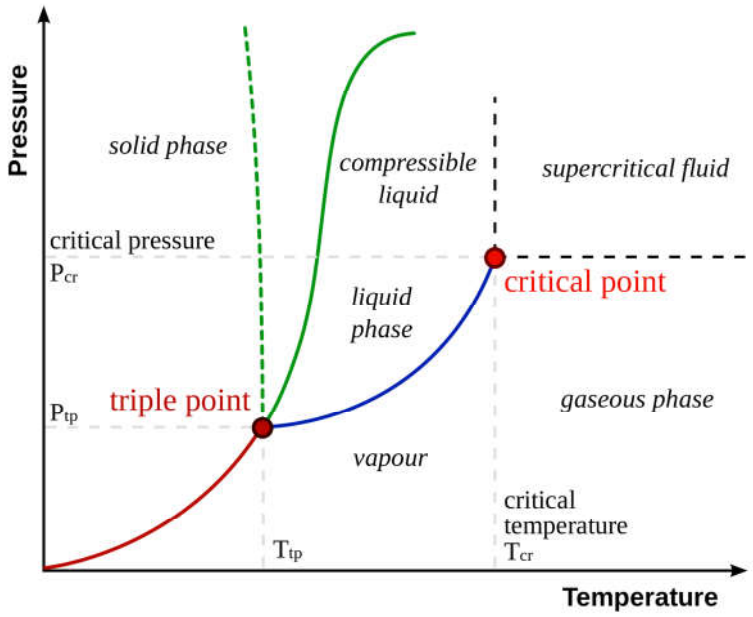

Figure 1.1 Temperature pressure phase diagram of water

But in the case of the Cantor alloys (see table 1.1) the degrees of freedom would be from 3 to 13, indicating that not only are the solid solutions formed stable at variable temperature and pressure combinations but also they are insensitive to variations in chemical composition. The implications of the Gibbs phase rule have been discussed in a recent review by Miracle and Senkov [5]; where it was pointed out that the rule only made a statement of the maximum permissible number of states under equilibrium and that a lower number of states are often observed in binary, composition-temperature phase diagrams and that care should be taken not to place too much significance on the fact that fewer than the maximum number of phases are present. For example metals with complete solid solubility such as silver and gold, which may form a continuous solid solution across the entire composition range, have an excess number of degrees of freedom (3) which is greater than the number of variables available. By this measure, electrum, the naturally occurring alloy of silver and gold could also be declared an HEA.

Table 1.1: selected alloys from [3]

Composition	Components	Phases	Degrees of Freedom
FeCrMnNiCo	5	1	6
FeCrMnNiCoNb	6	1	7
FeCrMnNiCoCu	6	1	7
FeCrMnNiCoTi	6	2	6

Although Miracle [5] makes the point that often fewer than the maximum number of phases are observed he does concede that the number of phases is also rarely the minimum possible of one, this infers that the number of degrees of freedom is rarely the maximum possible as observed in HEAs. In a typical binary system the number of degrees of freedom are rapidly consumed by the occurrence of more phases even in a two-phase field, where the number of degrees of freedom is usually calculated as 2 a change in temperature will change the ratio of the phases present by the lever rule, unless the composition is adjusted, therefore the number of degrees of freedom is not actually 2. The alloys discovered by Cantor et al each exist with an excess number of degrees of freedom and so they can react to change in a fundamentally different way than conventional alloys.

1.1.2 Compositional Complexity in High Entropy Alloys

In an *n* component alloy the sum of all the fractional component concentrations may be written as below:

$$\sum_{i-1}^{n} C_i = 1 \qquad \textit{Equation 1.2}$$

For a binary alloy there is only one degree of freedom as concentration of component B may be defined as one minus the concentration of component A. But for a multi component alloy change in the concentration of component *n* can be accommodated by the remaining *n-1* components:

$$\sum_{i=1}^{n} dC_i = 1 - dC_n \qquad \textit{Equation 1.3}$$

and $dC_i/(n-1)$ will be small with an almost infinite number of ways to accommodate the change in composition. This infers that the solid solution phases of Cantor's alloys may be stable for a range of compositions so long as dC_n is not so large that the component's chemical potential becomes more or less influential than those of the remaining elements. The definition of an acceptable range of concentration for each component must be a key parameter to be determined for an HEA system. Yeh [4] attempted to do this in his

definition of an HEA: an alloy of 5 or more components with atomic concentrations of from 5 at% to 30 at%. However for practical purposes the insensitivity to concentration variation must be sufficient to allow accommodation of solidification effects such as dendrite formation and coring. Because affinity (measured in terms of enthalpy) of the constituent metals for one another affects solidification features *and* the stability of any final solid solution phase. Then enthalpy of mixing of the constituent metals affects both the thermodynamics of HEA formation and the kinetic ability to form a microstructure that is within the limits of thermodynamic stability and it becomes clear that Enthalpy is a key parameter in the stability of an HEA composition.

A further effect of enthalpy of mixing of the alloy is on the viscosity of the melt; it has been established by various authors [6,7] viscosity of alloys is increased by a more negative enthalpy of mixing and by large differences in atomic size of the constituents. This is because these parameters encourage clustering and stickiness between the clusters of atoms, described for example by the Budai-Benko-Kaptay equation [6] and Andrade [7], which show a linear relationship between the enthalpy of mixing and the viscosity of the liquid metal.

The usual explanation for the ability of HEAs to form simple solid solution phases is that the configurational entropy of the solid solution is sufficient to suppress the formation of intermetallics by lowering the free energy of the solid solution. The stability or otherwise of a phase or microstructure is due to

the energy of that state. All systems will attempt to move towards the state of lowest energy for the combination of components, pressure and temperature. The expression below (equation 1.4) describes the Gibbs free energy of a state in terms of the enthalpy of formation (*H*) and statistical likelihood (*TS*), or in terms of internal energy (*U*), the work done on the system by its surroundings (*PV*) and the statistical likelihood of the state (*TS*)

$$G = H - TS + U + PV - TS \qquad \textit{Equation 1.4}$$

The free energy is a measure of the amount of external work required to hold the system in a particular state. A system will seek to reduce free energy and state changes, which reduce the Gibbs free energy of the system, are favoured. The change in Gibbs free energy for a change of state is simply the energy of the final state minus that of the initial state as shown in equation 1.5.

$$\Delta G = H_2 - H_1 - S_2T + S_1T \qquad \textit{Equation 1.5a}$$

$$\Delta G = \Delta H - T\Delta S \qquad \textit{Equation 1.5b}$$

In this form the expression has applications in many branches of science and engineering. For our purposes some additional terms are required. Real metallic systems include interfaces and surfaces between different phases, precipitates, or grains of different orientation. These surfaces cause a change in the nature of the bonding, usually a decrease in the number of bonds formed. As bond formation releases energy there is an energy penalty for creating an interface or surface where species have unused valence and so the interfacial

energy, γ_i, is a positive (retarding) term [8,9].

The free energy of the system also depends upon the energy absorbed or released when components react to form new phases such as intermetallic precipitates. The enthalpy (ΔH^{ron}) and entropy (ΔS^{ron}) of formation of such phases must be accounted for in the overall free energy calculation.

Addition of substitutional elements to the solid solution results in strengthening of the alloy through reduced dislocation mobility. However embedding a different sized atom into the lattice results in a strain (ε), which requires work to be done against the bulk modulus (B) of the crystal. This strain energy (w_ε) limits the size differences of metal atoms, which can form continuous solid solutions [8,9,10]. The modified expression for the free energy of the solid solution is shown below, equation 1.6

$$\Delta G = \Delta H^{mix} - T\Delta S^{mix} + \sum_i [\Delta H_i^{ron} - T\Delta S_i^{ron} + A\gamma_i] + w_{\varepsilon ss} \qquad \textit{Equation 1.6}$$

Equation 1.6 is an energy balance for the possible microstructural changes of the system. A common mechanism for reducing the free energy of an alloy is through precipitation, but this is favourable only when the energy released by forming the intermetallic or ceramic precipitate and relieving the strain outweighs the interfacial energy.

$$H^{f\_ss} - TS^{conf\_ss} < H^{f\_IM} - TS^{conf\_IM} \qquad \textit{Equation 1.7}$$

That is that the free energy of the solid solution is lower than that of the mixture of intermetallic phases. For an intermetallic the configurational entropy tends to zero and so the stability depends mainly on the magnitude of the negative enthalpy of mixing, for the random solid solution the bonding pairs are by definition not optimised and the enthalpy of formation should have a value much less favourable than for the intermetallic system, in an ideal solution, effectively nought. Thus the solid solution is stable when the entropy term is great enough to overcome the enthalpy of formation of the intermetallic mixture. This makes entropy of the solid solution a key variable in the stability of an HEA, according to Boltzmann's Law;

$$S = k_b \ln|\Omega| \qquad \textit{Equation 1.8}$$

where k_b is Boltzmann's constant, S is the entropy and Ω is the number of equivalent microstates (atomic arrangements) which may be present in the macrostate (solid solution alloy) (for use with molar concentrations equation 1.8 can be multiplied by Avogadro's number to give S in J/mol/K). The number of microstates is the number of ways the constituent elements may be arranged on the non-equivalent lattice points of the solid solution:

$$\Omega = \frac{N!}{n!(N-n)!} \qquad \textit{Equation 1.9a}$$

$$\Omega = -x_i lnx_i - x_j lnx_j -, \ldots . \qquad \textit{Equation 1.9b}$$

Where N is the number of components n the number of choices and $x_{i/j}$ the mole fraction of a component. Stirling's approximation equation 1.9b, may be used to calculate the configurational entropy, [8]. Table 1.2 shows the configurational entropy for an up to ten component equiatomic high entropy alloy.

Table 1.2: Configurational entropies calculated by Stirling's approximation

***N* Components**	**Mole fraction of x_i**	**Configurational entropy /Jmol^{-1}K^{-1}**
1	**1.000**	**0**
2	**0.500**	**5.76**
3	**0.333**	**9.13**
4	**0.250**	**11.53**
5	**0.200**	**13.38**
6	**0.167**	**14.90**
7	**0.143**	**16.18**
8	**0.125**	**17.29**
9	**0.111**	**18.27**
10	**0.100**	**19.14**

The data above show that configurational entropy increases with the number of components in the system; but that the rate of increase falls off at higher orders.

Takeuchi et al [11] used compositional configurational entropy diagrams based on plotting the configurational entropy divided by the ideal maximum configurational entropy versus the number of components as shown in equation 1.10.

$$Z = \frac{S_{conf}}{S_{ideal}} = \left[\frac{-\sum c_i \ln c_i}{\ln N}\right] \qquad \textit{Equation 1.10}$$

Because c_i is equal to $1/N$ differentiation of equation 1.10 with respect to N gives the result

$$\frac{dZ}{dN} = \frac{1}{N^2} \qquad \textit{Equation 1.11}$$

Therefore the increase in configurational entropy due to increasing number of components reduces very rapidly and tends to zero as shown in figure 1.2 and there is a diminishing return. This result is of some importance and will be discussed further in chapter 5.

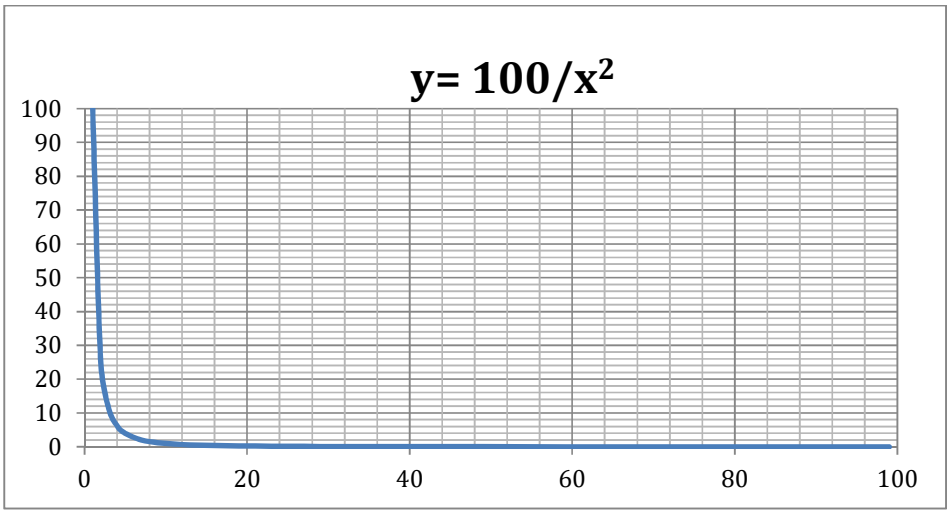

Figure 1.2 Arbitrary units. Illustrates that the rate of configurational entropy increase scales with $1/N^2$ and quickly asymptotes to zero

If HEAs are entropy stabilized solid solutions then the opposing force is the effect of the enthalpy of mixing of the constituent elements to form the alloy, which if negative will favour ordering of unlike neighbours and directional/covalent bonding and if positive will promote segregation and clustering of like atoms.

1.1.3 Enthalpy: a source of frustration to disorder

In ideal solutions the component elements are considered to have no chemical interactions and therefore no tendency to order or to cluster/segregate. In reality metallic systems all have an associated heat of mixing (ΔH^{mix}); this may be positive or negative depending on each metal's affinity for the other. A positive heat of mixing, such as between silver and chromium [10] results in poor mixing of the melt and clustering in the solid alloy. A highly favourable negative enthalpy of mixing indicates that the metals have a preference for unlike neighbours and are likely to order to achieve the maximum density of unlike bonding pairs. When enthalpy of mixing approaches zero the metal atoms show little preference for one or other species as neighbour, indicating that the metals are chemically very similar; such metals include the gold–silver alloys. The magnitude and sign of the enthalpy of mixing is determined by the bonding involved; as discussed in section 2.3 this is primarily an electron effect. Elements, which are very different in size, electro-negativity and electro-chemical potential, are very likely to have large negative heats of mixing, *eg* Y-Pt [10] where ΔH^{mix} = -83 kJmol^{-1}. This is due to the large differences in size, electro-negativity and chemical potential: 177.6 pm, 137.3 pm, 1.22, 2.28 and 5 eV, 9 eV for Y and Pt respectively. The large difference in electro-negativity results in platinum scavenging electrons from yttrium and the bonds become more directional and covalent in nature, the difference in activities means that when the molecular orbitals form there will be a significant lowering of energy by bond formation, because the number of electrons involved in the bonding of the metal pairs is 13 (4s + 3d) all the bonding orbitals are filled and only one anti-bonding

orbital half filled, which results in a large reduction in energy on mixing of the two metals. The ordering also helps to accommodate the large size differences by distributing the yttrium evenly through the lattice. That is a different lattice comes into being in order to minimize strain and maximize bonding efficiency both, this phenomenon has also been noted in HEAs where the 'expected' lattice strain is absent [5]. In the case of chromium and silver, the electro-chemical potentials are very different (8 eV and 5.5 eV) so again there is a large band gap between bonding and anti-bonding orbitals. In this case the number of electrons involved is 17 and the anti-bonding orbitals are being filled; this gives poor bonding between unlike pairs and repulsion. The small difference in electro- negativity means there is no great driving force to exchange electrons, nor are the sizes of the metal atoms very different: 124.9 pm, 127.8 pm, quite similar, so a random distribution or a clustering of like atoms would not cause a great amount of strain, thus the heat of mixing is positive and one of the largest amongst transition metal pairs.

Calculation of bond enthalpies is quite possible from first principles, however this is time consuming and, a more convenient method of estimating mixing enthalpies of alloys was developed by Miedema et al [10]. The model is a semi empirical model with a physical basis and has been used to predict enthalpies of mixing with very good accuracy. The model was applied to the case of the HEA AlCrFeNiCu [11] and gave the first insight into the thermodynamic stability of HEAs. The Miedema model is likely to provide a useful tool in the analysis and design of HEAs and will be discussed in more detail.

Miedema's model [10] is a semi-empirical model, which is based on the

physical parameters most important in the mixing of alloys. When the metals are brought together, to their equilibrium spacing, the electrons at the Fermi surface interact with those of the other atom(s). These interactions are obviously affected by the electron densities of the atoms involved, so the first Miedema parameter is the electron density of the Wigner-Seitz cell (first Broullion zone) n_{ws}. This parameter may be calculated for the free electron metals [13,14,15] (groups I, II, III, Sn Pb) by assigning the valence appropriate to the group (1, 2, 3, or 4) to the metal ion and then dividing this by the volume of the cell described by the planes which bisect the nearest neighbor distances. For transition metals it is more difficult to assign valency, however n_{ws} has been shown, experimentally and theoretically [10], to be related to bulk modulus K by equation 1.12.

$$(n_{ws}^{1/3})^2 = \frac{K}{V} \qquad \textit{Equation 1.12}$$

This relationship allows n_{ws} for transition metals to be obtained conveniently and to a good degree of accuracy. The second parameter is the electro-negativity of the metal which indicated the direction of charge transfer and the likelihood of ionisation of the metal, there are several systems of electronegativity, the one chosen by Miedema et al [10] was the work function of the metal φ. The final physical parameter was the molar volume of the metals V which is readily available and gives some information about the size of the metal ions and equilibrium separation. The Miedema model takes the form shown below in equation 1.13, the F and g are determined from n_{ws} , φ and V.

$$\Delta H^{mix} = Fgp\left[\frac{q}{p}\left(\Delta n_{ws}^{\frac{1}{3}}\right)^2 - (\Delta\emptyset)^2\right] \qquad \textit{Equation 1.13}$$

$$F = x_{is}x_{js} \qquad \textit{Equation 1.13b}$$

$$g = \frac{\left(2x_i V_{ia}^{2/3}\right)+\left(2x_j V_{ja}^{2/3}\right)}{\left(n_{wsi}^{1/3}\right)^{-1}+\left(n_{wsj}^{1/3}\right)^{-1}} \qquad \textit{Equation 1.13c}$$

$$V_{ia}^{2/3} = V_i^{2/3}\left(1+\left(\mu c_i \Delta\phi\right)\right) \qquad \textit{Equation1.13d}$$

$$x_{is} = \frac{c_i V_{ia}^{2/3}}{c_i V_{ia}^{2/3} + c_j V_{ja}^{2/3}} \qquad \textit{Equation 1.13e}$$

The constants *p, q* and μ are experimental fitting factors, *i* and *j* refer to the species being mixed *c* is concentration in mole fraction and the suffix *a* refers to the properties of the mixed "alloy". The model has been extended to multi-component alloys by use of the regular melt model. Miedema's model has been used in this thesis as a convenient method for calculation of enthalpies of mixing of alloys.

1.1.4 Review of some High Entropy Alloy compositions

Since the discovery of HEAs interest has gathered a pace and a large number of compositions have been investigated by different groups in the US [5,16],

China [12,17-30], Japan [11] and elsewhere [31,39]; some examples are shown in table 1.3:

Table 1.3 selected HEA compositions

Composition	Phases	Ref
WTaNbMo	bcc	16
WTaNbMoV	bcc	16
CoCrFeNi	fcc	28
CoCrFeNiAl	bcc	28
CoCrFeNiTi	fcc	29
$CoCrFeNiAlCu_xTi_{x-1}$	fcc + bcc	18
CoCrFeNiZr	fcc + IM	30
CoCrFeNiAg	bcc + fcc	30

The compositions above consist mainly of transition metals and aluminium; the early compositions were mainly based on the 3d transition metals particularly Fe, Ni, Co, Cu, Mn and Cr. Later alloys contained more exotic alloying elements such as refractory metals or rare earths. The main features of some of the HEA systems reported will now be discussed briefly.

1.1.5 Five Component HEAs

The early 5 component HEAs reported included; CoCrFeNiMn [3], CoCrFeNiTi, CoCrFeNiCu and CoCrFeNiAl. Their reported phases are summarised in table 1.3. The first four alloys solidify dendritically to form fcc solid solutions, Cu was found to segregate preferentially to the interdendrite regions, but not to a sufficiently large degree that the structure was destabilised. The presence of aluminium was found to promote the formation of a solid solution with a bcc crystal structure [30], and this was attributed to size mismatch between the late transition metals (atomic radii approximately 125pm) and aluminium (atomic radius 143 pm) being accommodated by the more open, lower symmetry bcc lattice. However the fact that Ti (atomic radius 145 pm) does not cause a similar effect even though it may form a bcc phase in the pure state casts doubt on this simplistic argument and suggests that other factors than atomic radius play a more important role; such as electronic structure and the shape of bonding orbitals.

The interesting alloy WNbMoVTa was synthesised by Miracle et al [16] and found to solidify as a bcc solid solution, it was also shown that the elastic modulus, density and lattice parameter of the alloy could accurately be predicted by using simple weighted average/rule of mixing type models, this suggests that the bonding behaviour of the metals in the alloy is no different to their behaviour in the pure state and the behaviour follows Vergard's law. Miracle also observed that the relationship was less accurate for a 4-component alloy WNbMoTa and that the rule of mixing relationship breaks down completely for 3 component alloys. This supports the 'entropy

stabilised' solid solution definition of an HEA as the entropy of mixing of an ideal solid solution increases with the number of components

1.1.6 Six component HEAs

The HEA community has attempted to develop the field by further 'parametric' studies involving the addition of a 6^{th} element to known quinternary high entropy alloys. These alloys usually draw on the usual palette of elements employed in the 5 component alloys for example: CoCrFeNiAlxTi1-x [29] where additional complexity has been added by substituting both Al and Ti into the system, or CoCrFeNiCuAl [33] in which both Al and Cu are added to the other common HEA metals Co, Cr, Fe and Ni. The effect of these further alloying additions was to increase the yield strength of the alloys and modify the phases present: CoCrFeNi adopts an fcc structure, addition of Cu or Ti to create a 5 component alloy maintains the fcc structure and Al promotes a bcc structure in the 5 component alloy. When Al is added to either CoCrFeNiTi or CoCrFeNiCu the yield strength is further increased as would be expected but the bcc crystal lattice is also promoted leading to duplex crystal structures. The occurrence of microstructures based on duplex crystal structures has not been explored extensively but does raise the possibility of developing precipitation strengthened or transformational (allotropic) microstructures. However should the elements segregate extensively to different crystal structures then there is a risk that the configurational entropy of the alloy is not sufficient to support a random solid solution and the HEA effect is lost.

1.1.7 Higher Order HEAs

The search for novel HEA compositions has naturally led to exploration of 7 or more component compositional space. Indeed the early paper by Cantor et al [3] included the compositions of up to 14 components. More often the higher order alloys are still based around the common transition metals Co, Cr, Cu, Fe, Ni, Mn, Ti plus Al, such as the seven component system CoCrNiFeCuAlTi [18]. Reports of such alloys have not shown any significant departure either positive or negative from the high hardness and good plasticity demonstrated by lower order HEAs. As observed by Miracle et al [5] the exploration of higher order compositional space is a huge undertaking and examination of individual seven or more component alloys really cannot help to build a meaningful picture of the systems. Any attempt to do so would have to rely on combinatorial methods borrowed from organic/pharmaceutical chemistry. Multiple target sputtering such as that used by Ilika [34] and rapid throughput phase analysis and nano indentation may provide one solution to this problem.

1.2 Amorphous Alloys (metallic glasses)

HEAs have mostly been investigated by groups with interests metallic glass (MG) research, this is probably due to the fact that the manufacturing route for small scale sampling and testing is similar for both alloys (so the equipment is available in these groups), both HEAs and MGs are novel and much of the research is reported in similar journals. However there is an important difference between the two systems.

The terms; amorphous or glassy metal refer to alloys which do not exhibit long range order in the same way that crystalline lattices do. The phenomenon was first observed by Kelmet, Willens and Duez in 1960 [39]. Because there is no crystal lattice metallic glasses do not exhibit microstructural features such as grain boundaries cause by mismatched lattices nor can dislocations be transmitted through the random structure. This leads to many interesting properties such as high yield strength, low magnetic coercivity, high electrical conductivity and low elastic modulus.

Metals may be caused/forced to adopt amorphous structures in various ways; Irradiation damage of Zr has resulted in amorphous structure being observed, high energy ball milling [40] and PVD [41] can also result in a glassy structure. But the most common way to produce metallic glasses is through solidification processing of a bulk melt. Whereas the other methods can be used to create amorphous structures in pure or low alloyed metals, through very high energy input, physically breaking down (or preventing development of) the crystal structure; glass formation through solidification processing is extremely sensitive to the composition of the alloy. This is because solidification processing requires that crystallisation is retarded until the material is completely solidified and cool enough that the constituent atoms do not have sufficient energy to rearrange themselves into energetically favourable crystal structures. And a key strategy in preventing crystal structures to form is by increasing the viscosity of the melt thus reducing the mobility of atoms required to stack into crystal units. The viscosity of a liquid is sensitive to the interactions between its constituent species and so the viscosity of liquid alloys is very dependent on chemistry. This is analogous to

the formation of glassy structures from silica melts, SiO_2 is described as an acidic slag/oxide because it does not dissociate to form free oxygen ions; instead it forms networks of SiO_4 tetrahedra this means the liquid silica has very high viscosity and on cooling there is no opportunity for molecules to re-arrange into a crystal lattice [42]. To promote glass formation in metallic alloys the chemistry is chosen to promote the formation of clusters of atoms in the melt, such clusters have been observed and characterised experimentally [44]. These clusters are based on dense packing of the alloy atoms around a central core atom, due to atomic size differences in every alloy composition there will be efficient (and therefore most favourable) cluster structures, this leads to a few favoured structures and the presence of short range order in metallic glasses. The rules for good glass forming compositions proposed by Inoue [43]: three or more components, large atomic size differences and negative heats of mixing, come directly from the need to promote high viscosity through clustering by allowing high packing efficiency and showing attraction between constituents. Other considerations such as compositions close to deep eutectic features in the phase diagram and improve glass formability by making the kinetics of solidification more favourable.

However they are formed, amorphous structures in metals are a meta-stable phenomenon caused by the triumph of kinetics over thermodynamics. They can be broken down by heat treatment above the crystallisation temperature the normal result is that crystalline intermetallic phases precipitate. The presence of intermetallics after crystallisation should be expected as all of the requirements to promote bonds of a directional/covalent nature are present in Inoue's rules.

In sections 1.1.2 and 1.1.3 the relationship between entropy and enthalpy in promoting simple crystal structures and random solid solution HEAs was discussed, the balance of these thermodynamic terms may allow HEAs to adopt simple structures due to a window of thermodynamic stability from the melting point down to some other temperature. This differs from metallic glasses because the liquid structure is never thermodynamically favourable below the melting point. This leads to two conclusions. A metallic glass may potentially transform into an HEA if the re-crystalisation temperature is within the HEA stability range. Both terms refer to a condition of the alloy which may not be permanent and so the alloys should be described as having HEA or glass forming potential and only as *HEAs* or *glasses* when in the actual condition. Considering these conclusions it is apparent that an alloy with both glass forming ability and HEA (simple random solid solution) forming ability has not been demonstrated [45, 46], but there is no reason why it should not be possible.

1.3 Commercial Alloys

Novel alloys such as Bulk Metallic Glasses or HEAs are often thought of as academic trivialities. But the study of these systems can often give insights into the behaviour of other alloys either as models or analogues. This is particularly true of the HEAs which on first inspection have outlandish chemistries but which are actually not dissimilar to some commercial Super Alloys as table 5 shows:

Table 5 compositions of some commercial alloys with multiple principal elements

Grade	Fe / wt%	Ni / wt%	Co / wt%	Cr / wt%	Others / wt%
IN718	18	53	1	20	Nb 5 Mo 3
IN783	30	30	30	3	Nb 3 Al 5.5
Nimonic 903	40	36	17		Nb 3, Al 1, Ti 1
Nimonic 909	45	37	16		Nb 4.5 Ti 1.5
Haynes 556	31	20	18	22	W 2.5, Mo 3

The alloys shown above are all commercially available and are established for use in aero-engines, they have undergone thousands of hours of testing to attain this level of trust and acceptance, but they are strikingly similar to the 'blue sky' HEA compositions described in earlier sections. The development of what are now known as super alloys started in the 1930s [35] to service the need for more creep resistant materials for aero engine superchargers and later gas turbine components, materials to replace the stainless steels then in use.

The matrix phase of all super alloys is an austenitic solid solution of nickel, iron or cobalt and often all three elements are present in substantial

concentrations along with 6-30 wt% chromium. It was seen in section one that these elements form the basis of most of the successful reported HEAs and in section two that the rate of change of the stabilising configurational entropy with respect to concentration of an individual component of a 5 element solid solution is almost at its minima at around 6 at% which for the elements Cr, Fe, Co, Ni is approximately 6 at% of a component. The result of this is the extreme microstructural stability of the super alloys at high temperatures. Addition of Al and Ti to super alloys results in the formation of the Ni_3Al gamma prime phase, which precipitates coherently with the matrix, Co and Cr have an interesting effect on the precipitation of gamma prime; Co can substitute for Ni in gamma prime and this increases the configurational entropy of the phase causing an elevation in its solvation temperature, Cr cannot and so increasing Cr additions have the opposite effect on solvation of gamma prime. This effect was noted and alloy compositions adjusted accordingly through several generations of super alloys: IN713 has reduced chromium (12 wt%) to increase operating temperature, IN939 had increased chromium (19 wt%) to improve resistance to harsh operating environments but this was mitigated by high cobalt (19 wt%) to maintain high temperature capability.

When these developments were being made it was on an incremental and experimental basis, this can be seen in the evolution of super alloys from nickel stabilised austenitic stainless steels to their current form.

Seventy plus years of incremental alloy development has generated a class of alloys, which are unique in their degree of complexity. No other system of

alloys relies on so many alloying elements and in such concentrations. The synergistic relationships between the components of super alloys and the matrix elements are far too complex to be studied in controlled manner and understood fully. And this has lead to the development of the electron vacancy number (N_v) approach to predict properties of super alloys.

Various models exist to predict the average electron valence number of the solid solution; after the formation of carbides and other precipitates have depleted the concentrations of certain elements the average valence electron concentration is calculated; thus contributions from all elements present in the alloy are considered and N_v is in effect a dimensionless number which can be used to study composition property relationships. Reminiscent of the sixty year old work of Hume-Rothery, N_v can reliably predict the threshold at which deleterious phases may form [35,36,37] and has recently been related to castability of alloys such as 713LC and MM002, where it is thought to be related to solidification behaviour of the alloy [38].

The power of N_v for predicting properties of Super alloys is in its simplifying effect, accounting for all the synergies and complexities of the alloy chemistry in a simple figure. And this must have implications for the investigation of HEAs, which share so many of the characteristics of Super alloys. To this end the development of the electron theory of metals will be discussed in the next section.

1.4 Electron Theory of Metals

Bonds are normally classified as ionic, covalent or metallic. An ionic bond exists due to the electrostatic attraction between an anion and a cation, the ions are formed when an electro-positive element donates an electron to/ reacts with an electro-negative element. Hence for an ionic bond a large difference in electro-negativities is required between the ion forming species; *ie* there is an energetic benefit to each species such as removal of an unpaired electron or completion of an octet or half orbital which is greater than the energetic cost of charge imbalance in the new ion or for removal an electron from the electropositive species. In ionic crystals nearest neighbours are usually of opposite charge and second nearest neighbours with like charges are thus shielded from each other. Typically ionic bonds are expected between a metal and a non-metal and are characterised by electron donation *and acceptance*. A covalent bond exists where atomic orbitals overlap and a pair of molecular orbitals is formed: a low energy bonding orbital and a high-energy anti-bonding orbital, when the electrons from the original atomic orbitals occupy the bonding orbital their kinetic energy is reduced and thus the formation of the bond lowers the energy of the system and is favourable. Because the formation of a covalent bond requires overlap of atomic orbitals and orbitals have a spatial orientation determined by their wave function a covalent bond is also geometrically constrained and the atoms in covalent molecules must maintain a fixed distance and angle from each other. Typically a covalent bond exists between non-metals and is characterised by sharing electrons and covalent lattices adopt crystal systems determined by the orientation of the *directional bonds*. A metallic bond is formed between metal atoms and the

nature of the bond is the origin of the many unique properties of metals for which they are valued. The Mott theory of conduction band gaps helps to explain how a metallic bond may form; when a lattice of atoms of the same valence are bonded by covalent bonds an array of bonds are formed which are saturated with the available electrons, these bonds also constitute a deep energy well and the electrons are held in the bonds unable to move about the lattice, this is the origin of the band gap in insulators. When a foreign atom with a different valence is added to the lattice, say one more valence electron (and one more proton), the substituted atom has a slight polarising effect on the nearest and second nearest neighbours pulling electron density towards itself and the additional electron has to move through this environment. This has the effect of lowering the ionisation energy of the electron to the level of background thermal activation. The electron thus ionised, cannot be accommodated in the saturated covalent bonds and must move through the lattice as a free electron in the conduction band. The effect of the foreign atom is to reduce the band gap to a level that may be overcome by thermal energy. In a metal the Fermi energy lies in the conduction band this means that there is an overlap between the conduction and valence bands, and because the material is conductive it cannot sustain long range electrostatic fields, any positive or negative charge concentrations attract or repel charge carriers and shielding takes place. With this screening effect in place ionisation is easy and general ionisation takes place, resulting in unsaturated covalent bonding with a resonance effect, which allows electrons to move freely through the lattice. A metallic bond is formed when electrons are not bound tightly to an ion or held tightly in a covalent bond.

1.4.1 Metallic Bonding in Alloys

1.4.1.1 Electrons in Metals

Metallic bonding is often described as an arrangement of positive ions on a lattice surrounded in a sea or gas of electrons, the attraction between the positive metal ions and the free electrons providing cohesion. This section gives an overview of electron theory and how metallic bonding comes about.

Electrons possess the property of wave particle duality; they may be described as either waves or particles depending upon the context of the discussion. The wave-like nature of an electron is described by a wave function. The wave function is a solution the Schrödinger wave equation for that electron's quantum state and describes the probability distribution of it being located at any point. The Schrödinger equation is a hyperbolic second order partial differential equation, equation 1.14, and may only be solved analytically for the two-body problem of the hydrogen atom.

$$E\psi(r) = -\frac{h^2}{4\pi m}\nabla^2\psi(r) + V(r)\psi(r) \qquad \textit{Equation 1.14}$$

where h is Plank's constant m is the electron mass V is the potential energy and Ψ is the wave function with form e^{ikr}. According to Euler's equation, equation 1.15, the wave function may be represented by the sum of a real and an imaginary wave.

$$Ae^{ix} = A\cos(x) + Ai\sin(x) \qquad \textit{Equation 1.15}$$

This form of the wave function illustrates that the function is periodic and that allowed wavelengths and frequencies therefore depend on the integration boundaries of the problem and the periodicity of the function. The first solution and lowest energy state corresponds to a wave with the longest possible wavelength (knowing that $E=h\omega=hc/\lambda$), so $\lambda=L$ where L is the size of the potential field which the nucleus exerts on the electron. The first solution describes a spherical surface about the nucleus and has no net angular momentum. The second lowest energy solution occurs at $\lambda=L/2$. The periodicity of the standing wave with respect to L must always be an integer and is known as the principal quantum number n. The second quantum number, l (0, 1, 2,...), describes the angular momentum of the electron and results in further splitting of the principal energy levels into p ($l=1$) and d ($l=2$) orbitals. The solutions for the hydrogen atom are used to approximate the behavior of electrons in more complex systems with a good degree of accuracy. The Pauli exclusion principle forbids electrons to occupy the same quantum state and so only two electrons with opposing spins may occupy the same energy level, for this reason additional electrons must move up into energy higher orbitals. As the orbitals increase in energy they expand further out from the positive nucleus and are less tightly bound.

When two metal atoms come into close proximity their outermost electron shells may overlap resulting in a new wave function that is the sum of the original atomic orbitals [14,15]; this is known as the linear combination of atomic orbitals theory (LCAO). Over the extent of a metallic lattice this results in the formation of a conduction band of very similar but discrete “molecular”

orbitals, which the outer electrons can navigate freely. So in a metal we may consider two distinct kinds of electrons; the inner tightly bound electrons and the nearly free electrons. The inner electrons of the s and p block metals play no part in the cohesion between the metal ions. The outer electrons of these metals are able to move around the crystal with a long wavelength Bloch function with a periodicity of *a*, the lattice parameter, these electrons form the sea of negative charge which holds metals together. Note that the metal ions are not stripped of all their electrons; they are described by pseudo-potentials, which attempt to describe the positive potential exerted by the partially shielded nucleus and the extent of its influence [14,15]. The presence of d orbitals in the transition metals increases the cohesion of the transition metals and results in much higher strengths than those of the s and p block metals. The d orbitals do not delocalise as the s and p electrons do, however they do overlap to form strong bonds with neighboring metal ions. The overlap of the atomic d orbitals results in splitting and formation of molecular orbitals, the splitting occurs because when the d orbitals overlap their wave functions may interfere constructively or destructively. As the metals are the same the wave functions will have the same amplitude and interference will double the amplitude or result in a node. The physical significance of the amplitude is the probability of the electron being located at a point in space. Constructive interference results in a low energy bonding orbital, destructive in an anti-bonding orbital. Each metal has five d orbitals so five bonding and five anti-bonding orbitals are formed, filling of these orbitals is sequential and bonding is strongest when all bonding orbitals are filled and the anti-bonding orbitals are empty [10,14,15] this is the reason that cohesion of the transition metals

peaks in the centre, as indicated by the trend in melting points of the d block elements.

1.4.2.2 Electron density of states

As discussed above the electronic structure of a bulk material is built up by the summation of the atomic electron orbitals. The orbitals with the highest energy, the outer atomic orbitals or outer shell electrons, are the ones which are able to combine with those of other atoms to form molecular orbitals and are known as the valence orbitals. Orbitals with lower energy do not combine with those of other atoms because they do not extend far enough from the nucleus for them to overlap with orbitals from other atoms. For this reason they are often called core electron orbitals. The Fermi energy (ε_F) is the energy of the highest occupied electron orbital at zero Kelvin and therefore lies in the valence shell at normal temperatures [14]. As discussed above all of these orbitals in the core or the shell exist as discrete energy levels with nodes between, *ie* they are quantized. According to equation 1.15 and the discussion of solutions to the wave equation frequencies the energy differences between the higher order orbitals must reduce very quickly according to the form $1/L^2$. When the higher energy valence orbitals are combined, into molecular / bonding orbitals, the recombination increases the number of orbitals and further reduces the energy differences. This means that although the orbitals are discrete the energy differences between them are often very small. As a result a valid state exists at almost any energy between the Fermi energy and the ionization energy. This is the origin of the term “band”, to describe the upper electron orbitals in solid materials. The band is made up of all of the allowed electron states and at each electron energy level there may be a

number of states of equivalent energy. This leads to the concept of the density of states (DOS), *ie* the number of available states at a particular energy or radial distance from the nucleus. These states are filled sequentially starting with the lowest energy core states and continuing until all of the available the last electrons have been accommodated, somewhere in the conduction band, for metallic materials. Electronic structures with high density of states at low energy levels have a lower overall energy and are therefore more stable than those with few low energy states to accommodate electrons [62]. Therefore if a "reaction" which increases the low energy DOS occurs it will increase the stability of an electronic structure, this is a statistical description of the molecular orbital theory.

But as DOS only describes the radial distribution of electron states it cannot give any insight to directionality. To describe the full band structure the density of states along the lattice vectors is required. Band structure diagrams show the number of energy states along a set vector, allowing information about the degree of atomic orbital overlap to be observed, the density of states in a particular direction is indicative of the strength of bonding in that direction and is important to predict mechanical properties and anisotropy.

1.4.1.3 Electrons in Alloys

Alloys contain several metals, which have different nuclear charge and so different energy orbitals and a different number of electrons arranged within them. The result of this is that when outermost electron orbitals combine the interference of the wave functions described above is more complex than that of a simple pure metal; there may be asymmetry of geometry or distribution of

energy states. This increased complexity may result in unanticipated properties which are not simply the average of the alloying elements behaviors. Such behavior could constitute a “cocktail effect” proposed for HEAs [4].

1.5 The Density Functional Theory Approach to Modelling Electronic Structure

1.5.1 Solving the Schrödinger Wave Equation

As discussed above the Schrödinger equation may describe the wave function of all the electrons in an atom, molecule or crystal but for any system more complex than a hydrogen atom the equation is a second order differential equation describing a many body problem and cannot be solved analytically in any meaningful way. This is because there are more variables to integrate than dimensions in the problem *ie* there are too many degrees of freedom. Furthermore using numerical methods to iterate a solution would be computationally unfeasible for most systems.

The Thomas-Fermi model of 1927 [47,48] offers a solution to the ground state of the system by defining the system in terms of electron density for example the energy of an atom may be described according to equation 3.1 in which E is energy, Z is the charge, r is a direction vector and ρ the electron density.

$$E_{TF} = \frac{3}{10}\left(3\pi^2\right)^{2/3} \int \rho^{5/3}(\mathbf{r})d\mathbf{r} - Z\int \frac{\rho(\mathbf{r}')}{r}d\mathbf{r} + \frac{1}{2}\iint \frac{\rho(\mathbf{r}_1')\rho(\mathbf{r}_2')}{r_{12}}d\mathbf{r}_1 d\mathbf{r}_2$$

Equation 3.1

Where the term consisting of the first integral and pre integral constant is the functional which expresses the kinetic energy of the system from Thomas-Fermi [74], the second integral describes the potential energy and the third the interaction energy. Because the solution to the problem (ground state energy) is described in three integrals with sufficient information to be solved, an analytical solution is possible. This is the basis of density functional theory and was further developed by Hohenberg and Kohn [48, 49], the beauty of the theory is that all of the integrals are described in terms of the electron density. The problem is then to describe the electron density and the exchange interactions of the electron gas.

1.5.2 Electron Density Approximations

The local density approximation (LDA) calculates the exchange correlation energy at a point in space and thus there is an implicit assumption that the electron gas is homogeneous (at least locally) and not changing with respect to position or time. The LDA assumes that the exchange correlation energy may be expressed in the form of equation 3.2

$$E_{XC}^{LDA}[\rho] = \int \rho(\vec{r}) e_{XC}(\rho(\vec{r}))\, d\vec{r} \qquad \textit{Equation 3.2}$$

And the exchange correlation energy is simply a function of the number of particles $\rho(\vec{r})$ and the energy of each particle e_{XC}.

Because the LDA does not account for the rate of change of density with respect to coordinate the exchange correlation energy is often overestimated when this approximation is used and so the LDA may find close packed

structures more stable than they actually are. However because these errors of 'low spatial resolution' may be averaged out for some properties the LDA may give very accurate results for such properties as lattice parameters.

1.5.3 The Generalised Gradient Approximation (GGA)

The accuracy of the electron density approximation may be improved by accepting that the electron density does change quite quickly with respect to position. The GGA adds further information to the calculation of the exchange correlation energy to account for the gradient of the charge density. The GGA therefore has the form shown in equation 3.3

$$E_{XC}^{GGA}[\rho_\alpha,\rho_\beta] = \int f(\rho_\alpha,\rho_\beta,\nabla\rho_\alpha,\nabla\rho_\beta)d\vec{r} \qquad \textit{Equation 3.3}$$

By accounting for the rate of change of charge density as well as the absolute density the GGA may give more accurate results for calculation of such properties as elastic moduli and the energy of a crystal structure. For these reasons and those given in 3.2 the GGA was used for the DFT calculations made in this thesis.

1.6 Conclusion

The term High Entropy Alloy is widely accepted to describe alloys which are compositionally complex, consisting of five or more elements in approximately equiatomic proportions. These alloys have attracted interest due to their unexpected properties, which include; the ability to form random solid solutions with simple crystal geometry, high strength and good ductility. The ability to form a solid solution has been attributed to the high configurational entropy of such a solution consisting of 5 or more elements, which may make a solid solution favourable over an intermetallic. This assumption is testable but has not yet been proven.

Current areas of research are focussed on discovery of new compositions and developing properties such as mechanical strength, wear resistance, corrosion resistance and electrical/magnetic properties. Whilst work is ongoing in these areas a universal design strategy has been lacking, even though tools to investigate complex alloys have been developed to describe the most compositionally complex alloys used today – Ni based super alloys, many of which bear a striking resemblance to HEAs. These tools such as electron vacancy number (N_v) and DFT modelling may offer a more efficient approach to the design of high entropy alloys. If each alloying addition to the HEA soup is considered in terms of its effect on the electronic structure of the alloy and the alloy itself is thought of in terms of its electronic structure, then maybe it will be possible to move away from 'fairy dust' metallurgy, where elements are added for one benefit only to cause other problems; such as the promotion of Laves phase by Re and W solid solution strengthening additions to single

crystal casting super alloys, leading to the reduction of Cr from these alloys to ‘make room’ (in the electronic structure) for the refractory metals.

High entropy alloys are exotic and most efforts in this field will produce new knowledge; in particular this review shows that there is an opportunity to investigate how these novel alloys form and how their properties arise; through applying the electronic theory of metals, which is well-established. The discussion on glass formation in alloys hinted that there may be some interesting links between HEAs and BMGs investigation of this possibility is likely to give some interesting insights to both material types.

2. Experimental Methods

2.1 Alloy Preparation

All alloys were prepared in-house either by Argon Arc Melting (AAM) or by Vacuum Induction Melting on the Small Scale Melting rig (SSM), described in sections 2.1.1 and 2.1.2 respectively. The choice of furnace was determined by the relative volatility of the alloying elements; for elements with a low melting point or high vapour pressure the SSM was preferred. For transition and refractory metal-based alloys the AAM was used.

Charge weights were calculated according to equation *2.1* below

$$M_i = \frac{C_i A_{ri}}{\sum_i^n (C_i A_i)} \qquad \textit{Equation 2.1}$$

where C_i is the concentration of element i in atomic percent A_r the relative atomic mass and M_i the weight percent required to obtain the desired atomic percent alloying concentration of i.

Raw materials in the form of virgin pure elements (table 2.1) were cut or filed to the required weight cleaned of oxide/surface contamination with steel wool, tissue paper and *propan-2-ol*. The charges of 5 g – 20 g were then either put directly into the furnace or stored under vacuum until required.

Table 2.1 details of virgin raw materials used in this work

Element	Source	Purity / wt%	Main Contaminants
Iron (electrolytic)	William Rowland Metals	99.98	C, O, N
Cobalt (carbonyl)	Alpha Aesar	99.98	C, Ni
Chromium (electrolytic)	Nikkelverk	99.6	C, S, N
Nickel (carbonyl)	Alpha Aesar	99.8	C, Fe, Co
Aluminium (ingot)	LSM/AMG super alloys	99.99+	O, S
Titanium (foil)	Alpha Aesar	99.998	O, Zr
Zirconium (foil)	Alpha Aesar	99.99	O, Ti, Hf
Manganese (electrolytic)	Alpha Aesar	99.7	C, Fe
Niobium (foil)	Alpha Aesar	99.998	Ta
Copper (rod)	Alpha Aesar	99.998	O
Lithium (wire)	Alpha Aesar	99.8	O, C, H
Magnesium (foil)	Alpha Aesar	99.98	O
Zinc (ingot)	Alpha Aesar	99.999	As, Sn

2.1.1 Argon Arc Melting

The arrangement for suction casting in an arc melter is shown in figure 2.1 the Buhler 'Mini Arc Melter' is shown in figure 2.2. The older Edwards Arc Melter was also used.

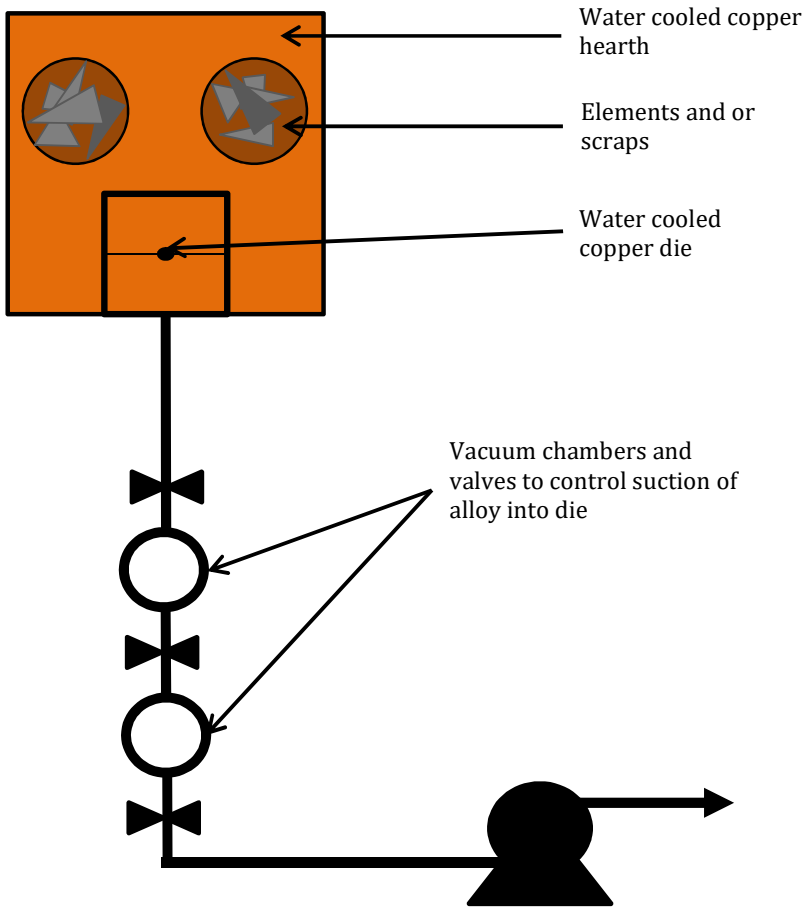

Figure 2.1 Schematic of hearth and suction casting arrangement.

Figure 2.2 Buhler Mini Arc Melter the hearth on this model is suitable for melting up to 6 alloy ingots at one time, the pumping system consists of an oil free scroll pump and high vacuum turbo molecular pump

Both furnaces were equipped with water-cooled copper hearths and were capable of achieving vacuum to $2x10^{-5}$ mbar.

The charges were placed into the furnace chamber with a Ti getter button; the chamber was evacuated to $7x10^{-5}$ mbar or better and back filled with argon to a pressure of 25 mbar. The Ti getter was melted to capture any remaining oxygen or nitrogen in the chamber; this was done before each time the alloy button was melted. All alloy buttons were melted and inverted 4 times to ensure thorough melting and homogeneity.

2.1.2 Vacuum Induction Melting

Alloys deemed unsuitable for arc melting were prepared by induction melting under vacuum. The small scale melter consists of a horizontal 50 mm diameter quartz tube connected to a two stage vacuum system, an induction coil is positioned around the centre of the quartz tube and alloy charges are placed in Boron-Nitride boats within the coil. The system is evacuated to $2x10^{-5}$ mbar and back filled with argon and the induction coil switched on until the charge is melted. Stirring is facilitated by the induction current and by agitation of the equipment. Figure 2.3 shows the small scale melter and induction generator.

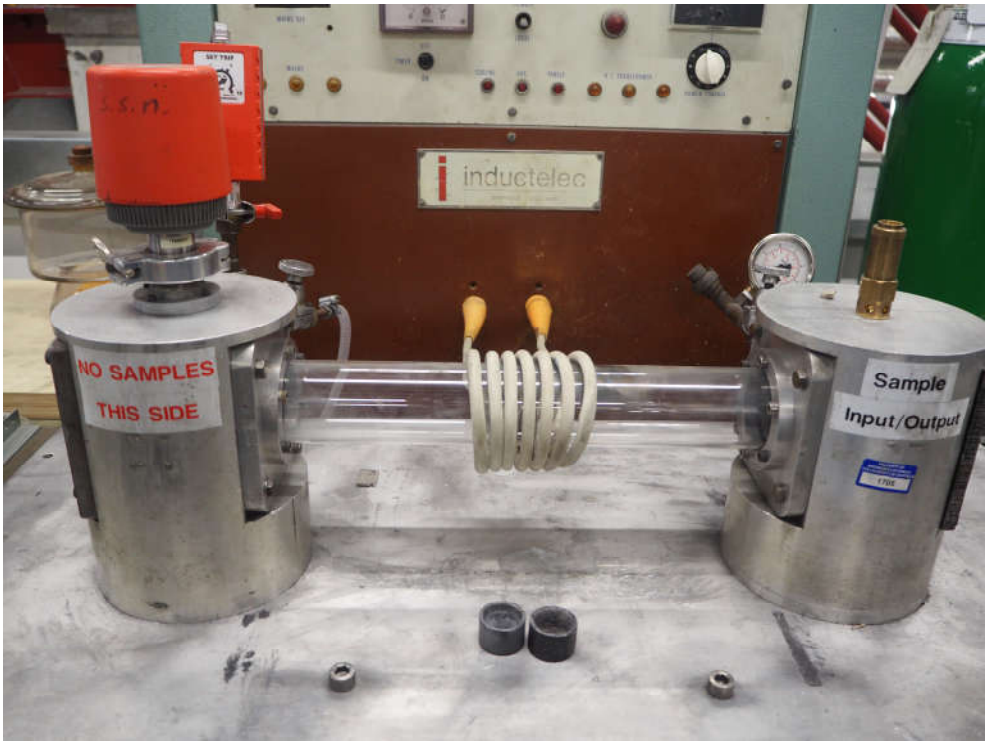

Figure 2.3 small scale melter used to prepare alloys with volatile or low melting point components

2.1.3 Casting / Solidification processing

The alloyed button ingots were re-cast for testing/characterisation. The form and method of solidification processing was selected as appropriate for the characterisation technique to be applied and the properties of the alloy. Most alloys were suitable for arc melting and suction casting which gave the best surface finish and lowest chance of defects, low melting point or viscous alloys were prepared by induction melting and injection casting and where a very high cooling rate was desired induction melt spinning was employed.

2.1.3.1 Suction casting

Material from the button ingot was placed into the AAM chamber on top of a copper split mould die set with the desired internal profile. The chamber is then evacuated as normal along with a secondary vacuum reservoir chamber, connected directly to the bottom of the die set; before the main chamber is backfilled with argon the reservoir is isolated. The alloy is then melted on top of the die set and once molten the valve isolating the secondary is opened and the pressure difference forces the melt into the die where it is rapidly solidified.

2.1.3.2 Injection casting

Pre-alloyed material was placed in a quartz crucible with a tapered nozzle at one end, the aperture size of the nozzle was controlled by grinding back the tip. The crucible was held in an induction coil over the die set with a retort stand

and clamp, the open end of the crucible was attached to a gas line. The whole apparatus was arranged inside a vacuum chamber and pumped down to $5x10^{-5}$ mbar before back filling with argon to 25 mbar. The alloy was melted by switching on the induction generator and forced through the nozzle into the mould by allowing argon top flow into the top of the crucible at 30-40 mbar.

2.1.3.3 Melt spinning

Melt spinning, shown in *figure 2.3* was used to obtain high cooling rates, the alloy to be cast was arranged as described above except that the nozzle was directed at a spinning copper wheel rather than at the opening of a die. This process resulted in the formation of a ribbon of metal approximately 20 μm thick. It was found that using helium rather than argon as the injecting gas gave a better surface finish and edge definition on the ribbons, this was ascribed to the He having less momentum and not causing turbulence in the liquid metal.

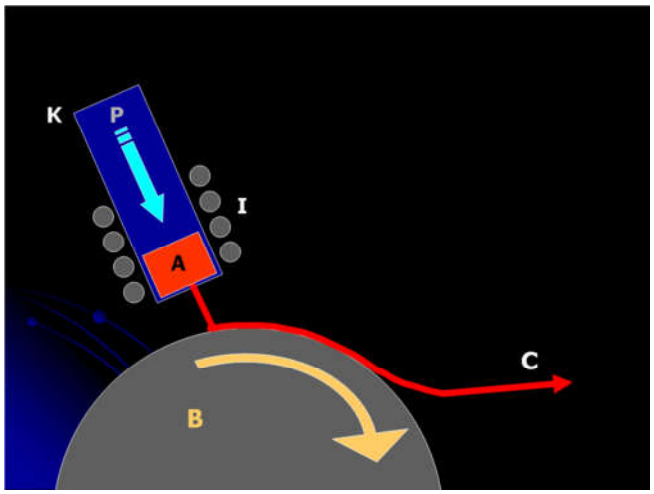

Figure 2.4 Schematic of the melt spinning process, the Metal A is forced through an aperture by gas pressure, the stream strikes the wheel B and a solidified ribbon is formed C

2.2 Microstructural Characterisation

Bulk alloy samples were prepared by wet grinding with SiC grit papers up to 4000 grade followed by polishing with colloidal silica to give a flat mirror surface. SEM and XRD were used to investigate the phases present.

2.2.1 Scanning Electron Microscopy

SEM was carried out using a n FEI Sirion equipped with a field emission gun, backscattered electron detector, EDS detector and Oxford instruments Inca EDS software. Backscattered electron images were collected at a working distance of 5 mm and accelerating voltage of 12 kV. EDS maps and spots were collected at a working distance of 5 mm and an accelerating voltage of 20 kV.

2.2.2 X-ray Diffraction

XRD was used to identify the phases present and the crystal structure of the alloys. Diffraction patterns were measured on a Siemens D500 equipped with a Cu source tube operating at 20 kV. Scans were made from 20° to 130° 2θ with a step size of 0.2°. Phases were identified with WinXPow, which automatically compares diffraction patterns with JCPDS cards. Where no phase could be identified a crystal structure was determined by manually indexing the diffraction pattern using the mathematical approach based on the $sin^2\theta$ method to determine cubic structures.

2.3 Mechanical testing

Mechanical testing was carried out to determine elastic moduli, yield strength, ultimate strength, plasticity and reduction/increase in area.

2.3.1 Compression testing

Vacuum suction or injection cast bars were cut to an aspect ratio of 1.5 to 1 (length to height) and ground to ensure the end faces were perpendicular to the long axis along which the load was to be applied. Compression testing was carried out on a Tinius Olsen testing rig fitted with a 100kN load cell. Cubic boron nitride platens were used to prevent the samples from embedding in the tools which if allowed to happen would be a source of error in the displacement measurements. The general compliance error was allowed for by using the Direct method described by Kalidindi et al [51], the testing rig was run without a test piece under the same conditions as used for sample testing. The load displacement data plotted and curve fitting was used to derive an expression (equation 2.2) for the compliance of the testing rig. Force measurements made during sample testing were used to calculate the machine displacement at that point in the test and this displacement was subtracted from the measured displacement to give the corrected deformation of the sample.

$$\text{Machine strain} = -4\text{x}10^{-}16\,P^4 + 6\text{x}10^{-12}\,P^3 - 3\text{x}10^{-08}\,P^2 + 9\text{x}10^{-05}\,P - 0.0072$$

Equation 2.2

Samples were tested at a loading rate of 1mm/min. Fracture surfaces and gauge diameters were examined by light microscope and SEM.

2.3.2 Ultrasonic measurements

Dynamic moduli were calculated from speed of sound data measured on cast bars of the HEA compositions.

Measurements were taken using an Olympus Epoch 600 send/receive ultrasonic inspection instrument equipped with longitudinal and transverse send/receive transducers.

The smallest available transverse wave transducer was 6 mm in diameter; therefore to obtain the strongest signal and reduce the noise to signal ratio, sample bars of 6mm diameter were cast for ultrasonic testing. The 6 mm bars were also suitable for longitudinal wave measurements using a 3 mm diameter transducer.

Coupling fluids were required to transmit the signal from the transducer face to the sample, it was found that glycerol was suitable for longitudinal waves and honey gave good transmission of sound for shear waves.

The samples were cut into cylinders with two faced perpendicular to the long axis to a nominal length of 7.5 mm and the length measured to ± 0.01 mm using a digital sliding calliper set.

Each sample was coupled to the transducer and the time for the wave to hit the "backwall" and be reflected back to the transducer measured. This time was then converted to a speed by dividing the accurate length by the measured time of flight. As per equation 2.2

$$c_{L/T} = \frac{2l}{tof} \qquad \textit{Equation 2.2}$$

where $c_{L/T}$ is the speed of a longitudinal or shear wave, l the length of the sample and tof the time of flight.

The elastic moduli can be calculated from the speed of sound according to equation 2.3

$$c_{L/T} = \sqrt{\frac{K}{\rho}} \qquad \textit{Equation 2.3}$$

where K represents either the elastic or shear modulus of the sample and ρ the density.

Density was calculated by weighing the sample in air and in water and applying Archimedes's principle.

$$\rho_{sample} = \rho_{water}\left(\frac{weight_{in.air}}{weight_{in.air} - weight_{in.water}}\right) \quad \textit{Equation 2.4}$$

The error in these measurements is estimated to be ± 0.065% on the length measurement and ± 0.165 % on the time of flight measurement so the overall uncertainty in the speed of sound determination is expected to be ± 0.295 %. The error on the density measurement is estimated to be ± 0.007 %. The overall uncertainty in the calculation of moduli is estimated to be ± 0.094 %.

2.4 Thermal Methods

2.4.1 Differential Scanning Calorimetry

Glass transition (T_g) and re-crystallisation temperatures (T_x) were measured on a Perkin Elmer Diamond DSC. Samples of approximately 0.2 g were placed in gold pans and the heating and cooling curves measured from room temperature to 1273 K at a rate of 10 °C min^{-1}. Glass transition which is a second order change of state may be seen on a DSC trace as an inflection point, crystallisation is an exothermic reaction and a corresponding peak appears on the trace.

3. Modelling methods

3.1 CASTEP and Materials Studio

3.1.1CASTEP

The Cambridge Serial Total Energy Package code was developed at the University of Cambridge Physics Department in the late eighties. The program is a code which was built to solve the many body Schrödinger wave equation using the DFT approximation of Hohenberg and Kohn [48, 49]. In order to reduce the computational expense pseudo potentials are used to approximate the effect of the nuclear potential and shielding on the outer electrons, CASTEP is compatible with all normally used pseudo potential approximations (LDA, GGA, super soft, on the fly etc). The code assumes that all electrons and nuclei are within the bounds of the model at all times *ie* no electrons escape above the calculation cutoff energy at any point: the system is adiabatic.

3.1.2 Materials Studio

Materials Studio is an atomic/molecular visualisation and building software which is interfaced with a suite of modelling calculation codes, including CASTEP. The visualisation and building module can be used to create lattices with the required symmetry, assign species to the lattice points and create a run file for any of the interfaced simulation codes. Once the code has been run the results file may be opened in Materials Studio and the structure viewed with the additional results, such as electron distribution, from the simulation

overlaid. The results files are also easily exported for data handling in other software such as excel/Igor.

3.2 Computational Methods

Super cells containing from 2 to 27 unit cells were built for: CoCrFeNi, bcc and fcc, CoCrFeNiAl bcc and fcc and for CoCrFeNiTi fcc, using the materials studio visualiser. Species were assigned randomly to the lattice points to simulate a solid solution with no nearest neighbour preferences, multiple arrangements were built and minimised to ensure the simulations were not affected by local minima. Where available in the literature [8,11,21] known lattice parameters were used, for the crystal structures not observed in reality lattice parameters were chosen to give the same starting density as the observed crystals. The electronic structure of the alloys was then calculated using the plane wave basis DFT code CASTEP using the graduated gradient approximation, cut off energy of 300 eV, Monkhurst-pack K-point grid spacing of 0.05 $Å^{-1}$ and SCF tolerance of $5x10^{-6}$. Figure 3.1 shows the expected linear trend – the energy of the reaction is a function of the amount of material involved. This infers that the calculated bonding in the alloys does not change as a feature of simulation size – the same bonds on average are being formed but the simulation is larger and the energies involved are correspondingly greater in magnitude. This means that the use of large simulations do not offer sufficient benefit in terms of accuracy to justify the computational expense.

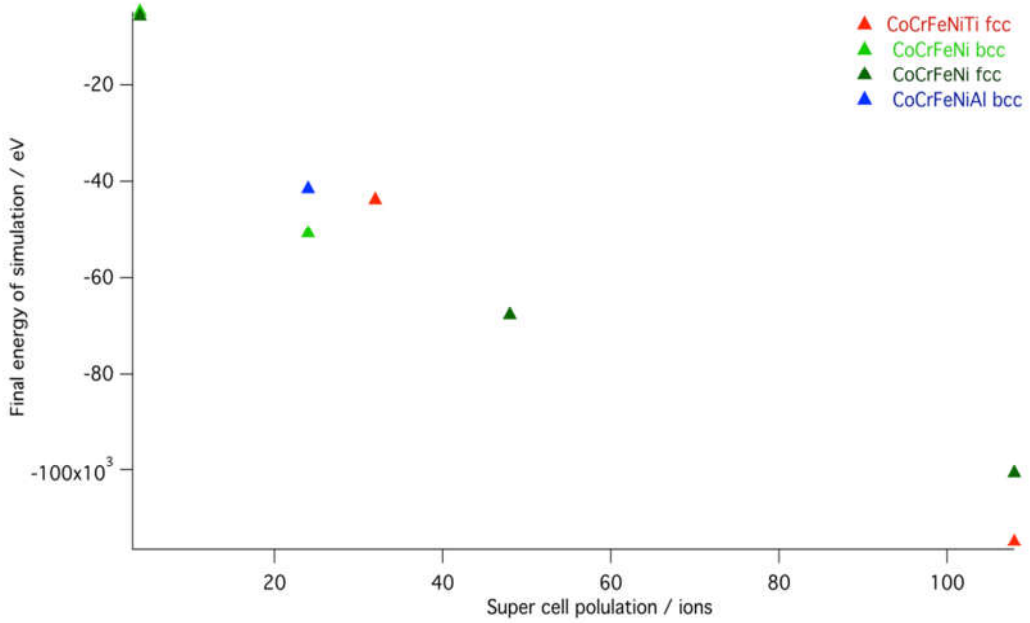

Figure 3.1 Change in minimisation energy with simulation size

Where super-cell size prevented, exact alloy stoichiometry to be simulated calculations were repeated with an excess of each species, the results of each simulation were compared to ensure repeatability.

The Fermi energy, electron density, band structure (BS) and electron density of states (DOS) were extracted from the CASTEP output files. The Fermi energy of each alloy for the smallest and largest simulation is given in table 3.1, the value of ε_F is largely unaffected by the size of the simulation which suggests that the electronic structures of the alloys are represented well by all the calculation sizes.

Table 3.1 Fermi energies of alloys for different size simulations.

Alloy	CoCrFeNi (fcc)		CoCrFeNiTi (fcc)		CoCrFeNiAl (bcc)	
Number of ions	108	32	108	32	72	24
ε_F / eV	2.83	2.77	10.9	11.36	2.2	2.05

Taken together the data in figure 3.1 and table 3.1 support the use of smaller simulations to give greater computational efficiency because calculation time increases with the cube of supercell size for no demonstrable improvement in the value of the data. This being the case smaller super cells (16-32 ions) were used for the majority of the calculations simulating rearrangements of species and changes in stoichiometry. The reduced calculation time allowed more simulations to be carried out.

3.2 Modelling of potential light HEAs

The potential light HEA in Chapter 7 was modelled as above in super cells with hcp, fcc and bcc symmetry to allow the density of states of each structure to be compared and allow the stable crystal lattice type to be determined. The starting lattice parameters for geometric optimisation were calculated from the estimated density of the alloys.

4. Design of Thermoelectric Power Measurement Equipment

4.1 Introduction

Recalling that all metals and alloys have a defined Fermi energy, the value of which depends on; the number of free electrons, the potential of the lattice and the overlapping of the atomic orbitals and that the electrons are distributed statistically according to the Fermi-Dirac distribution, figure 4.1.

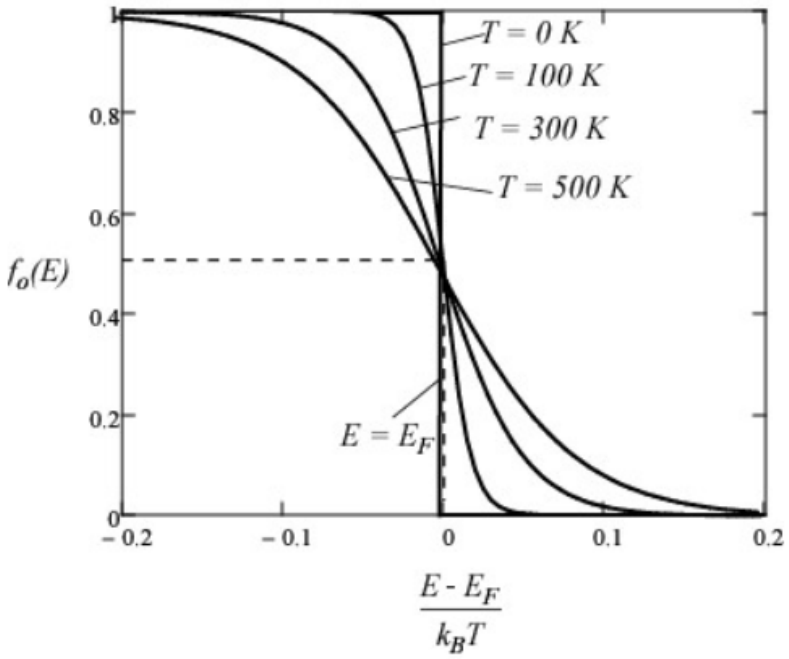

Figure 4.1 the Fermi-Dirac showing dependence of electron distribution on temperature [52]

The form of the distribution is given in equation 4.1 [52]

$$P(E) = \frac{1}{e^{(E-E_F)/k_BT}+1} \qquad \textit{Equation 4.1}$$

1. Changes in temperature will change the distribution of electron energies in a sample, higher temperatures giving rise to more energetic electrons filling higher level bands.
2. The level of the Fermi energy affects the sensitivity of the distribution to temperature (if the Fermi energy is high, more thermal energy is required to fill the unoccupied orbitals).

These two observations give rise to the Seebeck/Thermoelectric effect and the Thermocouple effect. In a thermocouple the two metals have different Fermi energies and therefore different distributions of electrons, it is possible for the energy of the system to be reduced by flow of electrons, and the potential difference across the thermocouple is a measure of this energy advantage. If two ends a sample of a metal or alloy are held at different temperatures the Fermi-Dirac distribution tells us that the electrons in the hot end will occupy more high energy states, and there will be some unoccupied states below the Fermi energy (fig 4.1), therefore if the circuit is closed electrons from the cold end may flow into the unoccupied low energy states, and the high energy electrons may fall into the vacated states at the cold end, in effect heat is being used to pump electrons.

This means that measurement of Thermoelectric power (TEP) is a means of directly sampling the conduction band of an alloy and provides a means of validating electronic structure models. A key output of DFT modelling is the fermi energy of the electronic structure; it is also possible to calculate the Fermi energy of a sample from a measurement of its TEP as may be seen from equations 4.2 - 4.4 [52].

$$TEP = S(T_2 - T_1) \qquad \textit{equation 4.2}$$

$$S = \frac{\pi^2 k_B T}{-2eT_F} \qquad \textit{equation 4.3}$$

$$E_F = \frac{T_F}{k_B} \qquad \textit{equation 4.4}$$

Where S is the Seebeck coefficient, T is temperature k_B is the Boltzman constant, e is the charge on an electron and T_F is the Fermi temperature. These relationships mean that measurement of TEP provides a means of directly comparing theoretical and experimental results. That is the measurements may be used to validate the models.

Equipment suitable for measurement of TEP was not available within the department or the wider University, nor was an off the shelf design available from equipment manufacturers at the time. Therefore the equipment to

measure TEP was designed and built by the author. And this chapter is concerned with the design, implementation and validation of the equipment.

4.2 Description of equipment requirements

Thermo-electric power is generated because when two ends of a sample are held at different temperatures the kinetic energy of the electrons at each point is different, this translates to a difference in electrical potential between the two ends. If a current is allowed to flow electrical power is released. So a simple experimental set up as shown in figure 4.2 is required to:

1. Cause the ends of the sample to be at different temperatures
2. Measure the temperature difference
3. Measure the potential difference between the two ends

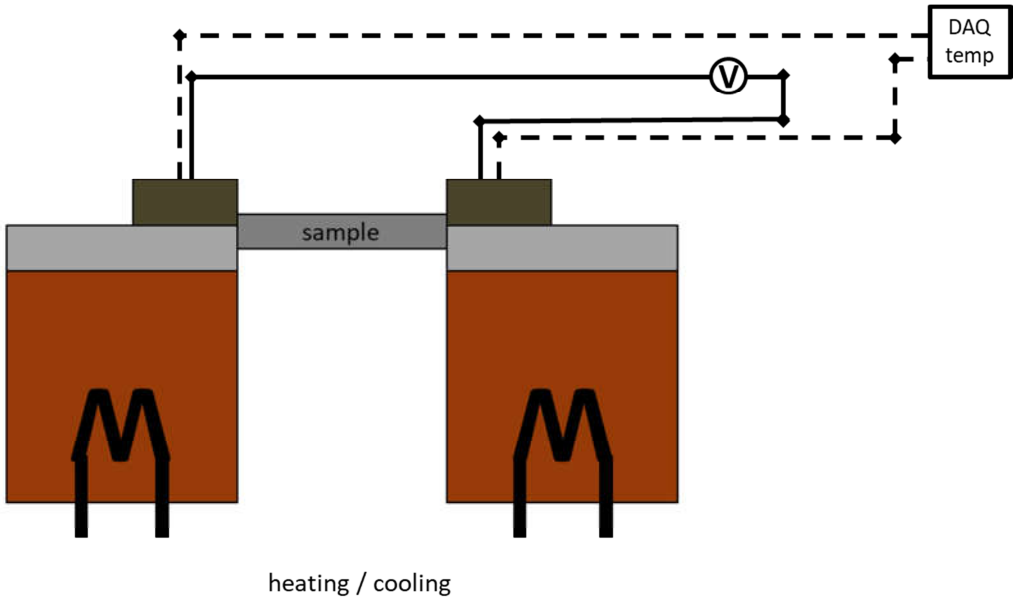

Figure 4.2 schematic of equipment for TEP measurement

In addition to points 1-3 above to get usable data requires:

- Accurate and repeatable measurement of voltage in the μV range
- Accurate measurement of temperature
- Control of temperature
- Stable temperature

4.3 Equipment solution

4.3.1 Voltage measurement

To get an accurate measurement a volt meter with high internal resistance is required, this minimises the voltage drop across the circuit, allowing an accurate measurement of the TEP voltage.

A Keighley 2000 voltmeter with 1 nV sensitivity, measurement reproducibility better than 10 nV and internal resistance over 200 MΩ was obtained. In metals the Seebeck coefficient is normally of the order of 1 μV-10 μV, and so a voltmeter with a resolution in the μV range is required. The 2000 series volt meter will gave sufficient resolution and repeatability to measure the TEP of alloys to the 2^{nd} decimal place, for a temperature difference of 10 K this will allow calculation of the Seebeck coefficient to at least 2 decimal places with a good degree of confidence.

4.3.2 Temperature measurement

Temperature measurements will be made at each end of the sample using K type thermocouples and an NI DAQ436 which connected to a laptop PC running National Instruments' lab-view software to collect data. The difference between the temperatures is used to calculate the Seebeck co-efficient of the metal from the TEP measurement according to equation 4.1.

The normal accuracy of a K type thermocouple in the range 250 K – 500 K is ± 1.5 K (°C). Because a temperature difference is being calculated from the temperature measurements and so long as the thermocouples are checked to be in agreement over the range of temperatures, thermocouple error will be cancelled out during the calculation of the parameter *S*.

4.3.3 Temperature controlled sample holding blocks

To generate a measurable voltage the ends of the sample must be held at temperatures which are sufficiently different to allow a large enough signal. The availability of an accurate and sensitive voltmeter means that a difference of 10 – 100 degrees across the sample is acceptable

The equipment will consist of two copper blocks one capable of reaching and holding a temperature of 473 K, the second to act as a heat sink for the cold end of the sample will have internal water-cooling. At low measurement

temperatures the water cooling may be required to draw thermal energy out of the cold end, at higher temperatures the heat losses from the system are expected to be greater and the cold end may not require water cooling.

Once the desired temperature difference is achieved it is important that the temperature of the ends remains stable. This is best achieved by having a sufficient thermal mass that the temperature will not fluctuate due to small environmental changes, to this end the hot and cold stations were specified to be two 50 x 50 x 50 mm cubes of copper with a mass of approximately 220 g each. Each heat sink was therefore approximately ten times the mass of the largest possible sample size (8 mm dia x 50 mm length). To achieve good thermal contact for a range of sample diameters an inter-changeable sample holder with an appropriate sized slot was designed to be attached to the heat sink. The holders were machined from aluminium and screwed down firmly to the heat sinks. Each sample holder was equipped with a clamp, which provided insulation of the sample end, allowed for fixture of probes and ensured good thermal contact with the hot or cold station. An example of the block is shown below, figure 4.3

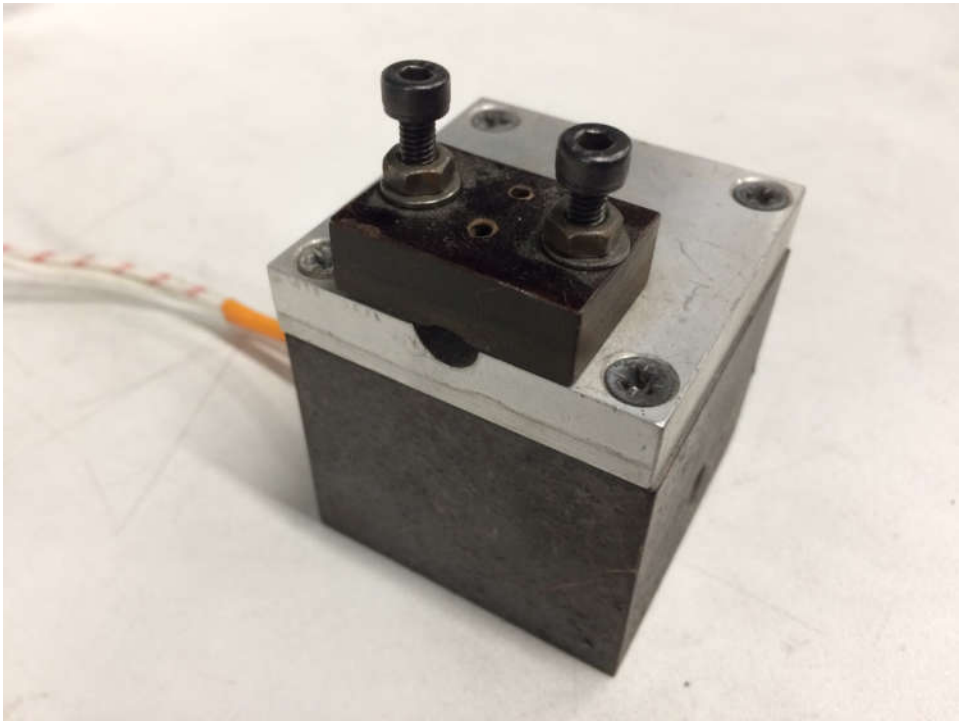

Figure 4.3 Sample holder block showing from bottom up; copper block, aluminium sample plate, tufnol hold down clamp. Heater cable extends from rear left

In order to specify the required power for the heating power the load was calculated including the losses due to convection and radiation:

The convective heat loss is given by equation 2.5, where A is surface area and T_∞ and T_S are the temperatures of the surroundings and the surface of the heat sink respectively:

$$Q_{Conv} = hA(T_S - T_\infty) \qquad \textit{Equation 2.5}$$

The determination of the heat transfer coefficient h requires dimensionless analysis using the relationships between the Grashof (Gr), Raleigh (Ra), Prandtl (Pr) and Nusselt (Nu) numbers in equations 2.6 – 2.8

$$Nu = \frac{h\delta}{k} = CRa^n \qquad \textit{Equation 2.6}$$

where k is the thermal conductivity of air, δ is the characteristic length (volume of object / surface area) and C and n are constants which can be found in tables; for this geometry 0.46 and 0.33 were used.

$$Ra = Gr \times \mathrm{Pr} \qquad \textit{Equation 2.7}$$

$$Gr = \frac{g\beta(T_S - T_\infty)\delta^3}{\nu^2} \qquad \textit{Equation 2.8}$$

where v is the viscosity of air. At 473 K the heat loss was calculated to be 2 W. The radiative heat loss may be calculated according to equation 2.9.

$$Q_{rad} = \varepsilon\sigma A(T_S^4 - T_\infty^4) \qquad \textit{Equation 2.9}$$

where ε is the emissivity of oxidized copper (0.78) and σ is the Stefan-Boltzmann constant. For the apparatus at 473 K the radiative heat losses were calculated to be 22W. In order to cope with the losses and still allow a reasonable ramp rate a 100 W heater was specified.

4.4 Equipment validation

Before measurements could be made on unknown samples the equipment had to be calibrated. Calibration is the process of comparing a measurement to a known value. This allows the accuracy of the measurement system to be quantified and if necessary corrected.

Rods, Ø 6 mm x 40-50 mm, were produced from high purity iron, aluminium and copper by argon arc melting. The Seebeck coefficients of these metals are known, see table 4.1.

Table 4.1 Seebeck coefficients of some pure metals [53]

Element	Absolute Seebeck co-efficient / μVK^{-1}
Iron	2.5
Aluminium	-1.5
Copper	1.5

Measuring the thermo-electric power of the pure metal rods allowed results from the instrument to be compared to a known standard. The measured values were used to calculate the accuracy of the equipment and correct the results as required.

During the initial validation of the method it was found that it was very important to ensure the rod was clamped down tightly with the voltmeter fly wire trapped between the rod and the clamp. Trials were carried out to measure the pure metal rods 20 times, the average measured results were very close to the expected values. But there was a degree of scatter in the data sets. Figures 4.3 - 4.6 show the measured Seebeck coefficients of the three metals and the expected values.

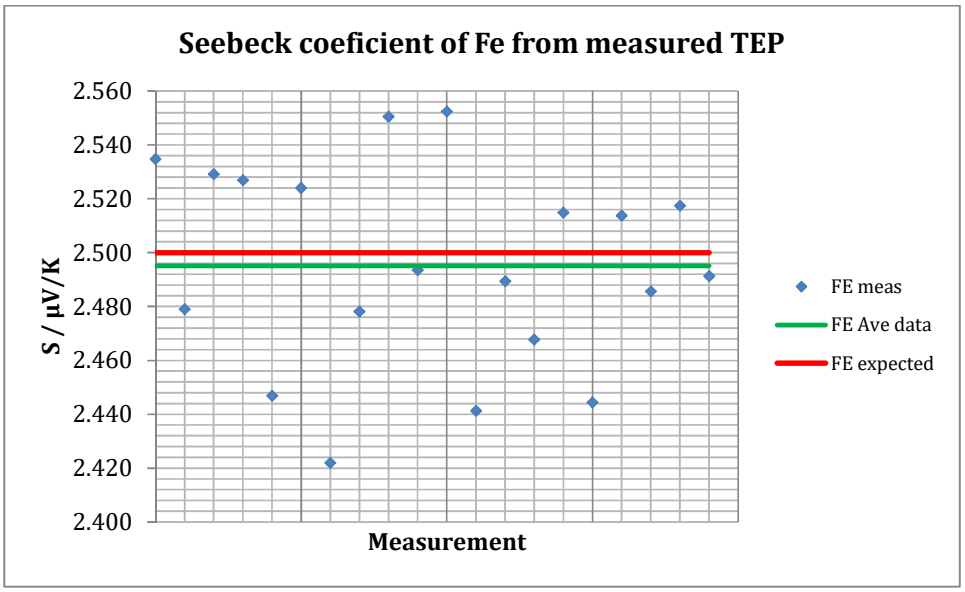

Figure 4.3 Seebeck coefficient of iron calculated from TEP measurements made using the equipment described above

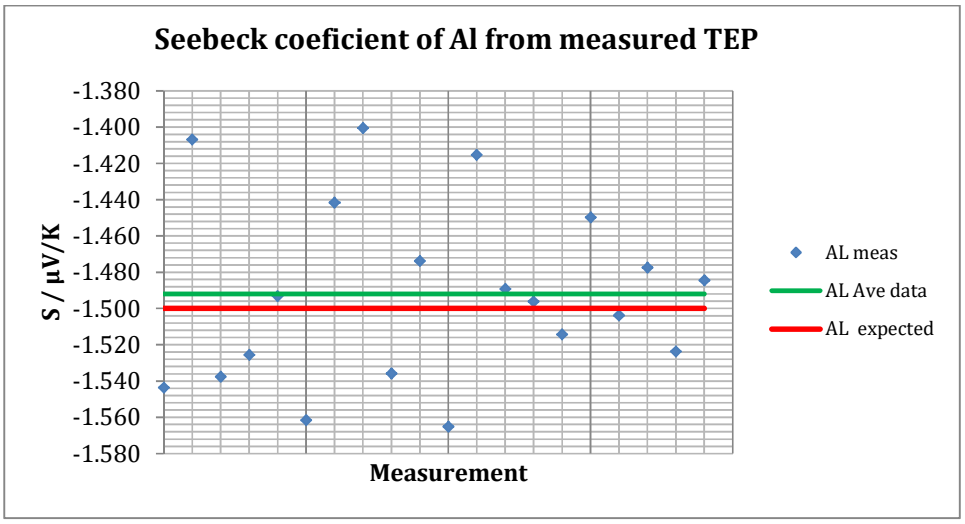

Figure 4.4 Seebeck coefficient of aluminium calculated from TEP measurements made using the equipment described above

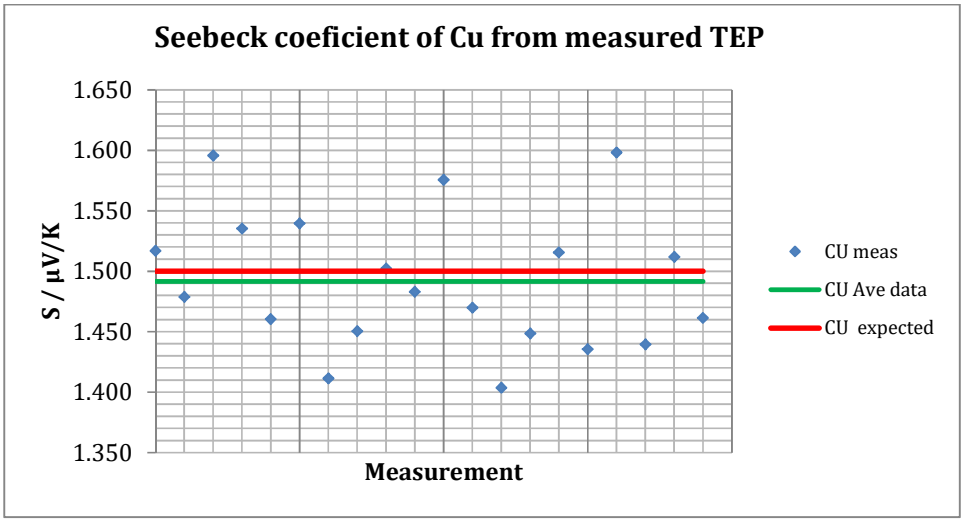

Figure 4.5 Seebeck coefficient of copper calculated from TEP measurements made using the equipment described above

The differences between average and actual value for iron, aluminium and copper were: 0.005 μVK^{-1}, -0.008 μVK^{-1} and 0.008 μVK^{-1} respectively. The standard deviations of the measurements were 0.037 μVK^{-1}, 0.048 μVK^{-1}, 0.055 μVK^{-1} for iron, aluminium and copper respectively. An attempt could have been made to use these data to create a correction factor for results

measured on unknown samples but as the differences between average and expected are small compared both to the measurements and the scatter it is not worthwhile.

Before an unknown sample was measured the original pure metal rods were measured to confirm that the equipment was performing properly. The acceptance criteria was that the value on the day should fall in the range of plus or minus two standard deviations from the expected value of the Seebeck coefficient for the rod material.

Table 4.2 Acceptable results ranges from check samples

Element	Minimum / μVK^{-1}	Maximum / μVK^{-1}
Iron	2.43	2.57
Aluminium	-1.59	-1.44
Copper	1.39	1.61

If pretesting checks failed, cleaning the sample and contacts and re-clamping usually corrected the issue.

4.4 Conclusions

In order to use TEP measurements as a validation tool for DFT modelling suitable equipment was designed and built. The requirements of each component were specified, based on design calculation, to give adequate performance for measuring TEP on metals in the range from room temperature to approx. 200 °C. The accuracy of the measurements was shown to be good when samples of known Seebeck coefficient were analysed, this has been taken as confirmation that the errors in measuring temperature and voltage directly are minimal and the equipment is suitable for analysis of unknown samples subject to satisfactory pre-analysis checks.

5. An Electronic Structure Approach to Properties Prediction in High Entropy Solid Solution Alloys

5.1 Introduction

In this Chapter the implications of Guo and Miracle's work discussed in the literature review are explored. Miracle [16] produced refractory HEAs, MoNbWTa and MoNbWTaV, and by using a simple rule of mixing formula predicted the lattice parameter and densities of the resulting bcc solid solution alloys. The accuracy of such a simple approach was impressive and improved as the high entropy solid solution basis of the alloys was increased [4, 16]. Guo [58] attempted to relate valence electron concentration (VEC) of HEA compositions to their crystal structure in the way Hume-Rothery did for copper alloys [37]. Guo found that HEAs with VEC less than 6.87 formed bcc solid solutions, those with VEC greater than 8 formed fcc solid solutions and alloys with intermediate VEC formed a mixture of bcc and fcc solid solutions. These two results are remarkable because they were achieved with models developed for ideal pure and dilute systems. This suggests that HEAs are indeed acting as *"good metals"* and that the bonding in HEA solid solutions is predominantly free-electron-metallic in nature. A further example of free electron nature of HEAs is illustrated in figure 5.1, the elastic modulus of the elements is known to vary with atomic number (table 5.1) and reaches a peak in each period in the centre of the transition block where the maximum number of bonding orbitals are filled and anti-bonding orbitals are yet to be populated. The observation

that HEAs also follow this trend is intriguing, and suggests that the bonding is in similar nature to that of a pure metal.

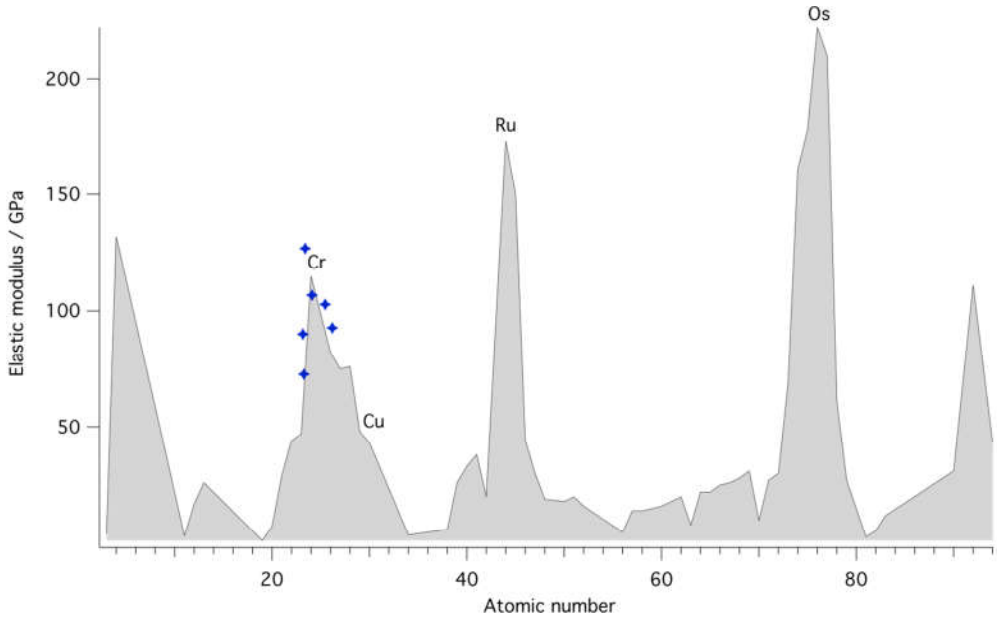

Figure 5.1 Illustrating the trend of elastic modulus with atomic number (electronic structure) of the elements and HEAs detailed in table 5.1.

Table 5.1: Elastic moduli of some HEAs

Composition	**Average atomic number**	**Elastic modulus /GPa**	**Reference**
$Ti_{0.5}CoCrFeNiAl$	23.3	72	Wang [8]
CoCrFeNiTiAl	23.33	90	Zhang [9]
AlCoCrFeNi	23.6	127	Zhang [9]
$CoCrFeNiTiAl_{0.5}$	24.28	106	Zhang [11]
$Ti_{0.5}CoCrFeNiAl_{0.25}Cu_{0.75}$	25.63	102	Zhang [11]
$Ti_{0.5}CoCrFeNiTiCu$	26.36	92	Wang [8]

Table 4.1 shows the elastic moduli and average atomic number of some HEAs reported in the literature, although these moduli are from quasi static data the trend as illustrated in figure 5.1 is still remarkable and the warrants further investigation.

It is a natural next step to investigate how far these simple models can take us in our understanding of HEAs and their properties; in this work we propose that high entropy solid solutions may be treated as pseudo-pure metals, each with a characteristic electronic structure on which as in a pure metal, many fundamental properties of the alloys are assumed to depend.

Relationships between electron density and Fermi energy and physical properties of metals were discussed in the literature review and are summarised in table 5.2. Such equations were derived for pure metals or dilute alloys and would not be expected to hold for concentrated and complicated systems such as HEAs, however the observations above hint otherwise [16,58].

Table 5.2: Relationships between electron density and Fermi energy and physical properties of metals

Property	Relationship	Reference
Thermo electric power / μVK^{-1}	$S = \frac{\pi^2 k_B T}{2(-e)T_F}$	Ziman [19]
Bulk Modulus /GPa	$\frac{1}{B} = \frac{15}{2n\varepsilon_F}$	Tanner [20]

In this work rather than using VEC or e/a which are simplified models; DFT modelling is used to calculate the Fermi energy, electron density, band structure and density of states of the reported high entropy alloys shown in table 5.3.

Table 5.3 HEAs investigated using pseudo pure metal approach and their calculated mixing properties

Alloy	Enthalpy of mixing / $kJmol^{-1}$	Entropy of mixing / $Jmol^{-1}K^{-1}$	Critical temperature / K	Alloy first reported
CoCrFeNiTi	-22	13.38	1644	[11]
CoCrFeNiAl	+17	19.14	888	[8]
CoCrFeNiCu	+8.9	13.38	935	[13]
CoCrFeNi	+4.3	11.5	374	[22]

This approach has allowed accurate predictions of bulk modulus and thermoelectric power of the alloys, these properties being intrinsic and largely insensitive to microstructure. The pseudo-pure metal treatment has also allowed us to explain the role of aluminium as a bcc stabiliser in HEA systems, an observation which until now has not been satisfactorily explained in the current literature having been attributed to the lattice strain of accommodating the large Al ion in a close packed crystal structure.

5.2 **Results and discussion**

5.2.1 Band structure and DoS

5.2.1.1 CoCrFeNiAl alloy

The simulation of bcc CoCrFeNiAl returned a value of 2.05 eV for the Fermi energy of the alloy and an electron density of 1.7×10^{28} m^{-3}, the DoS of the alloy are shown in figure 5.3.

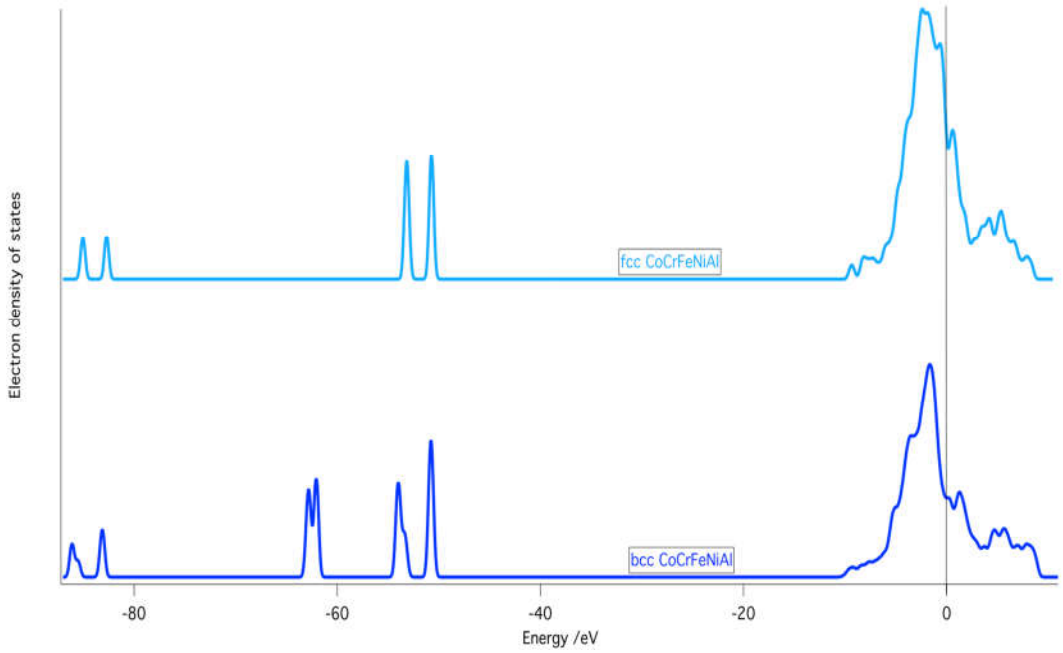

Figure 5.3 DoS plot of (top) fcc and (bottom) bcc CoCrFeNiAl

The fcc form of the alloy was predicted to have Fermi energy of 1.8 eV and electron density of 1.1×10^{28} m^{-3}. The band structure of this alloy is shown in figure 5.3 top.

The bcc band structure shows stronger s, p nature than that of the fcc lattice with an sp couplet at -65 eV not seen on the fcc DOS, this is due to the octahedral nearest neighbour geometry of the fcc lattice lending itself to hybridisation of the p orbitals. This results in a lowering of the fcc Fermi energy but more high energy states overall in this band structure.

5.2.1.2 CoCrFeNiTi alloy

CoCrFeNiTi was modelled as an fcc crystal, as it appears in nature, the Fermi energy and electron density of the alloy are; 11.36 eV and 17.39×10^{28} m^{-3}. The DoS are shown in figure 5.4; comparison with figure 1 shows that the addition of Ti increases the number of electrons accommodated in the conduction band compared to Al. Numerous attempts were made to simulate the bcc CoCrFeNiTi alloy but the computation would not minimise for any cell size, cut of energy or pseudo-potential combination tried by the author. It was assumed that the structure is fundamentally incapable of distributing the available electrons in a repeatable consistent function.

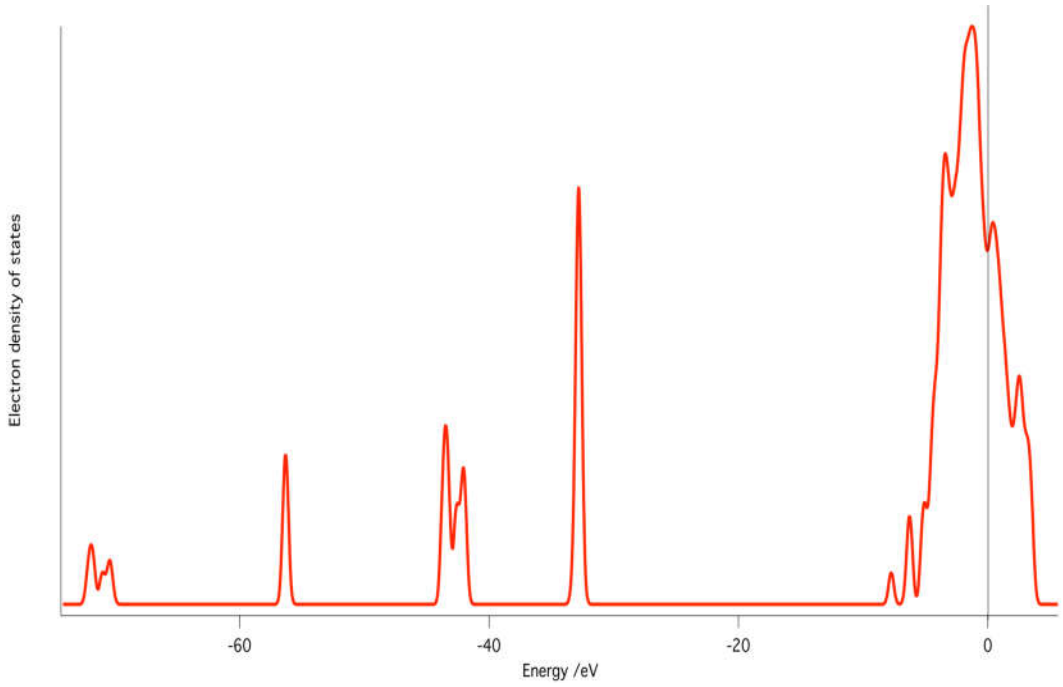

Figure 5.4 DoS plot for CoCrFeNiTi

5.2.1.3 CoCrFeNi Pseudo-base metal

The pseudo base metal common to both the above high entropy alloys was modelled to calculate the electronic structure, in which the Ti and Al additions would be embedded. The electron DoS of the bcc and fcc CoCrFeNi alloys are shown in figure 5.5 The Fermi energies and electron densities of the two lattices were calculated to be: 3.49 eV, 2.96×10^{28} m^{-3} and 2.77 eV, 2.09×10^{28} m^{-3} for the bcc and fcc symmetries respectively.

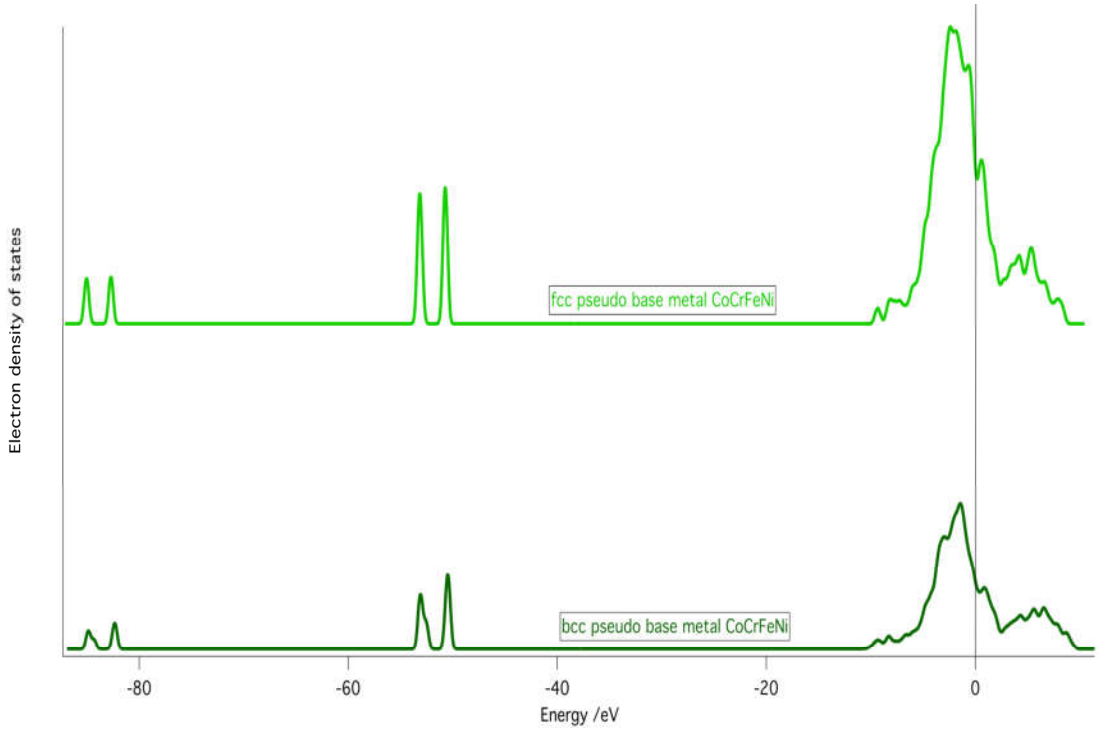

Figure 5.5 DoS diagram of; top fcc and bottom bcc CoCrFeNi pseudo base metal

5.2.2 Structural Stability

It is commonly observed that Al additions to HEAs promote the formation of bcc crystal phases [22, 23]. It has been suggested that this effect is due to the size mismatch between Al (r_a=143 pm) and the late transition metals ($r_a \approx$125 pm) commonly used in HEA compositions, the large atomic radius of Al forcing the HEA to adopt a less closely packed structure in order to reduce lattice strains. The problem with this explanation is that it cannot explain the observation that Ti (r_a=145 pm) substitution into CoCrFeNi and other HEA compositions does not promote the formation of a bcc lattice. The lattice strain associated with accommodating a hard Al or Ti atom in an fcc CoCrFeNi lattice is approximately 3.6 % and 4.0% respectively the accompanying increase in internal energy is about 1- 1.5 $eVmol^{-1}$ for both cases. The difference in lattice strain caused by Al is less than that of Ti so lattice strain cannot account for the behaviour of Al and in any case the energy costs of accommodating the strain are negligible. The work of Guo [58] hints that HEAs should follow the "electron phases" behaviour Hume-Rothery described. A more fundamental approach to the origin of phase stability in alloys was proposed by Paxton, Methfessel and Pettifor [62], they suggested that the accommodation of electrons in the respective band structure of the different alloy crystal structures was the key to understanding their relative stabilities. By comparing the band structure energies of the competing symmetries it is possible to elucidate the crystal structure with the lowest energy and therefore greatest stability. The band structure energy is related to the Fermi energy of the alloy and DoS according to equations 3 and 4 respectively.

$$\frac{dE_{bs}}{dn} = \varepsilon_F \qquad \textit{Equation 3}$$

$$\frac{d^2E_{bs}}{dn^2} = \frac{1}{g(\varepsilon_F)} \qquad \textit{Equation 4}$$

It should be noted that this analysis is based on behaviour modelled a temperature of absolute zero and as mentioned above there is evidence to suggest high entropy solid solutions are high temperature phases; for the purposes of this study it is assumed that in the case of high entropy solid solutions the electronic structure contribution to the crystal stability would dominate rather than vibrational entropy.

The DoS and band fillings can therefore be used to find the relative stability of the crystal structures [62].

Following Paxton's approach DOS curves were integrated numerically and plotted together in figure 5.6 for comparison.

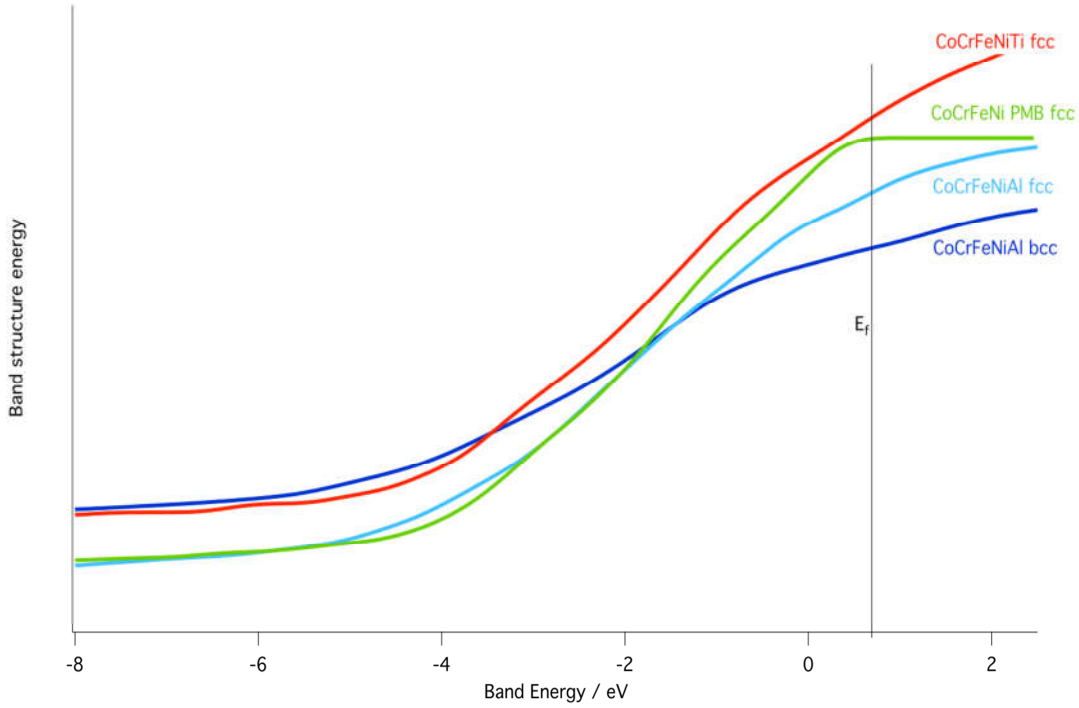

Figure 5.6 Band structure energies of the CoCrFeNi- pseudo metal based (PMB) high entropy alloys about the Fermi energy

The bandstructure energies of each crystal structure are shown together. Using this diagram we can observe the effects of alloying additions on the band structure energy of the fcc structure. Al alloying additions decrease the band structure energy compared to the pseudo base metal.This is likely due to the ability of Al to accommodate electrons in p-orbitals, which are unavailable in the late transition metals, thus at higher electron numbers fewer high energy bands are filled and the overall structure is lower in energy. The lowest energy band structure however belongs to the bcc lattice of CoCrFeNiAl. The bcc symmetry allows more electron density to be kept within the core bands because the nearest neighbour geometry does not favour p orbital

hybridisation, thus lowering the energy of the band structure whilst resulting in a slightly higher Fermi energy than for the fcc analogue. Figure 5.7 shows the electron density iso-surfaces (2.5) for both the fcc and bcc lattices of CoCrFeNiAl, the greater directionality of the fcc iso-surface can be observed.

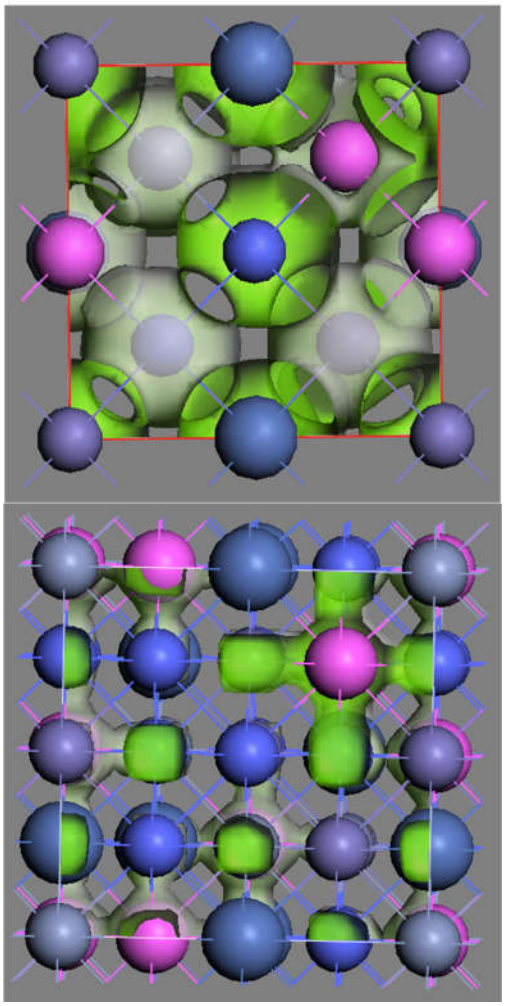

Figure 5.7 Illustration of electron density iso-surfaces of top; bcc and bottom; fcc CoCrFeNiAl lattices.

5.2.3 Properties

The predictive power of this modelling approach to the problem of HEAs was tested by comparison of measured values of thermoelectric power, bulk modulus, and specific heat capacity and those calculated using only data generated by electronic structure calculations performed in CASTEP. The alloys in this section were chosen as they can be described as CoCrFeNi pseudo base metal-derived, *ie* a 20 at% alloying addition of Al, Cu or Ti to the four element high entropy solid solution.

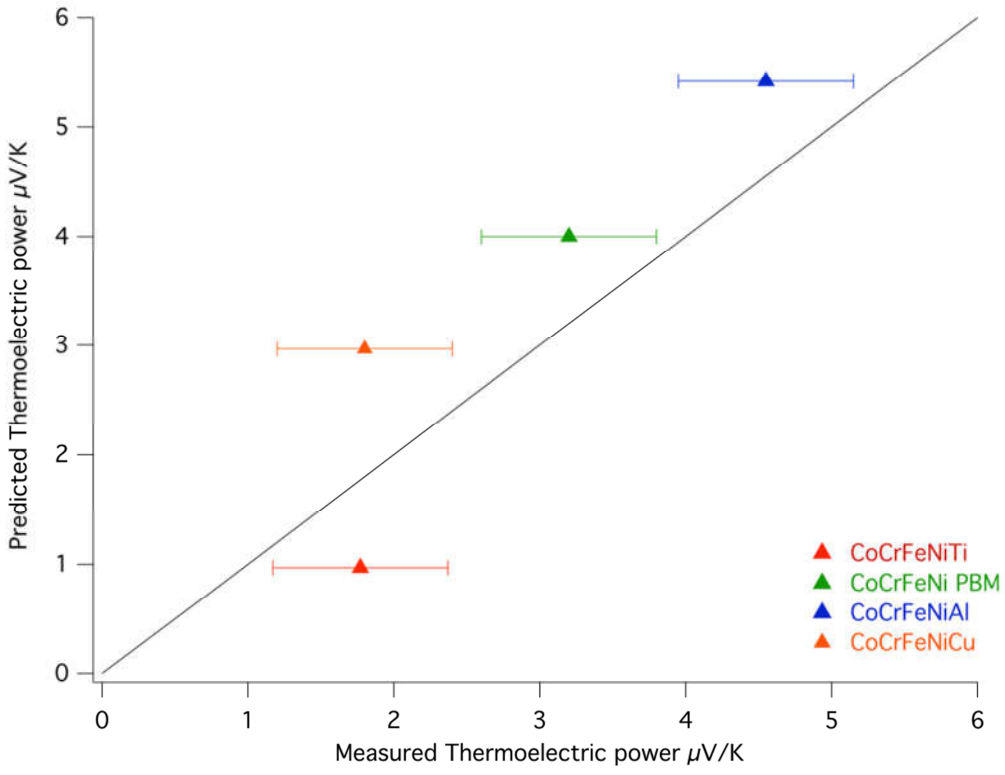

Figure 5.8 Calculated and measured thermoelectric power of HEAs in this study

Measurement of thermoelectric power, unlike resistivity, is insensitive to microstructural features of an alloy such as grain boundaries and provides a way to directly sample the Fermi energy of the alloy as shown by the expression in table 5.2. The measured and calculated values of TEP are compared in figure 5.8, the pseudo base metal CoCrFeNi shows the best correlation of theoretical and experimental values, which is expected at it has the lowest critical temperature T_c (321 K) [32] of the alloys and therefore the most high entropy alloy character and most likely to conform to the pseudo pure metal analysis. Substitution of Al into the PBM increases the thermoelectric power of the alloy because Al has the effect of lowering the Fermi energy of the alloy, and despite its higher T_c (888 K) the calculated and measured values are in good agreement. Alloying additions of early transition metal Ti to CoCrFeNi reduce the thermoelectric power of the alloy by increasing the Fermi energy and the DOS at that energy, the calculated values of CoCrFeNiTi are unique in that they underestimate the thermoelectric power of the alloy, this may be due to the rather high T_c (1600 K) of this alloy indicating only marginal HEA nature and thus more covalent nature of its bonding and so a lower Seebeck effect would be expected.

Table 5.5 Calculated and measured (ultrasonic) values of bulk modulus for high entropy alloys in this study

Bulk Modulus /GPa	CoCrFeNi	CoCrFeNiTi	CoCrFeNiAl	CoCrFeNiCu
Calculated	85	41	230	118
Measured	100	56	256	144

Bulk modulus was calculated using the Birch–Murnaghan equation, the calculated and measured values are shown in table 5.5. Figure 5.9 shows the accuracy of the electronic based approach compared to a simple rule of mixtures calculation. The DFT based values follow the observed values very closely whilst slightly underestimating the bulk modulus of each alloy; the correlation is all the more remarkable because DFT modelling methods are known to underestimate bulk modulus by approximately 10-15 % [63]. The rule of mixtures approach gives very poor predictions because it assumes that each metal in the alloy maintains its own electronic structure and that the properties of the alloy are merely the average of its component parts. This may be appropriate for dilute alloys where an impurity donates a number of electrons to the system but has little effect on the overall lattice potential. This is clearly very different to the case of an HEA where free electrons interact with a very different lattice potential to that of the component metals, and it is

thus essential to calculate the new electronic structure if reliable properties predictions are to be made.

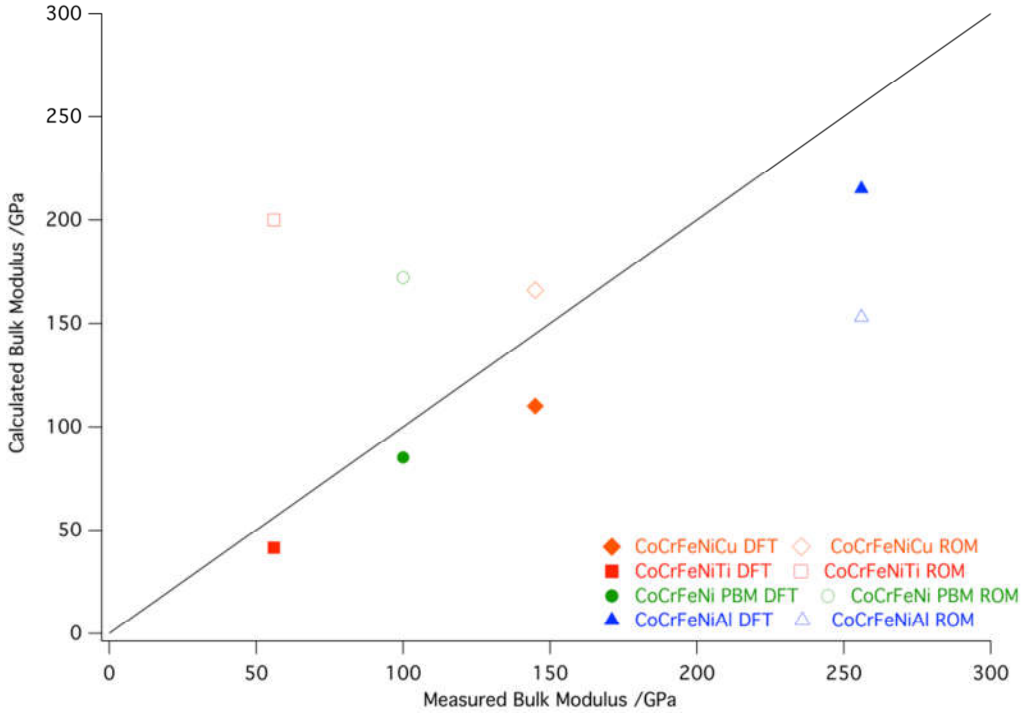

Figure 5.9 Comparison of calculated and measured values of bulk modulus. The use of DFT offers greater accuracy than the standard rule of mixtures approach

This is further demonstrated in figure 5.10 which shows the trend of bulk modulus of the elements and proton number with the three HEAs of this study superimposed. CoCrFeNiAl with an average atomic number of 23.6 shows that a peak in bulk modulus exists for a “pseudo pure metal” between vanadium and chromium. A well in bulk modulus also exists when proton number equals

25.4. These features could not be calculated except by chance using rules of mixing or valence electron configuration.

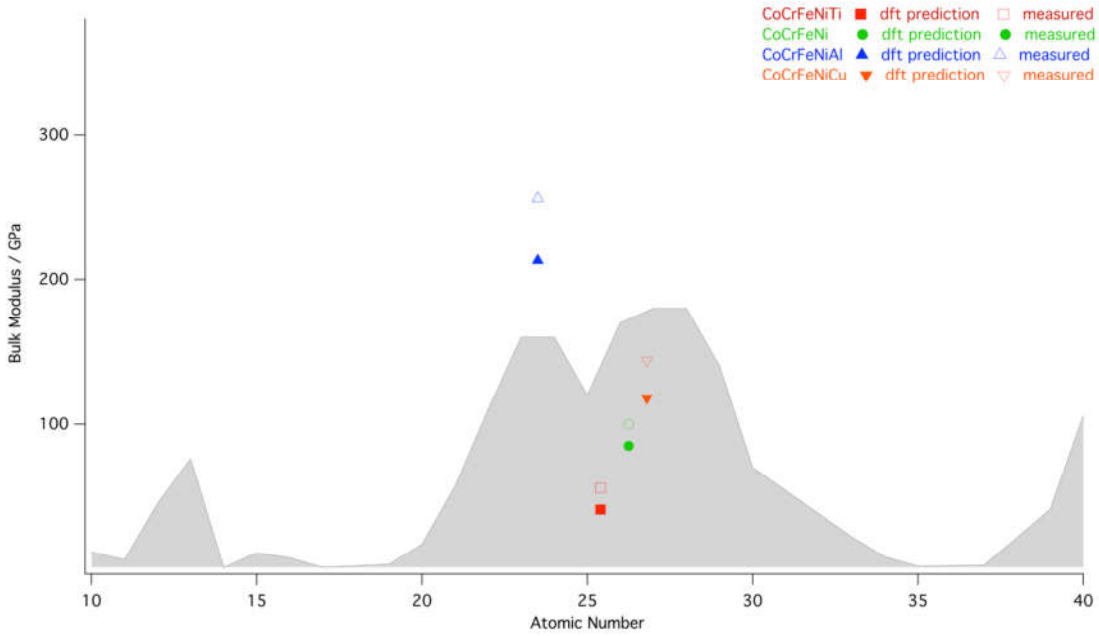

Figure 5.10 Bulk moduli of the HEAs in this study follow the same trend as those of pure elements filling the empty spaces between integer values of atomic number.

5.3 Conclusions

Here is presented a new approach to the problem of HEA properties prediction; based on the observation that HEAs' elastic moduli vary in the same way as a pure metals' with regard to proton number and the success of approaches such as Guo's [58] and Miracle's [16], we assumed that a true HEA with a random solid solution could be treated as a pseudo-pure metal with a characteristic electronic structure, from which many of the physical properties of the alloy can be predicted. This approach has allowed us to predict the stable crystal structure of HEAs and physical properties; thermo electric power and bulk modulus with a high degree of accuracy. The method of treating HEAs is easily adaptable to other systems and different properties of interest such as GUM or SIM alloy systems and by adjusting the potentials used, to be more suitable for highly alloyed systems and incorporating molecular dynamics simulations to account for high temperature behaviour; even greater accuracy may be achieved. The work also hints at the potential of HEAs to deliver tailored and or novel properties, through the nudging of electronic structure by doping with special alloying additions as seen in the recently reported magneto-caloric alloy CoCrFeNiPd [64]. As Kubaschewski predicted in 1984 [65] entropy has allowed us to produce alloys with simple microstructures, but what he may not have realised is that this effect would allow us to tune the properties of alloys by allowing access to new electronic structures. It could therefore be that the unusual mechanical, magnetic [66] and electrical properties of HEAs are only the beginning of a new era of alloy development.

6. Glass Formation in a High Entropy Alloy System by Design

6.1 Introduction

Along with HEAs another novel form of alloys are the amorphous or glassy alloys which have been extensively studied, resulting in a good understanding of the essential considerations for obtaining glass formation. Models to predict glass forming compositions are based on the need for a high density of atomic packing. Inoue proposed three parameters that promote glass formation by encouraging dense random packing; a large negative enthalpy of mixing between atom pairs, three or more components and large differences in atomic radii between the constituent species [39]. BMG compositions also tend to occur close to eutectic compositions, where the melting point is suppressed and so the temperature difference between it and the point at which the glassy structure is frozen in (termed the glass transition temperature, T_g) is at a minimum. Mutual frustration of several possible competing eutectic phases also aids in shifting the nose of the crystalline phase field on a time-temperature-transformation (TTT) diagram to the right, reducing the critical cooling rate for glass formation [68].

As of 2011, no high entropy solid solution alloy system, consisting of 5 or more elements and forming a simple fcc or bcc solid solution [4] with the ability to form an amorphous phase on rapid cooling has been reported. Identification of an alloy system which forms both an HEA solid solution and

a glassy phase would allow novel processing routes for high entropy alloys and raise the possibility of HEA reinforced amorphous alloy composites but would also force a re-evaluation of the explanation of HEA formation. The compositions $(TiZrNbCu)_{1-x}Ni_x$; x= 0.125, 0.15, 0.20, 0.25 fulfil the main requirements of a glass former:

- At least three components
- Components should have a range of sizes with a 12 % mismatch in atomic radius
- The alloying elements should have a negative heat of mixing between pair

The high S^{conf} of the HEA solid solutions must be large enough to overcome the enthalpy of mixing of the metals composing the alloy. Many of the reported HEA compositions have positive heats of mixing when calculated using the Miedema model [10] and the regular melt model [71]. The compositions CoCrCuFeNiAl (fcc) [22] and WNbMoTaV (bcc) [16] have heats of mixing 18.7 $kJmol^{-1}$ and 13.9 $kJmol^{-1}$ respectively and would normally be expected to segregate, though at high temperature the configurational entropy of each solid solution of 22.5 $JK^{-1}mol^{-1}$ and 19.1 $JK^{-1}mol^{-1}$ respectively would make a random solid solution the more stable state. It may be that compositions with positive heats of mixing and therefore prone to segregation form HEAs more readily than those with negative mixing enthalpy; as the increase in entropy from a segregated alloy ($S^{conf} \rightarrow 0$ $JK^{-1}mol^{-1}$) to a random solid solution is greater than that for a theoretical poly-substituted intermetallic to a random solid solution [72].

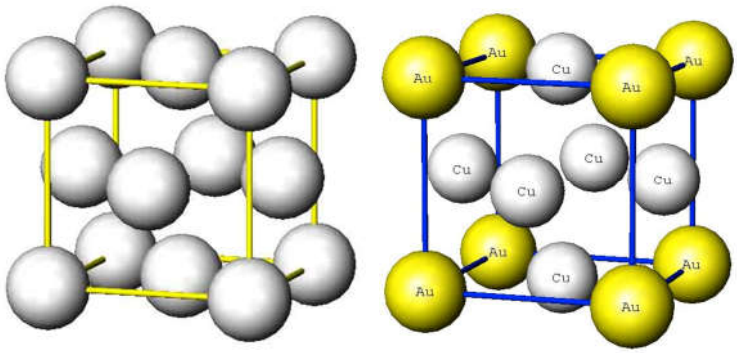

Figure 6.1 A1 fcc crystal structure with 4 unique lattice points and the $L1_2$ Cu_3Au type lattice with 1 + 3 non-equivalent points [26]

For example consider the alloy CoCrNiFeTi [29] reported to exhibit a random fcc / A1 solid solution (Ω = 5) with a configurational entropy of 13 $JK^{-1}mol^{-1}$ the alloy could potentially adopt an ordered $L1_2$ structure; $(Ni,Fe,Co)_3(Cr,Ti)$ (Ω = 3) which would have a similar configurational entropy of 9 $JK^{-1}mol^{-1}$.

If the formation of random solid solution phases in HEAs depends wholly upon sufficiently high entropy of mixing then a zero or positive value of enthalpy of mixing must be a requirement of the alloy system, and one that is incompatible with glass formation.

6.2 Experimental Procedures

Four alloys in the $(TiZrCuNb)_{1-x}Ni_x$ system with x = 0.125, 0.15, 0.20, 0.25, named: A-HEA1, A-HEA2, A-HEA3 and A-HEA4 respectively and the reported HEA compositions CoCrNiFeTi [29] and CoCrNiFeAl [30] were prepared as described in Chapter 2. Ribbons with a thickness of approximately

20 microns of each alloy were generated by melt spinning. The suction cast rods were investigated by: 1) X-ray diffraction (XRD) 2) scanning electron microscopy. The melt-spun ribbons were also analysed by XRD and by differential scanning calorimetry (DSC)

The proposed alloys; $(TiZrNbCu)_{1-x}Ni_x$; x= 0.125, 0.15, 0.20, 0.25) have negative ΔH^{mix} in the range -35 to -55 $kJmol^{-1}$ [2,14], the size mismatch of the alloys varies from 12.0 % to 12.5 % and the kinetic glass index, *m*, was calculated using the method of Park et al [17] to be the intermediate value of 42 (based on theoretical elastic moduli) see Table 6.1. The compositions also all fulfil the requirements of an HEA former, except for the inferred requirement for a positive enthalpy of mixing. In this work the extent to which this alloy system may form an HEA solid solution or amorphous phase depending on chemistry and cooling rate will be investigated and the extent to which the sign of the enthalpy of formation is important will be discerned.

Table 6.1 Theoretical elastic moduli (calculated from the method in [30]) and kinetic fragility index, m (m=12(B/G+0.67)) [72]

Alloy	Δr (%)	ΔH^{mix} (kJmol^{-1})	G (GPa)	B (GPa)	m
A-HEA1	12.0	-35	43.4	124.5	42
A-HEA2	12.15	-40	43.9	125.6	42
A-HEA3	12.36	-49	45.0	127.8	42
A-HEA4	12.5	-55	46.2	130.0	42

6.3 Results and Discussion

The A-HEA alloys solidified to form the dendritic microstructure seen in figure 6.3 and EDS analysis found that the dendrites consisted mainly of Nb. XRD traces, figure 6.2, suggest that A-HEA1 solidified to form two phases, the first corresponding to closely to niobium and the second a bcc HEA phase with a = 2.51 nm.

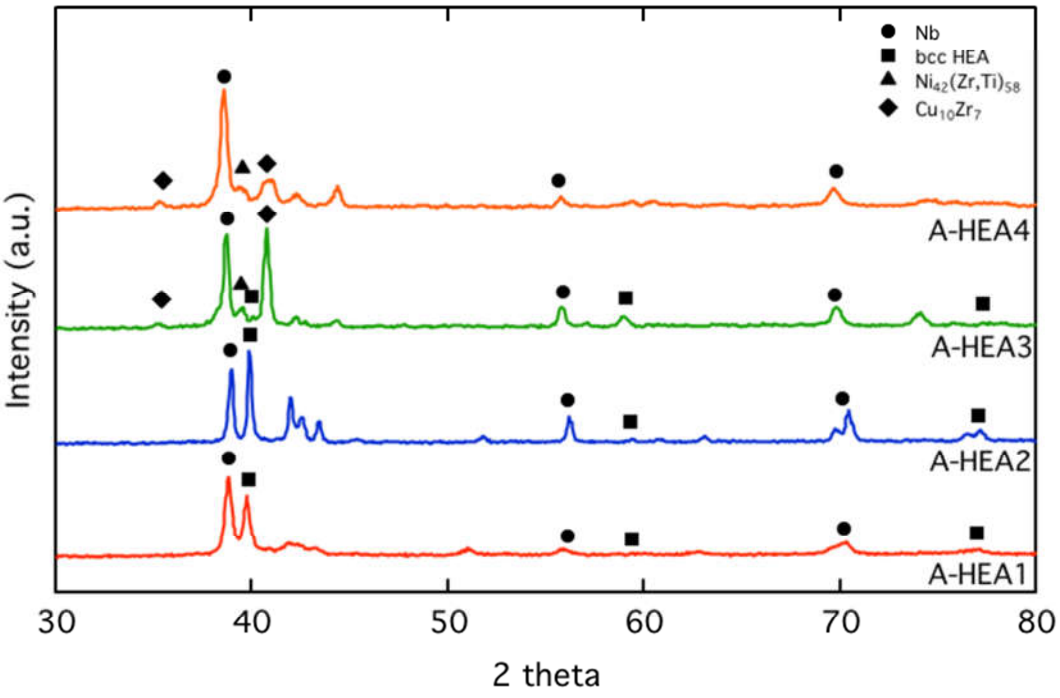

Figure 6.2. XRD traces show of as cast A-HEAs. AHEA-1 forms a dual phase microstructure consisting Nb and another bcc HEA phase, other alloys show multiple phases

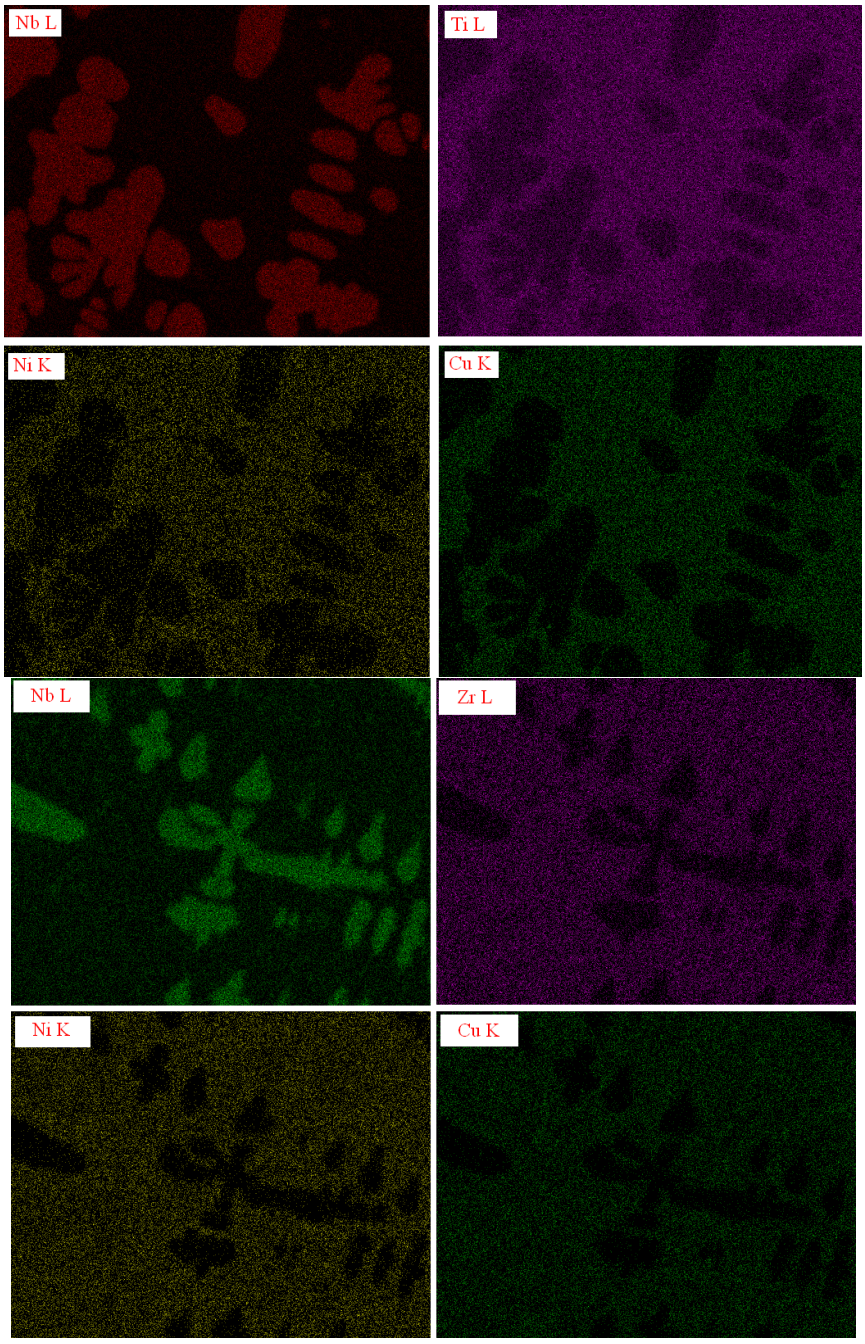

Figure 6.3. left, EDS maps of A-HEA3 Nb partitions mainly to dendrites the remaining elements partition mainly to the matrix phase

The compositions A-HEA3 and A-HEA4 also precipitated niobium dendrites but the HEA peak is suppressed in the XRD trace of A-HEA3 and absent in A-HEA4, being replaced by peaks which may be due to $Ni_{42}(Ti,Zr)_{58}$ and $Cu_{10}Zr_7$ signals. Although these intermetallics have been identified by indexing only one or two peaks they allow a possible mechanism to be proposed; increased intermetallic precipitation corresponds to increased Ni content, which causes the enthalpy of mixing of the alloys to become more negative. High concentrations of Ni could therefore push the equilibrium between the solid solution and the decomposition products towards formation of Ni-X intermetallic phases. Heats of mixing calculated using the Miedema model [10] imply that at these compositions Ni would react most favourably with Ti and Zr to form intermetallic phases of the type $Ni_{42}(Ti,Zr)_{58}$, ΔH^{mix} -64kJmol^{-1}. Should this occur, the alloy would then be depleted in Ti and Ni. The remaining composition may then have insufficient configurational entropy to form an HEA random solid solution phase, resulting in favourability for Zr and Cu to form the intermetallic $Cu_{10}Zr_7$. This mechanism appears to fit the observed XRD peaks. The proposed mechanism, gives an explanation of why at some value of x between 0.15 and 0.2 the enthalpy of formation of the intermetallic phase is such that the entropy of a random solid solution is insufficient to suppress ordering. Yeh [4] states the ability of an HEA to form a simple solid solution results from the high configurational entropy of the system. The configurational entropy of the 5 component bcc solid solutions was calculated as described above, with enthalpy of mixing of the alloys used to estimate a critical temperature for the suppression of intermetallics, T_c; (*ie*

when the difference in free energy of the solid solution and the intermetallic phase $\Delta G^{IM\text{-}SS} = 0$) Equation 6.1.

$$T_c = \frac{\left|\Delta H^{mix}\right|}{\Delta S^{conf}} \qquad \textit{Equation 6.1}$$

The T_c of each alloy is shown with H^{mix} in Table 6.2. The melting point of each alloy was outside the range of DTA measurements and therefore known to be greater than 1723 K; the rule of mixtures (RoM) melting point is shown in Table 6.2 for comparison. It is noteworthy that the T_c of A-HEA1, which shows least sign of ordering in the XRD trace, is significantly lower than the RoM melting temperature of the alloy, whilst those for A-HEA3 and A-HEA4, which both show a clear tendency toward ordering have values of T_c greater than the predicted melting temperature and would therefore be expected to solidify directly to the ordered structure. This is indeed what was observed. For A-HEA2 the melting and critical temperatures are very similar and the XRD data shows both the HEA & Nb peaks seen in A-HEA1 plus the unattributed possibly ordered peaks observed in A-HEA4.

Table 6.2 Transition temperatures of the alloys

Alloy	T_g (K) ± 5 K	T_x (K) ± 5 K	ΔT_x (K)	$RoM\ T_m$ (K)	T_c (K)
A-HEA1	648	721	73	2000	1781
A-HEA2	651	717	66	1992	2130
A-HEA3	662	731	69	1977	2582
A-HEA4	678	743	65	1961	2880

The method of calculation of the enthalpy of mixing and melting points of the alloys neglects vibrational entropy, resulting in ambiguity in the prediction for this alloy, being as it is on the cusp of HEA formability. These alloys are unable to form a high entropy phase when the critical temperature for HEA formability is higher than the solidus temperature of the alloy; this supports Yeh's explanation of the HEA phenomenon [4]. In a similar calculation Zhang [74] discussed a HEA formability parameter, $\Omega = 1000\Delta S^{mix}/\Delta H^{mix}$ where if $\Omega < 1$ a HEA will be formed; 1000 K is approximately $0.6T_m$ for the alloys reported in [20] below which diffusion would be sluggish and the HEA phase would be meta-stable, thus Zhang's model predicts whether an alloy can remain in the HEA solid solution phase on cooling. For the alloys reported here the melting temperature is not known and so a suitable value of $0.6T_m$ to substitute into Zhang's equation is not available. Equation 6.1 may also be deployed to explain observations in other HEA systems; the alloy

CrMnFeCoNi has been observed to precipitate a Cr rich sigma phase when held at 1000 K [27,28] and this has been used to suggest that the alloy is not an HEA. However application of Equation 6.1 shows that for this alloy (S^{conf}= 13.9 JK^{-1}) the critical temperature for precipitating a CrMn sigma phase (H^{mix}= -10.7 $kJmol^{-1}$) from the fcc HEA (H^{mix}= +1.8 $kJmol^{-1}$) the critical temperature would be about 900 K. Within the limitations of the model this is a very close estimate of the temperature at which the HEA would break down. And as the alloy is shown to be entropy stabilised above 900-1000 K then it should still be described as an HEA.

The CoCrFeNiTi and CoCrFeNiAl melt spun ribbons did not form an amorphous phase during solidification, and instead precipitated crystals. However, XRD traces of the melt-spun A-HEA alloys reported here (Figure 6.3) show amorphous traces, with a characteristic broad peak between approximately 60° and 80° 2θ.

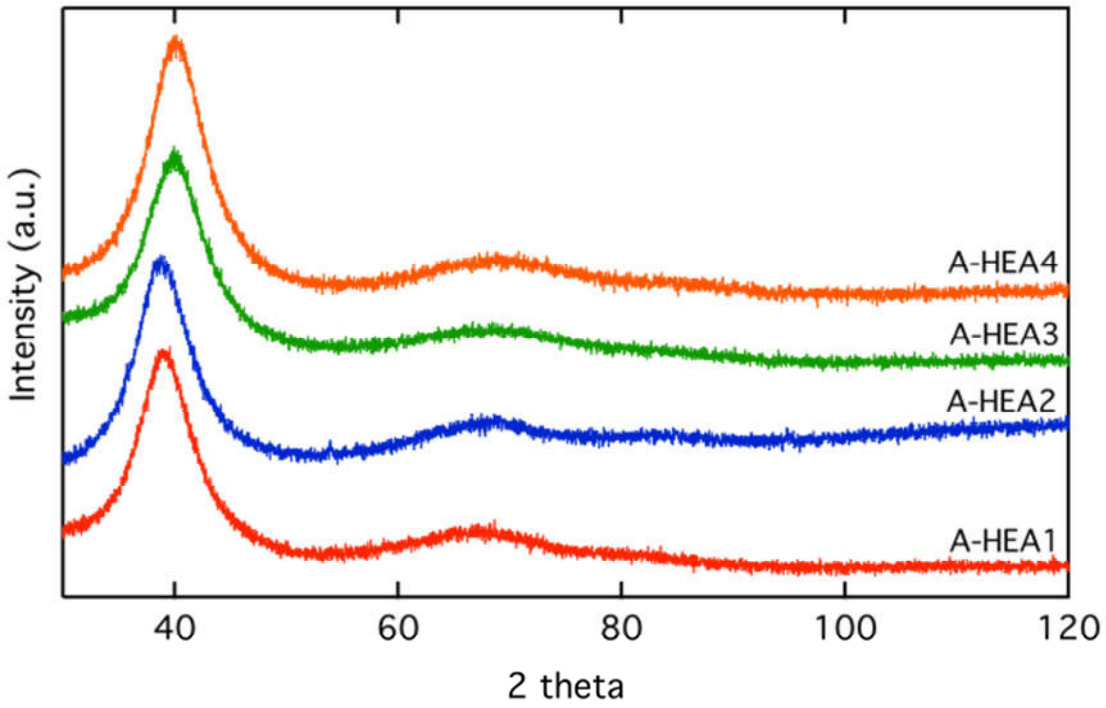

Figure 6.3. XRD traces of the A-HEA alloys after melt spinning showing amorphous halo

The DSC data show the glass transition and crystallisation start temperatures of the alloys, T_g and T_x respectively, also confirming glass formation. These were taken as the onset values and are shown in Table 6.2. In general both T_g and T_x increase with increasing Ni content. This is due to the effect of increasing Ni content on the glass formation parameters of Inoue [39] as a result of the increasing atomic misfit from 12.0 % to 12.5 % further lowering of the enthalpy of mixing of the alloys and in A-HEA3 and A-HEA4 competition between intermetallic formation. DSC traces show two crystallisation peaks for A-HEA1, A-HEA 2 and A-HEA3 and three peaks for

A-HEA4. The increasing area of the first crystallisation peak with Ni content indicates an increase in volume fraction of the intermetallic phase.

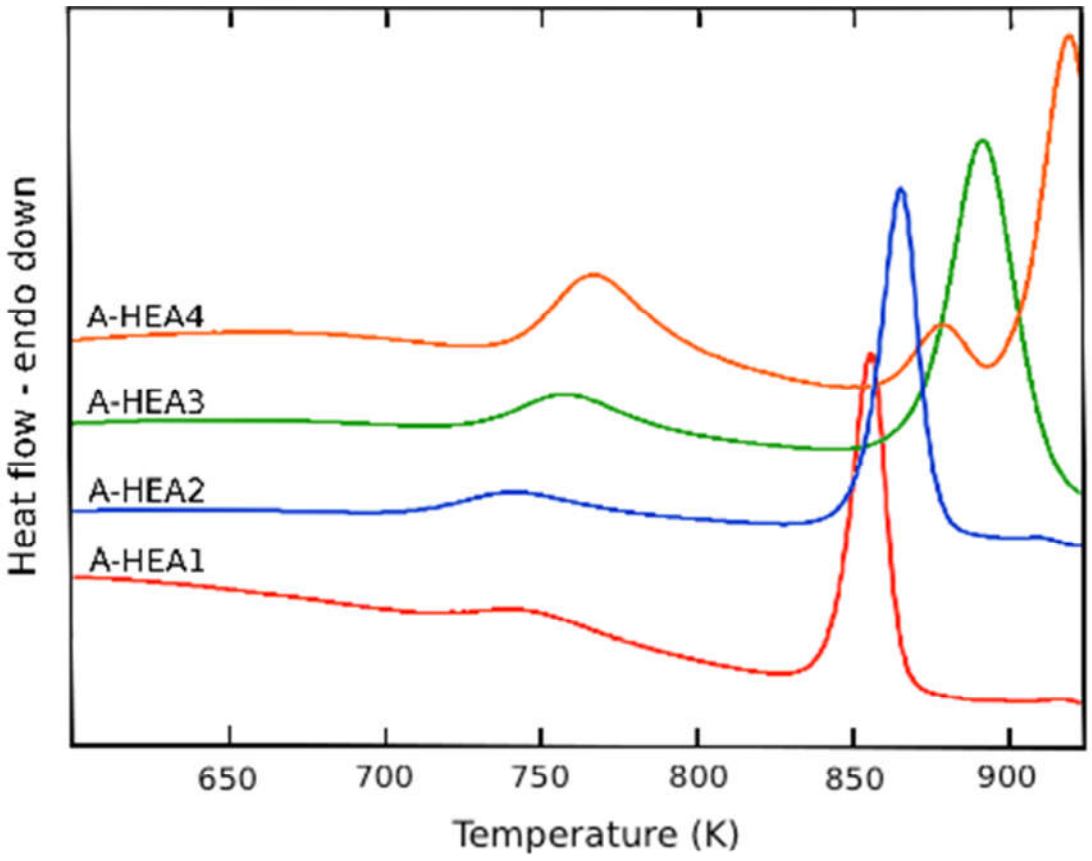

Figure 6.4. DSC traces of A-HEA alloys, showing T_g and T_xs

The devitrificaton products in A-HEA1 and A-HEA2 are the bcc-HEA phase and Nb solid solution and these crystallisation events correspond to peaks 1 (occurring between 725 K and 800 K) and 2 (825 K – 900 K) respectively in the DSC traces of these alloys in Figure 6.4. As Ni content is increased in A-HEA3 and A-HEA4 there is an additional increase in peak 1 area,

corresponding to an increase in the volume fraction of the Ni-rich intermetallic phase. The remaining material then crystallises to form a mixture of Nb solid solution and the $Cu_{10}Zr_7$ phase, causing a broadening and eventual splitting of the second peak to give 3 distinct peaks starting at 750 K, 860 K and 900 K respectively. That devitrification of these alloys results in the formation of Nb, $Ni_{42}Ti_{58}$ and $Cu_{10}Zr_7$ indicates there is a cooling rate effect in the formation of the HEA phase; on slow cooling from the melt the HEA phase is observed because the nose of the HEA phase field on a TTT type diagram occludes any intermetallic phases, but when crystallisation occurs from the metastable amorphous phase, the alloy decomposes to form binary intermetallics. This suggests the HEA phase does not replace intermetallics as the most stable phase but that it is the most readily formed when cooling from the randomly distributed melt phase.

The vast majority of reported HEA compositions contain Fe, Ni and Co which are all able to substitute onto the face centred positions of the L_{12} γ' phase when the two other common HEA components, Ti and Al, are present [70]. Increasing the ratio of Al to all other elemental constituents (Fe, Co, Ni and Ti) to greater than a 3:2 ratio disrupts this arrangement, leading to decomposition of the solid solution and the formation of binary intermetallics [75]. Similar reasoning would also account for the disruption of HEA formability with increasing Ni in this series of alloys, as Ni promotes the Ni-Ti/Zr intermetallics and the whole system then decomposes to binary and ternary intermetallics. This strongly suggests that the ability of some alloys to form apparent high entropy phases results from their constituent metals' abilities to substitute for one another in ordered cubic structures. This would allow the formation of

glassy and high entropy phases in a single system. The observation that there is a kinetic contribution to the formation of HEAs suggests that they are not the most thermodynamically stable phase of the system. Indeed, the FeCoCrNiAlCu [20] alloy is known to precipitate intermetallic phases after heat treatment. If the entropy of mixing were solely responsible for the formation of a random solid solution then the microstructure would be more stable at elevated temperatures and elements would be expected to remain in solid solution.

Work by Pan [77] showed a link between vacancy formation energy of an alloy, where they devised the figure of merit $\Delta H_h \Delta H^{mix} S^{conf}$ and discovered that there was a strong trend between the magnitude of this value and the critical diameter (or critical cooling rate to form a glassy phase) of an amorphous alloy. It was suggested that this link is due to the relationship between vacancy formation energy and crystallisation temperature, where the formation of vacancies permits self-diffusion, promoting crystallisation. The ability to form vacancies also improves the structural stability of ordered compounds with respect to chemistry. Vacancy formation energies of the alloys in this study were calculated in Table 6.3 using the method in [77], along with those of reported CoCrFeNiTi and CoCrFeNiAl HEAs, intermetallic alloys and glass forming alloys. The low vacancy formation energy of the intermetallic alloys allows the structure to be maintained despite variations in stoichiometry.

Table 6.3 Vacancy formation energies of various alloy types

Alloy	Vitralloy 1	A-HEA1	A-HEA2	A-HEA3	A-HEA4	CoCrFeNiTi	CoCrFeNiAl	NiTi
ΔH_h / kJmol^{-1}	283	281	280	274	266	225	212	133

It is interesting that the HEAs thus far reported have lower vacancy formation energies than glass forming alloys, suggesting that they are also capable of accommodating some variation in chemistry whilst still maintaining their structure. This allows for the large number of degrees of freedom when the Gibbs phase rule is applied to HEA compositions [3] while, conversely, the A-HEAs in this study have high vacancy energies similar to that of the good glass former Vitreloy 1 [78] The high vacancy binding energy of the A-HEAs complements the atomic size variation, negative enthalpy of mixing and multiple components, enabling them to form amorphous alloys on rapid cooling. These properties separate them from many of the reported HEA compositions, which are unable to form glassy phases by rapid solidification.

6.4 Conclusions

If HEA formability depends only on the entropy of mixing overcoming the enthalpy of mixing to suppress precipitation of intermetallics it would be difficult to produce a system capable of forming both HEA and amorphous phases, due to the requirement for glassy alloys to have low enthalpies of mixing.

Here the A-HEA1 a member of the $(TiZrNbCu)_{1-x}Ni_x$ system has been shown to be capable of solidifying as a glassy alloy and as a crystalline solid solution alloy with minimal ordering, depending upon cooling rate. Other members of the family with higher Ni compositions ($x > 0.15$ atomic fraction) show reduced or poor HEA formability they also show more decomposition products when devitrified in the DSC. The reduction in HEA formability may be due to the affinity of Ni for Ti, promoting the formation of Ni-Ti intermetallics. Thus reducing the possible stabilising entropy of the HEA and therefore causing a domino effect of de-alloying and intermetallic reactions; as the system attempts to minimise its free energy through the reduction of enthalpy by bond formation.

The observation of both a glassy and an HEA phase in one system, suggests that there is more determining the formation of HEA phases than simply the entropy of mixing. A possible mechanism, not at odds with the requirements of a good glass former, is suggested, *ie* that the high vacancy binding energies of the A-HEAs retards crystallisation during rapid solidification. However, regardless of mechanism, an alloy system with the capacity to form both a high entropy solid solution and an amorphous phase opens up the possibility of

novel processing routes for producing HEAs with nanocrystalline microstructures and metallic glassy alloys toughened with HEA crystallites.

7. A-Priori Modelling Approach to Producing a Novel HEA Composition with Low Density

7.1 Introduction

By their nature and definition high entropy alloys do not have an obvious base metal from which to extrapolate their properties, this makes prediction and design of their behaviour very difficult and many researchers are relying on an experimental approach. Such an approach is not practical when the number of potential HEA forming alloy compositions is so vast. With up to 90 metals or metalloids from which to choose components, the number of potential alloys is astronomical, even where only equiatomic compositions are considered as shown in Figure 7.1.

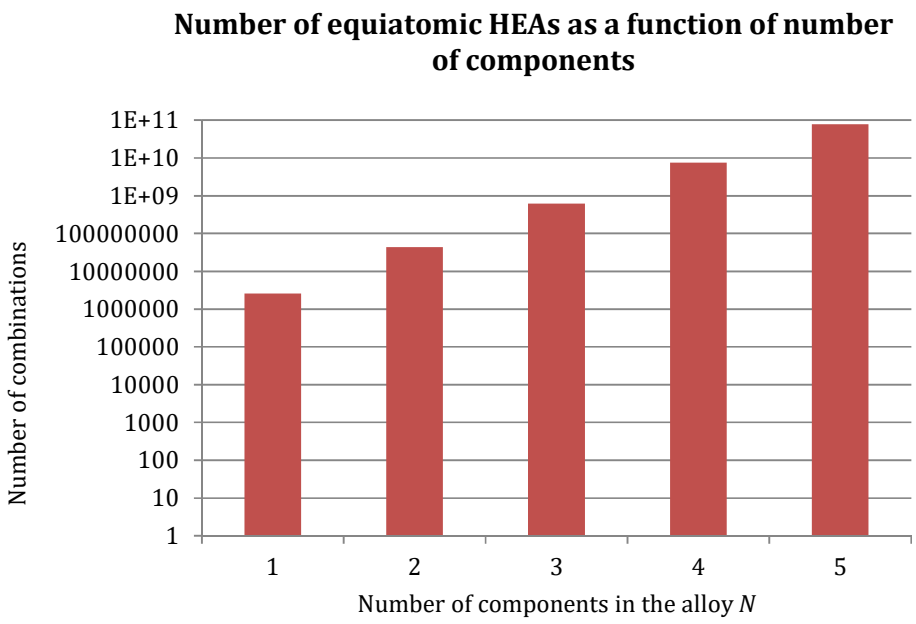

Figure 7.1 The number of potential compositions is vast and increases exponentially with N

For this reason alone a reliable method to predict compositions capable of forming an HEA solid solution alloy and then to predict or screen their properties is an essential tool in the exploitation of the phenomenon.

In this chapter the requirements for HEA formation, as laid out in chapters 5 and 6 are applied to predict a suitable composition for a low-density, high entropy solid solution forming alloy. The modelling methods developed in Chapter 5 are then applied to predict the properties of the alloy. Finally the alloy was been prepared and some characterisation carried out to test the predictive power of the approach.

At the time of when the initial work of this chapter was carried out no light/low density HEA fitting the description of "multi principal component solid solution alloy" had been reported. For example in 2009 Juan et al [83] reported the composition $Al_{20}Be_{20}Fe_{10}Si_{15}Ti_{35}$ but it formed a number of phases rather than the desired fully single solid solution.

7.2 Candidate Alloys

In search of a lightweight HEA we naturally look to the light metals Mg, Al and Li, however it is extremely doubtful that the configurational entropy a three-component solid solution of these elements would be sufficient to suppress the formation of their intermetallic phases. We therefore must choose some other metals to substitute into the alloy, to increase the configurational entropy and if possible to reduce the enthalpy of mixing of the alloy and increase its melting point. The elements Cu, Zn and Co were chosen, as the most suitable as the enthalpy of mixing of these elements with Mg, Al and Li are small in *magnitude* table 7.1. The effect of this is that the net effect of adding Cu, Co and Zn is to stabilise the high entropy solid solution by increasing the configurational entropy significantly but not increasing the magnitude either positive or negative of the enthalpy of mixing by their presence.

Table 7.1 Enthalpies of mixing of alloying components

Enthalpy / $kJmol^{-1}$	Cu	Co	Zn	Mg	Al	Li
Cu	-	11.25	3.06	-5.69	-0.1	-9.66
Co	-	-	26.94	17.02	15.95	16.99
Zn	-	-	-	-8.10	18.14	-15.97
Mg	-	-	-	-	-12.01	-0.77
Al	-	-	-	-	-	-48.92
Li	-	-	-	-	-	-

The composition $Al_{20}Co_{10}Cu_{10}Li_{20}Mg_{20}Zn_{20}$ referred to as ACL-3 was chosen for its small enthalpy of mixing -6.11 $kJmol^{-1}$, low estimated density 4.2 gcm^{-3}, low calculated T_c: 272 °C and estimated melting temperature above its T_c: 639 °C.

The density and melting temperature were estimated using the rule of mixing method, which has been shown to give good results for HEAs [16].

7.3 Results and Discussion

7.3.2 DFT Modelling of ACL-3$Al_{20}Co_{10}Cu_{10}Li_{20}Mg_{20}Zn_{20}$

The hcp, fcc and bcc super cells used in the calculation are shown in figure 7.5, with electron density iso-surfaces overlaid the Fermi energies of the structures were calculated to be 9.8 eV, 5.6 eV and 2.6 eV respectively.

The band structure and DOS curves of each crystal structure of the alloy are shown in figures 7.6-8, the hcp lattice shows an increased DOS at the Fermi energy in the Q direction in the Broullion zone which would indicate stronger bonding between the basal planes and possibly a reduced axial ratio c/a. However the integrated DOS curves in figure 7.9 indicate that the most stable structure is the fcc lattice [62]. This structure does not show any great tendency towards directionality in its bonding as shown by the relatively homogeneous appearance of the band structure with respect to lattice vector.

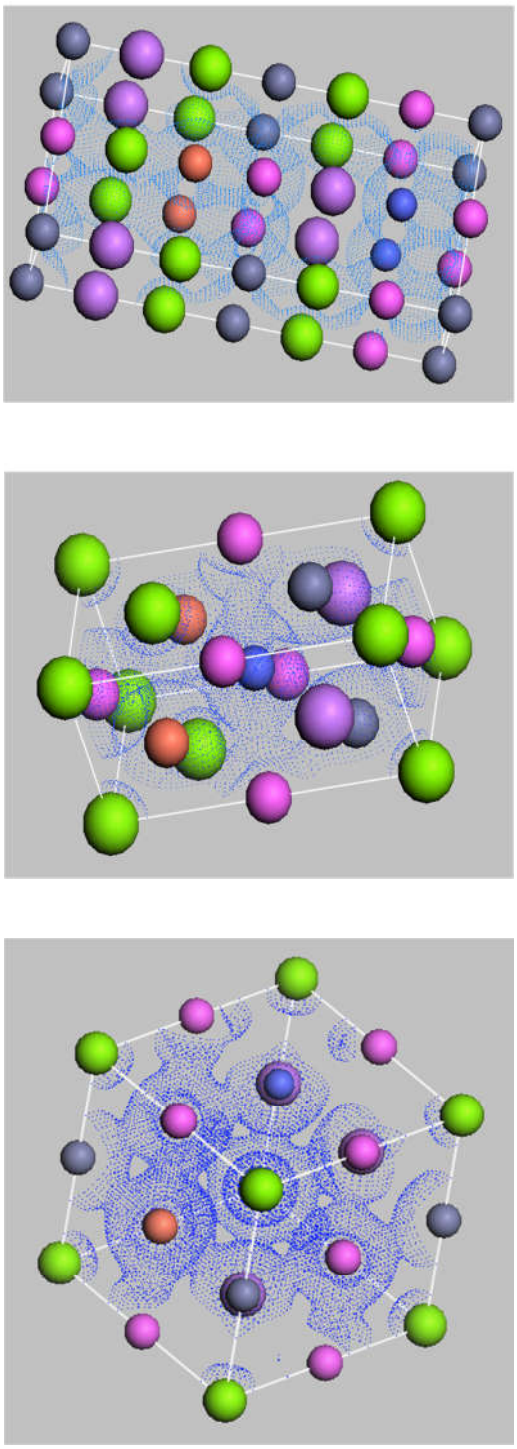

Figure 7.2 hcp, fcc and bcc super cells of ACL-3

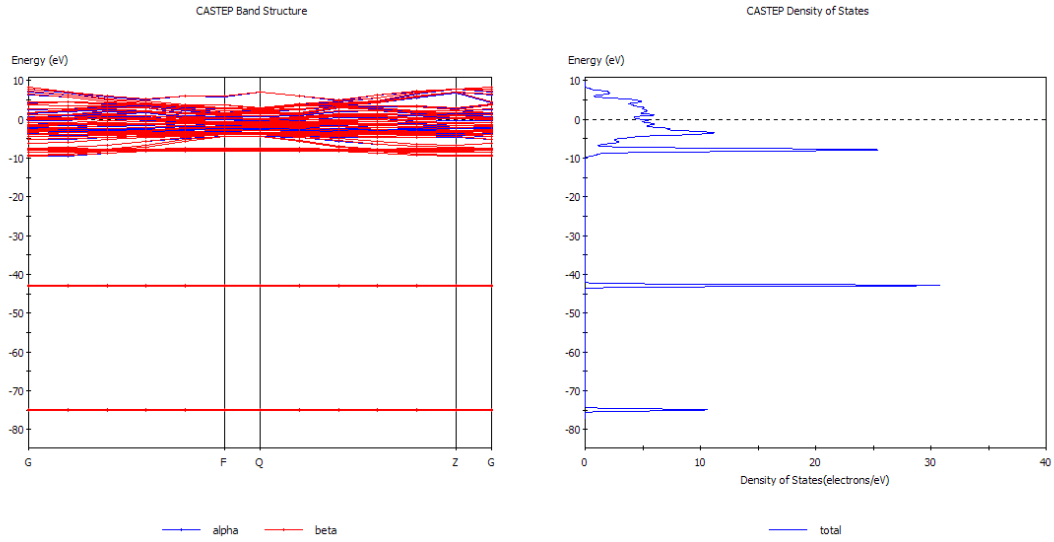

Figure 7.3 Band structure and DOS curves for hcp ACL-3

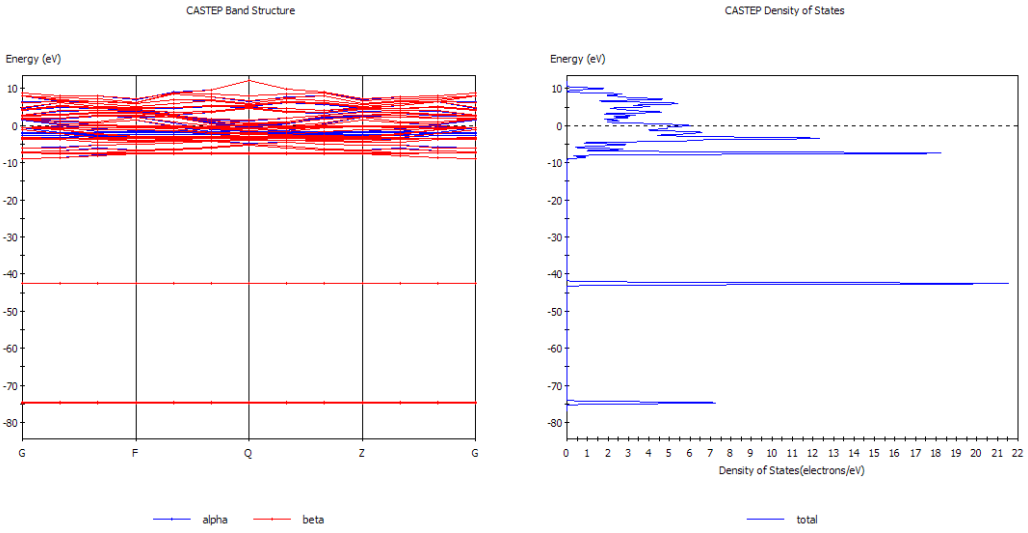

Figure 7.3 Band structure and DOS curves for fcc ACL-3

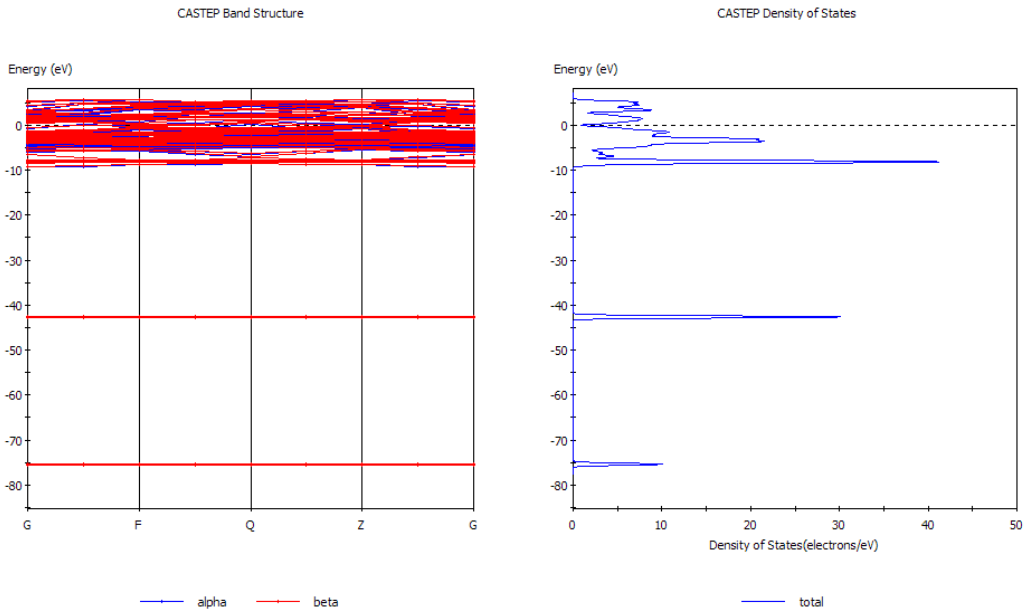

Figure 7.4 Band structure and DOS curves for bcc ACL-3

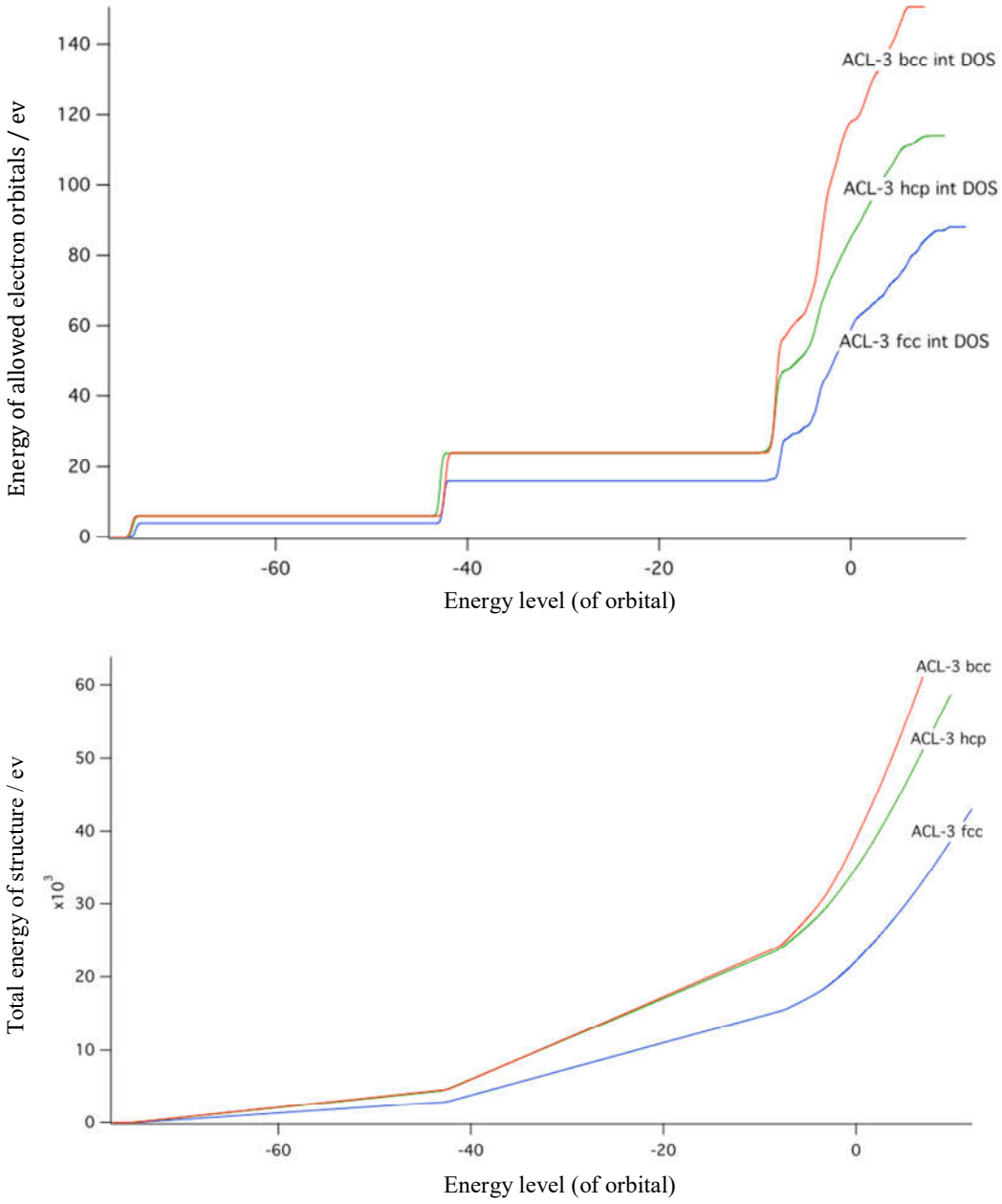

Figure 7.5 Integrated DOS and second integral of DOS curves of ACL-3

7.3.2 Experimental Investigation of Light High Entropy Alloy

7.3.2.1 Synthesis: ACL-3

To test the accuracy of the modelling of the light high entropy ACL-3 was produced and characterised as described below.

Because of the volatility of the elements to be alloyed vacuum induction melting was used rather than argon arc melting which is more aggressive and may have caused the light elements, particularly lithium, to boil off. The elements were weighed out and melted as described in chapter 2 to meet the composition $Al_{20}Co_{10}Cu_{10}Li_{20}Mg_{20}Zn_{20}$. After consolidation/alloying the ingot of ACL-3 was injection cast into a copper mould of 5 mm diameter for characterisation. The samples were then sectioned for XRF and SEM, polishing was carried out using cerium oxide in a paraffin suspension to prevent oxidation of the samples.

7.3.2.2 Results and discussion of ACL-3 characterisation

The XRD trace of as cast ACL-3 is shown in figure 7.10. The trace shows a large number of peaks which is indicative of the presence of more than one phase. It was not possible to index all of the peaks with sufficient confidence and this further suggests that the alloy chemistry has resulted in some complex phases and that the lattice parameters of any recorded phases have been affected according to Vegard's Law.

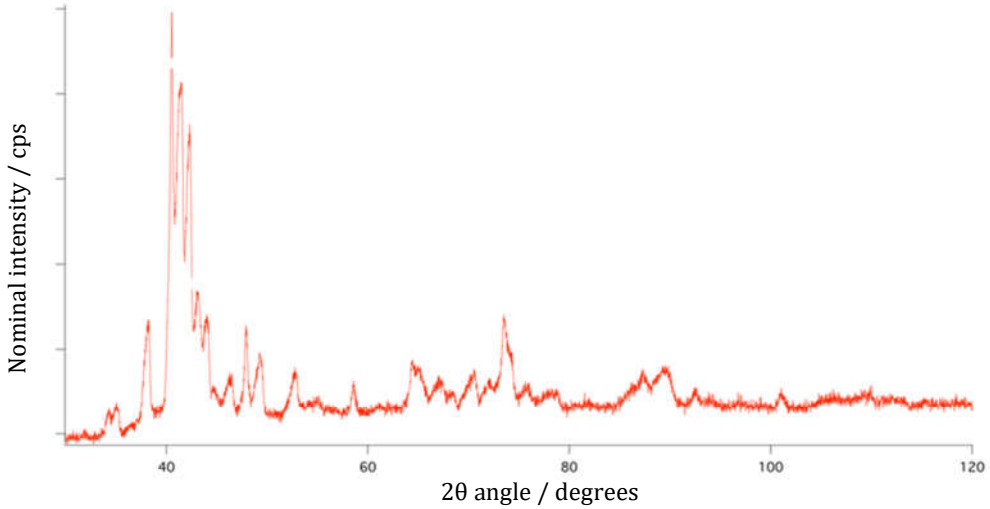

Figure 7.6 XRD trace for ACL-3 Copper K_α 2θ vs intensity

Figure 7.7 shows an SEM image of the as cast microstructure of the alloy. There are at least three distinct contrasts in the back scatter image; A shows up lightest and comprises approximately 50% of the area with a dendritic morphology, B makes up the next highest area and has the darkest contrast, the morphology of the phase B is quite rounded and globular, The final major contrast is an intermediate grey, C, which has a lace like perhaps eutectic morphology.

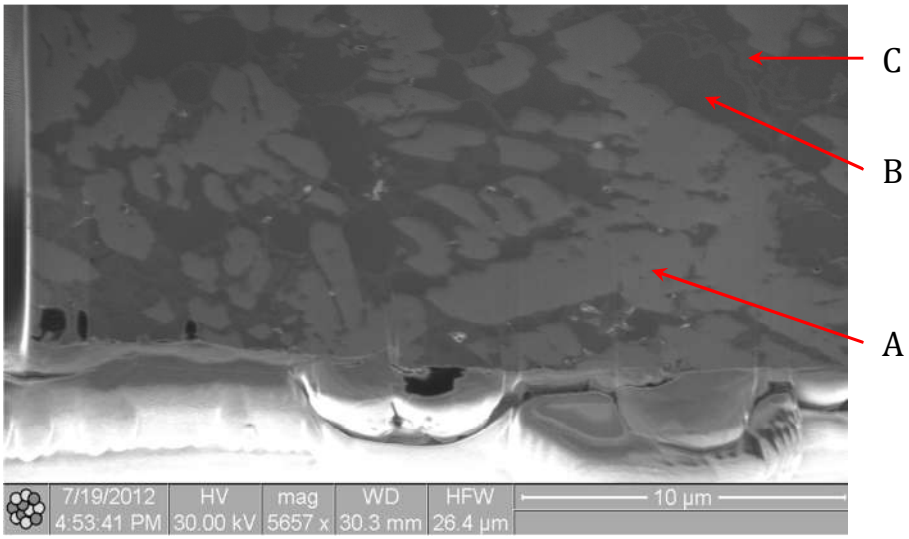

Figure 7.7 FIB-SEM image of microstructure of ACL-3

The micro structure and phases identified suggest that the alloy has solidified dendritically resulting two main phases, corresponding to the dendritic (A) and inter-dendritic (B) material. EDS analysis has been carried out on the alloy ACL-3, results of the spectra are given in tables 7.2 - 7.4. Unfortunately the technique is not capable of analysing Li due to the low energy of its characteristic X-ray line.

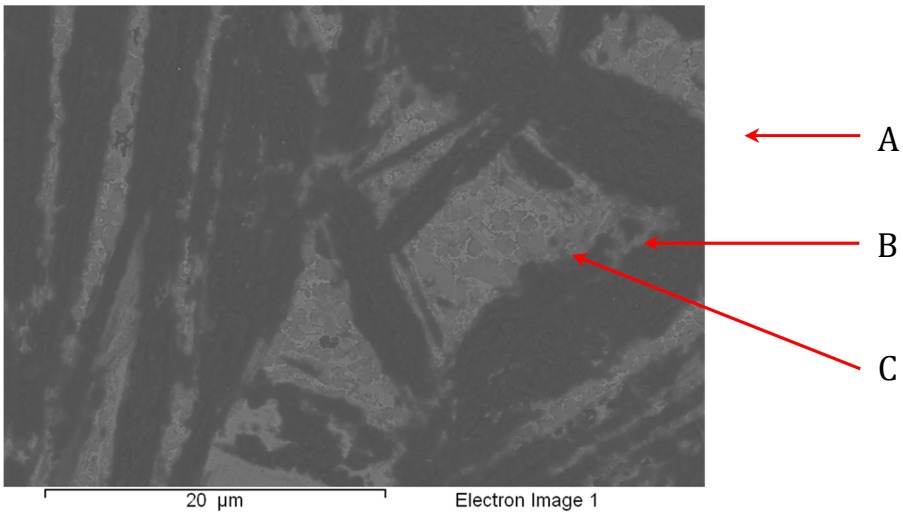

Figure 7.8 SE - SEM image of microstructure of ACL-3

Table 7.2 EDS analyses of each of the phase "A" identified in Figs 7.7 & 7.8

(A)	Scan 1	Scan 2	Scan 3	Average
Element	Atomic%	Atomic%	Atomic%	Atomic%
Mg	0	0	0	0
Al	3	1	1	2
Cu	1	0.5	0.6	0.7
Zn	0.6	0.5	0.3	0.5
Co	95.6	97	98	96.9

Table 7.3 EDS analyses of each of the phase "B" identified in Figs 7.7 & 7.8

(B)	Scan 1	Scan 2	Scan 3	Average
Element	Atomic%	Atomic%	Atomic%	Atomic%
Mg	9	8	11	9
Al	69	72	74	72
Cu	4	4	2	3
Zn	18	16	14	16
Co	0.1	0	0	0.0

Table 7.4 EDS analyses of each of the phase "C" identified in Figs 7.7 & 7.8

(C)	Scan 1	Scan 2	Scan 3	Average
Element	Atomic%	Atomic%	Atomic%	Atomic%
Mg	2	4	3	3
Al	10	16	19	15
Cu	27	22	8	19
Zn	61	58	69	63
Co	0.30	0.50	0.30	0.37

The dendritic material identified as A is shown to consist mainly of cobalt to the point where it has consumed almost all of the cobalt available in the alloy. The major constituent of B is Al at about 72 at% a significant amount of Zn and Mg 16 at% and 9 at% respectively are also present, The average Z number of this material is about 16 and so it would be expected to appear darker in a BSE image such as 7.7. The Constituent C is mainly Zn based, 63 at% with a significant amount of Cu, 19 at % and Al 15 at%. The average atomic number of this phase is about 26.5 and so it appears slightly darker than the phase A in Fig 7.7. It should be noted that "C" is intimately associated with B and has quite a fine scale so there may be some interference signals from B in the analysis of C. The EDS analysis should not be taken as absolute, but it can be seen from the chemistry of A, B and C that there are three distinct phases present with quite different compositions.

It is clear that ACL-3 is not a high entropy alloy in the sense that it can solidify to form a simple solid solution phase, the reason for this may be due to the likely solidification path. As cobalt has the highest melting point of all the constituent elements (1495 °C) and it has a positive heat of mixing with each of the components (table 7.1); it is reasonable to suggest that on cooling a Co rich phase was the first to form, this would be "A" in figure 7.7. This would leave a liquid consisting of mainly Mg, Al, Cu, Zn and Li. These remaining

elements all have negative heats of mixing with one another except for Cu-Zn (+3 $kJmol^{-1}$) and Al-Zn (+18 $kJmol^{-1}$). The disaffinity between Al and Zn may be the cause of the separation of the remaining liquid into two chemically different solid phases; one with higher Al, the other enriched in Zn. But by forming two separate phases and limiting the potential for Al-Zn bonding:

1. The alloy reduces the potential configurational entropy of a solid solution
2. At the same time reducing the enthalpy of mixing of the two phases due to the separation of Al and Zn

These points and the absence of the Co may be the reason why ACL-3 was not able to form a solid solution alloy. Other attempts to produce a low density HEA through the melting route have similarly failed to get $Mg_x(MnAlZnCu)_{100-x}$ [84, 85] or $Al_{20}Be_{20}Fe_{10}Si_{15}Ti_{35}$ [83] to form solid solution alloys. But Koch et al [86] were able to produce a single phase HEA from the composition $Al_{20}Li_{20}Mg_{10}Sc_{20}Ti_{30}$ by high energy ball milling – a solid state process route. Attempts to produce a low density HEA by the melt and solidification route may be susceptible to failure due to sequential solidification; the alloys above contain at least one element of significantly higher melting point than the "light metals" (small atomic mass) which must always be considered/included for use in a low density composition. If the range of melting points promotes a wide solidification range this may allow segregation and the formation of multiple phases. The method of mechanical alloying [86] avoids the solidification effects and allows the materials to be mixed in the solid state.

7.4 Conclusions

The alloy ACL-3 was proposed as a potential HEA solid solution forming alloy due to a favourable balance of configurational entropy and enthalpy of mixing. DFT modelling was used to predict that it would form an fcc crystal structure, as this structure possessed the lowest energy electronic structure. However XRD and SEM analysis of the alloy suggest that it decomposed during solidification, resulting in three or more phases, one mainly Co, one enriched in Al and another in Zn. These phases were able to form because of the high melting point of Co and the difference in melting points and positive heat of mixing of Al and Zn made the segregation energetically favourable. Other unsuccessful attempts to produce low density HEAs may have failed for similar reasons [83, 84, 85]. A solid state processing method [86] may overcome the problems of attempting to solidify all components of the HEA melt concurrently. The ability of an HEA to form a solid solution may be determined by the melting range of the alloy, this may have consequences for even "good HEA formers" when attempts are made to produce them on an industrial scale; *cf* the upper limit of about 22" diameter ingot for ESR processed IN 718 before freckle (gross buoyancy driven segregation) is unavoidable [35].

8. Summary and Conclusion of Thesis

8.1 Summary of thesis

The term high entropy alloy is widely accepted to describe alloys which are compositionally complex, consisting of 5 or more elements in approximately equiatomic proportions. These alloys have attracted interest due to their unexpected properties, which include; the ability to form random solid solutions with simple crystal geometry, high strengths and good ductility. The ability to form solid solutions has been attributed to the high configurational entropy available to a solid solution of 5 or more components. This interest has revealed a number of secondary properties of interest such as resistance to wear and corrosion and some magnetic and electrical behaviour, each of these properties may be attributed to the random solid solution nature of the alloys, high hardness, lack of easily corrodible precipitates causing grain boundary sensitivity and the generation of completely new electronic structure from the overlapping of the elemental metals' orbitals.

Whilst the work is ongoing into the field a design strategy has been lacking even though the tools to investigate complex alloys are available and have been developed to describe the most complex alloys currently in use: nickel based super alloys, many of which bear a striking resemblance to HEAs. These tools such as electron vacancy number and density functional modelling allow a more meaningful study of HEAs to be undertaken.

A number of compositions of HEA were produced and standard methods for the characterisation of metals were used including SEM, XRD, DSC were used and equipment for measuring thermoelectric power was developed.

In Chapter 5 DFT was used to model the electronic structures of a number of CoCrFeNi based HEAs. The modelled band structures were then used to explain the reported properties of the alloys. The question of the mechanism of alloying additions affecting crystal structure was satisfactorily answered, elastic moduli were calculated successfully and the thermo electric power of the alloys was predicted and then measured and confirmed. The accuracy of the modelled data when compared to the measured values validates the approach. The approach of modelling the alloy as a solid solution with a unique crystal lattice is only valid if the alloy may form such a structure and the atomic orbitals are able to overlap and form a band structure. This requires that the thermodynamics of the system favour a solid solution.

In Chapter 6 the nature of high entropy alloys and their thermodynamic stability was studied by exploring the relationship between HEAs and amorphous alloys. It was found that compositions based on $(TiZrCuNb)_{1-x}Ni_x$ were able to form either an HEA or an amorphous alloy depending on the processing route. As the nickel content of the alloy was increased from 0.125 at% to 0.2 at% the enthalpy of mixing was reduced and intermetallic phases were able to form, the formation of these phases reduced the potential configurational entropy of the solid solution and thus rendered it thermodynamically unfavourable. The balance between enthalpy of mixing, which influences the propensity for ordering or segregation in the alloy, and configurational entropy, which requires that the alloy be mixed chemically to manifest, was used to derive equation 5.1. Equation 5.1 describes a critical temperature (T_c) above which the entropy of the solid solution is sufficient to make it more favourable than the formation of an ordered of segregated

structure. It was shown that when the critical temperature is greater than the melting point then an alloy could never solidify to form a solid solution, but where T_c is low enough compared to the homologous temperature then the random solid solution is metastable at room temperature and the alloy may be described as a high entropy solid solution alloy.

In Chapter 7 the thermodynamic and modelling methodologies described in earlier chapters were applied to predict a suitable composition for a low-density high entropy alloy and to predict the properties of the solid solution that it would form. The alloy ACL-3 ($Al_{20}Co_{10}Cu_{10}Li_{20}Mg_{20}Zn_{20}$) was predicted to be capable of forming an fcc solid solution alloy at room temperature, experimental results confirm that the alloy did indeed adopt an fcc structure, however some intermetallics were present in the microstructure, this observation was attributed to the positive enthalpy of mixing of some elements.

The phenomenon of “high entropy alloys” provides a vast new compositional space for metallurgists and physicists to explore, some researchers have raced boldly into the hinterland of this new country and others have remained on the borders. In this thesis the thermodynamics, which allow the phenomenon, have been investigated and an approach based on modelling of the alloys proposed. This approach should be considered as a tool for those who wish to explore the high entropy space further.

8.2 Conclusions of thesis

Although HEAs are compositionally complex they may be modelled using DFT to calculate the overall potential of the lattice and the average electronic structure of the alloy. From these models physical parameters may be calculated with good accuracy. Such models would not be expected to produce accurate results if the alloys were intermetallic (highly covalent) in nature.

It is possible for an alloy to form either an HEA or glassy phase depending on the processing parameter. But some requirements of each system are not compatible and alloys which exhibit either a strong glass or HEA solid solution formability may be very poor HEA/glass formers. Thus finding alloy compositions which overlap both fields is a problem of optimisation.

Compositions which follow the current "rules" of HEAs: *small* enthalpy of mixing, five or more components in approximately equiatomic proportions from 5 at% – 30 at%, may still fail to form a solid solution alloy in situations where one or more components solidifies independently of the other constituent elements. Separate solidification may be promoted by one or more of the elements having a significantly higher melting point than the other components and or a significantly positive enthalpy of mixing with the other components. This may lead to another "rule" for HEA formers: that the solidification range cannot be too great. This rule is similar to the "off eutectic composition" rule for good glass formers.

9. Suggestions for Further and Future Work

This chapter is broken into two parts; the first outlines work which I would have liked to have carried out as part of the current work to explore some of the concepts presented in the Thesis, the second part consists of my thoughts on where HEAs may find applications.

9.1 Further work

9.1.1 Development of the pseudo base metal description of alloys

The work of chapter 5 could be developed into a methodology to predict the behaviour of alloying additions to a system, a similar but more powerful approach than electron vacancy number (N_v) or M_d-number calculations. In the N_v and M_d methods, used mainly for Ni based super alloys, the number of unoccupied orbitals (N_v) or the average energy of lowestunocupied molecular orbital (LUMO) and highest occupied molecular orbital (HOMO) between the base and substituted metals are used to estimate the compatibility of the alloying species' with the base element [90, 91]. In both methods, the further the alloying elements N_v or M_d deviates from that of the base metal eg Ni the more likely it is to form secondary phases with other incompatible elements. For example there is nothing special about an N_v of over 2.4 to indicate an alloy which may break down into TCP phases [90] except that it is quite different from that of pure Ni (0.61); Fe, Mo, Cr and Ti all exist as elements or in alloys with higher values. When a the metal is more heavily alloyed the

other elements present become important and the reference point shifts away from that of the base element, hence most Ni based alloys have different N_v limits. Calculating the electronic structure of the starting alloy, the "*pseudo-base metal*" is analogous to these methods, but differs in that the electronic environment is not that of a base element but of the alloy in which a species is to be embedded and so the influence of the potential additions on the structure of the alloy can be assessed. This approach was adopted in work with Zhao Leong (University of Sheffield 2013) the electronic structure of the PBM CoCrFeNi was split by adding the f orbital metal Pd to give a magnetic moment not present in the base metal.

9.1.2 Metallic glass – HEA in-situ composites

In Chapter 6 it was demonstrated that alloys with the composition $(TiZrCuNb)_{1-x}Ni_x$ were capable of forming either an amorphous phase or a HEA depending on the solidification conditions. A current topic of research is to reinforce metallic glasses with crystalline metals [92]. These amorphous-crystalline composites are usually produced by solidification from the melt and so the microstructures consist of crystalline dendrites in an amorphous matrix. Although the presence of softer dendrites does inhibit crack growth and so enhance toughness [86] the presence of a continuous brittle matrix limits the properties of the alloys; higher volume fractions of dendrites offer greater toughness but at the expense of high yield strength imparted by the amorphous material. This is a feature of the solidification processing method. The alloys described in chapter 6 could be developed to allow a new kind of glass

reinforced alloy. The crystallisation temperatures of the compositions were about 720 K, this allows a for a heat treatment window of about 1000 K where the alloy may be crystallised between T_x and T_m. If temperature of the treatment is chosen such that the HEA phase is stable then the result of a partial transformation would be a composite microstructure of transformed HEA grains and untransformed glassy particles. This material would be a tough HEA reinforced with hard chemically similar glassy particles, and should be resistant to corrosion and crack initiation, an advantage over the composites mentioned above.

Work in this area would require development of the $(TiZrCuNb)_{1-x}Ni_x$ system to identify a composition with improved glass and HEA formability, this may require some micro alloying additions (eg B, P, or RE elements) to promote glass formation. But the additions should be carefully controlled to avoid preventing the HEA formation. Heat treatment and microstructural characterisation experiments could be designed to optimise the properties of the alloy.

9.1.3 Investigation of the solidification range "rule" of HEA formation

In Chapter 7 it was suggested that the reason for the failure of ACL-3 to form a HEA solid solution was that its components segregated during solidification over a wide temperature range. Further work on this topic would include: further characterisation of the microstructure and phases present in the current alloy samples as cast this would help to support the conclusions made thus far; an attempt to produce the alloy ACL-3 by mechanical alloying and to test the

approach on some other compositions which have been suggested in the literature but which were not suitable for solidification processing. The work could be expanded later to investigate whether there is a link between solidification range and process ability of HEAs alloys. High temperature DSC/DTA could be used to determine solidification range and the results of controlled cooling rate experiments used to determine if a maximum part size exists and if this size is related to solidification range.

9.2 Future work

9.2.1 HEAs as Potential Structural Materials in Nuclear Applications

Apart from their excellent mechanical properties HEAs exhibit several, more subtle or functional properties worthy of further investigation as potential structural materials for future nuclear power generation applications:

High temperature phase stability: Because the solid solution phase is entropy stabilized it becomes more stable with temperature [2].

High vacancy binding energy: HEAs have high vacancy binding energies and so radiation induced defects such as Frenkel pairs or vacancies are less able to coalesce to form voids in the material [2]. *Slow diffusion kinetics*: The slow diffusion kinetics of HEAs [5], make them potentially resistant to radiation induced Gibbsian segregation and creep rupture.

Good solvation of impurities: The stability of the solid solution phase makes it insensitive to the presence of impurities such as those generated by absorption of material from the reactor or decay of the alloying elements. Such impurities

would be dissolved into the solid solution.

Potential nuclear damage recovery mechanism: HEAs have a characteristic temperature (*Tc*) above which the solid solution is thermodynamically stable. If an HEA component is subjected to radiation damage and then allowed to cool to a temperature just below *Tc* then a phase transformation will take place, originating at radiation induced and other defects, annihilating them, when the alloy is returned to the operating temperature it will reform a damage free solid solution.

Synthetic analogues: The pseudo-pure metal nature of the bonding in HEAs allows the properties of a metal to be replicated in an alloy without ever having to use the element itself. Thus it is possible to avoid elements such as molybdenum, which decompose to form dangerous isotopes.

These properties of HEAs are inherent resulting from their ability to form a solid solution phase and make them an ideal starting point for development into the next generation of nuclear materials.

9.2.2 Impurity Tolerant Alloys

The ability of HEAs to accept further alloying additions and yet maintain their simple solid solution structure may allow them to tolerate impurities which in conventional allows would normally be insoluble and exist as embrittling grain boundary precipitates. Elements such as Bi and Pb present in concentrations as low as 10 ppmwt are known to reduce the creep rupture life of Ni alloys by as much as 50%. Alloys that are impervious to these effects would be extremely sought after, and could be developed by adapting the band structure of the

alloy to be compatible with both the solute atoms and the desired crystal structure as an extension of the work of Pettifor and Chapter 5 of this Thesis.

10. References

1. Baker, C; *The Shape-Memory Effect in a Titanium-35 wt.-% Niobium Alloy.* Metal Science, **5,** 1 (1971) 92-100
2. Demetriou.M.D, LauneyM.E, Garrett.G, SchrammJ.P, HofmannD.C, JohnsonW.L, Ritchie.R.O; *A damage-tolerant glass*. Nature materials **10** (2011) 123-128
3. Cantor. B, Chang ITH, Knight.P, VincentAJB; *Microstructural Development in Multicomponent Alloys*, Materials Science and Engineering A **375-377** (2004) 213-218.
4. Yeh.JW, Chen.YL, Lin.SJ, Chen.SK; *High entropy alloys a new era of exploitation*, Materials Science Forum **560** (2007) 1-9
5. Miracle.D.B, Senkov.O.N; *A critical review of high entropy alloys and related concepts.* Acta Materialia article in press (2016), http://dx.doi.org/10.1016/j.actamat.2016.08.081
6. Budai.I, Benko.M, Kaptay,G; *Comparison of Different Theoretical Models to Experimental Data on Viscosity of Binary Liquid Alloys.* Materials Science Forum **537-538** (2017) 489-496
7. Andrade.E.N.DA.C; *A theory of the Viscosity of Liquids - Part A.* Philosophical magazine and Journal of Science **17** (1934) 497-511
8. Porter.D.A, Easterling.K.E; *Phase Transformations in metals and Alloys.* Nelson Thornes (1988)
9. Haasen.P, *Physical Metallurgy.* Cambridge University Press (1996)

10. Boer.F.R, Boom.R, Mattens.W.C.M, Miedema.A.R, Niessen.A.K; *Cohesion in metals transition metal alloys*, North Holland Physics Publishing (1988)
11. Takeuchi.A, Amiya.K, Takeshi.W, Kunio.Y, Wei.Z, Akihiro.M; *Entropies in Alloy Design for High entropy and Bulk Glassy Alloys.* Entropy **15** (9) (2013) 3810-3821
12. Hsu.US, Hung.UD, Yeh.JW, Chen.SK, Huang.YS, Yang.CC; *Alloying behaviour of iron, gold and silver in AlCoCrCuNi based equimolar high entropy alloys*, Materials Science and Engineering A **460** (2007) 403-408
13. Cottrell.A; *Concepts of the electron theory of alloys*, Institute of Materials Communications Ltd (1998)
14. Kittel.C: *Introduction to solid state physics*, Wiley (2005)
15. Barrett.C, Massalski.T.B; *Structure of metals*, Pergamon International Library (1980)
16. Senkov ON, Wilkes GB, Miracle DB, Chuang CP, Liaw PK; *Intermetallics* **18 (**2010) 1756-8
17. Zhou.YJ, Zhang.Y, Wang.FJ, Wang.YL, Chen.GL; *Effect of Cu addition on the microstructure and mechanical properties of* $AlCoCrFeNiTi_{0.5}$ *solid solution alloy*, Journal of Alloys and Compounds **466** (2008) 201-204
18. Chen.Y, Hu.Y, Tsai.C, Yeh.J, Chen.S, Chang.S; *Structural evolution during mechanical milling and subsequent annealing of CuNiAlCoCrFeTi alloys*, Materials Chemistry and Physics **118** (2009) 354-361

19. Wu.J, Lin.S, Yeh.J, Chen.S, Huang.Y Chen.H; *Adhesive wear behaviour of $Al_xCoCrCuFeNi$ alloys as a function of Al content*, Wear **261** (2006) 513-519
20. Shun.T, Hung.CH, Hung.CH, Lee.CF; *The effects of elemental Mo or Ti addition to $Al_{0.3}CoCrFeNi$ high entropy alloy on age hardening at 700 ºC*, Journal of Alloys and Compounds (2009), doi:10.1016/j.jallcom2010.02.032
21. Hu.Z, Zhan.Y, Zhang.G, She.j, Li.C; *Effect of rare earth addition on the microstructure and mechanical properties of high entropy AlCoCrCuNiTi alloys*, Materials and Design **31** (2010) 1599-1602
22. Tong.CJ, Chen.YL, Chen.SK, Yeh.JW, Shun.TT, Tsau.HC, Lin.SJ, Chang.SY; *Microstructure characterisation of $Al_xCoCrCuFeNi$ high entropy alloy system with multiprincipal elements*, Metallurguical and Materials Trans A **36** (2005) 881-893
23. FJ, Zhang.Y, Chen.GL; *Atomic packing efficiency and phase transition in a high entropy alloy*, Journal of Alloys and Compounds **478** (2009) 321-324
24. Li.BS, Wang.YP, Ren.C, Yang.C, Fu.HZ; *Effects of Mn, Ti, V on the microstructure and properties of AlCrCoNiCu high entropy alloys*, Materials Science and Engineering A **498** (2008) 482-486
25. Huang.YS, Chen.L, Lui.HW, Cai.MH, Yeh.JW; *Microstructure, hardness, resistivity and thermal stability of sputtered oxide films of $AlCoCrCu_{0.5}NiFe$ high entropy alloy*, Materials Science and Engineering A **457** (2007) 77-83

26. Zhang.Y Zhou.YJ, Hui.XD, wang.ML, Chen.GL; *Minor alloying behaviour in bulk metallic glasses and high entropy alloys*, Science in China Series G **51** (2008) 427-437
27. Tsai.CW, Chen.YL, Tsai.MH, Yeh.JW, Shun.TT, Chen SK; *Deformation and annealing behaviours of high entropy alloy* $Al_{0.5}CoCrCuFeNi$, Journal of Alloys and Compounds (2008), doi:10.1016/j.jallcom.2009.06.182
28. Chou.HP, Chang.YS, Chen.SK, Yeh.JW; *Microstructure, thermophysical and electrical properties in* $Al_xCoCrFeNi$ *(0<x<2) high entropy alloys*, Materials Science and Engineering B **163** (2009) 184-189
29. Zhang.KB, Fu.ZY, Zhang.JY, Wang.WM, Wang.H, Wang.YC, Zhang.QJ, Shi.J; *Microstructure and mechanical properties of* $CoCrFeNiTiAl_x$ *high entropy alloys*, Materials Science and Engineering A 508 (2009) 214-219
30. Li.C, Li.JC, Zhao.M, Jiang.Q; *Effect of alloying elements on microstructure and properties of multiprincipal element high entropy alloys*, Journal of Alloys and Compounds **475** (2009) 752-757
31. Varalakshmi.S, Kamaraj.M, Murty.BS; *Processing and properties of CuNCoZnAlTi high entropy alloys by mechanical alloying*, Materials Science and Engineering A (2008), doi:10.1016/j.msea.2009.09.019
32. Cunliffe.A.J, Plummer.J.D, Todd.I; *Glass formation in a high entropy alloy system by design,* Intermetallics **23** (2012) 204-207

33. Kuznetsov.A.V, Shaysultanov.D.G, Stepanov.N.D, Salischev.G.A, Senkov.O.N; *Tensile Properties on an AlCrCuNiFeCo HEA in as cast and wrought condition.* Mater Sci and Eng A **533** (2014) 428-441

34. Guérin.S, Guyomarch.A, Hayden.B, Soulié.J, Yakvolev.S, Cotton.J; *High-Throughput Synthesis and Characterization of Thin Film High Entropy Alloys Based on the Fe-Ni-Co-Cu-Ga System.* Procedings of TMS annual meeting (2015)

35. Simms.C.T; *A History of Superalloy Metallurgy for Superalloy Metallurgists.* TMS Super alloys (1984) 399-419

36. SAE intnl; *AS5491C Calculation of Electron Vacancy Number in Superalloys.* [2013]

37. Hume-Rothery.W, Mabbott.G.B, Channel Evans.K.M; *Philosophical Transactions of the Royal Society of London. Series A* **233** (1934) 1-97

38. Kantor,Bela; *Influence of Al and Nb on castability of a Ni-base superalloy, IN713LC.* International Journal of Cast Metals Research 22 (1) [2009] 62-65

39. Klement, W.; Willens, R. H.; Duwez, POL (1960). "Non-crystalline Structure in Solidified Gold-Silicon Alloys". *Nature*. **187** (4740): 869–870.

40. Lee.PY, Li.WC, Lin.CK, Huang.JC: *Fabrication of Mg–Y–Cu bulk metallic glass by mechanical alloying and hot consolidation.* Materials Science and Engineering A **449–451** (2007) 1095–1098

41. King, D.M.; Middleburgh, S.C.; Liu, A.C.Y.; Tahini, H.A.; Lumpkin, G.R.; Cortie, M. (January 2014). "Formation and structure of V–Zr amorphous alloy thin films". *Acta Materialia*. **83**: 269–275.

42. Nurnberg.K; *Schlackenatlas* Verlag Stahleisen mbH (1981)

43. Inoue, A. (2000). "Stabilization of metallic supercooled liquid and bulk amorphous alloys". *Acta Materialia*. **48**: 279–306.

44. Georgarakis.K, Hennet.L, Evangelakis.GA, Antonowicz.J, Bokas.GB, Honkimaki.V, Bytchkov.A, Chen.MW, Yavari.AR: *Probing the structure of a liquid metal during vitrification* Acta Materialia **87** (2015) 174-186

45. Wang.WH**:** *High-Entropy Metallic Glasses* JOM **66** (2014) 2067–2077

46. Takeuchi.A, Amiya.K, Wada.T, Yubuta.K, Zhang.W, Makino,A: *Entropies in Alloy Design for High-Entropy and Bulk Glassy Alloys.* Entropy **15 (**2013) 3810-3821

47. Thomas.L.H; *The calculation of atomic fields.* Proc. Cambridge Phil. Soc. **23** [1927] 542–548

48. Feynman.RP, Metropolis.N, Teller.E: *Equations of State of Elements Based on the Generalized Thomas-Fermi Theory.* Physical Review **75 (**1949) 1561-1573

49. Hohenberg.P, Kohn.W; *Inhomogeneous electron gas*. Physical Review **136** [1964] B864-B871.

50. *Kohn.W, Sham.L. J; Self-consistent equations including exchange and correlation effects. Physical Review. **140** [1965] A1133–A1138*

51. Kalidindi.S.R, Abusafieh.A, El-Danuf.E; *Accurate characterisation of machine*

52. A Kittel. C; *Introduction to Solid state Physics*. Wiley (2015) Eighth edition

53. *B Thermo-electric characteristics to British standard specifications*. Cambridge

54. Ranganathan.S; *Alloyed pleasures: Multimetallic cocktails.* Current Science, **85**, 10, (2003) 1404-1406

55. Hu.Q.M, Li.S.H, Hao.Y.L, Yang.R, Johansson.B, Vitos.L; *Phase stability and elastic modulus of Ti alloys containing Nb, Zr, and/or Sn from first-principles calculations.* Applied Physics Letters **93** (2008) 121902

56. Matsugi.K, Murata.Y, Morinaga.M, Yukawa.N; *An electronic approach to alloy design and its application to Ni-based single-crystal superalloys.* Materials Science and Engineering, A **172** (1993) 101-110

57. Ng.C, Guo.S, Luan.J, Shi.S, Liu.C.T; *Entropy driven phase stability and slow diffusion kinetics in an $Al_{0.5}$CoCrCuFeNi high entropy alloy,* Intermetallics **31** (2012) 165-172

58. Guo.S, Ng.C, Lu.J, Liu.C.Tl; *Effect of valence electron concentration on stability of fcc or bcc phase in high entropy alloys.* Journal of Applied Physics 109, (2011)

59. Ziman.J.M; *The Physics of Metals 1: Electrons.* Cambridge University Press**1969**

60. Tanner.BK; *Introduction to the Physics of Electrons in Solids*, Cambridge University Press **1995**

61. Lucas.M.S, Wilks.G.B, Mauger.L, Mun˜oz.J.A, Senkov.O.N, Michel.E, Horwath.J, Semiatin.S.L, Stone.M.B, Abernathy.D.L, Karapetrova.E; *Absence of long-range chemical ordering in equimolar FeCoCrNi.* Applied physics letters **100** (2012) 251907

62. Paxton.A.T, Methfessel.M, Pettifor.D; Proceedings of the Royal Society London A (1997) 1493-1513

63. Frederiksen.S.L, JacobsenK.W; *Bayesian Ensemble Approach to Error Estimation of Interatomic Potentials.* Physical Review letters **93** 16 (2004) 165501

64. Belyea.D, Bauer.C, Lucas.M, Horwath.J, Michel.E, Casey.W; *Magnetocaloric effect in NiFeCoCrPd$_x$ high entropy alloys.* American Physical Society, APS March Meeting (2012)

65. Kubachewski.O, *With one Auspicious and one Drooping Eye.* CALPHAD **8** 4 (1984) 355-358

66. Zhang.Y, Zuo.T.T, Cheng.Y.Q, Liaw.P.K; *High-entropy Alloys with High Saturation Magnetization, Electrical Resistivity, and Malleability*. Scientific Reports, **3** (2013) 1455

67. A.L.Greer, E.Ma; MRS Bulletin **32** (2007) 611-615

68. Waniuk, T.A., J. Schroers, and W.L. Johnson; Applied Physics Letters **78** (2001) 1213-1215

69. Mandle.F; *Statistical Physics*, Wiley (1998)

70. Stoloff.N.S, Sikka.V.K; *Physical Metallurgy and Processing of Intermetallic Compounds,* Springer (1995)

71. Li.A, Zhang.X; Acta Metallurgica Sinica (English Letters) **22** (2009) 219-224

72. Stoloff.N.S; International Materials Reviews **34** (1989) 153-183

73. E.S. Park, J.H. Na and D. H. Kim, Applied Physics Letters **91**, 031907 (2007)

74. Zhang.Y, Materials Science Forum **654-656** (2010) 1058-1061

75. Li.C, Zhao.M, LiJ.C, Jiang.Q; Journal of Applied Physics **104** (2008)

76. Wang.Y.P, Li.B.S, Fu.H.Z; Advanced Engineering Materials **11** (2009), 641-644

77. Xuilin.J, Pan.Y; Materials Science and Engineering A **485** (2008) 154–159

78. Loffler.J.F; Intermetallics **11** (2003) 529-540

79. Plummer.J, Figueroa.I.A, Hand.R.J, Davies.H.A, Todd.I; Journal of Non Crystalline Solids **355** (2009) 335-339

80. www.geocities.jp%2Fohba_lab_ob_page%2Fstructure4.html&psig=AFQjCNFmkRyRejxrLNkS9puFM6eroxLf9Q&ust=1495541611157011

81. J.Y.He, CZhu, D.Q.Zhou, W.H.Liu, T.G.Neih, Z.P.Lu; Intermetallics, **55** (2014) 9-14

82. E.J.Pickering, R.Munoz-Moreno, H.J.Stone, N.G.Jones; Scripta materialia, **113** (2016) 106-109

83. JuanC-C,YehJ-W,ChinT-S; Anovel lighthigh-entropy alloy Al20Be20Fe10Si15Ti35. Paper presented at: EMRS Fall Meeting, Symposium I; 2009 Sept 14–18; Warsaw, Poland.

84. Li R, Gao JC, Fan K. Study to microstructure and mechanical properties of Mg containing high entropy alloys. Mater Sci Forum. 2010;650:265 – 271.

85. Li R, Gao JC, Fan K. Microstructure and mechanical properties of MgMnAlZnCu high entropy alloy cooling in three conditions. Mater Sci Forum. 2011;686: 235 – 241

86. Youssef.KM, Zaddach.AJ, Niu.CN, Irving.DL, Koch.CC (2015): *A Novel Low-Density, High-Hardness, High-entropy Alloy with Closepacked Single-phase Nanocrystalline Structures*. Materials Research Letters, **3:2**, (2015) 95-99

87. Yeh.JW, Chen.YL, Lin.SJ, Chen.SK; *High entropy alloys a new era of exploitation*, Materials Science Forum **560** (2007) 1-9

88. Wang.FJ, Zhang.Y, Chen.GL; *Atomic packing efficiency and phase transition in a high entropy alloy*, Journal of Alloys and Compounds **478** (2009) 321-324

89. Pyczak.F, Mughrabi.H; *An overview of M_d number calculations as a tool for phase stability prediction in Ni-base superalloys*, Intermetallics and Superalloys Euromat 10 Wiley 2010

90. General Electric-Baker Hughes ITN07756.13 (REV 7)

91. Scientific RepoRts | 7:42598 | DOI: 10.1038/srep42598

92. Fan.J, Wu.F.F, Li.D; *Dynamic compressive response of a dendrite-reinforced Ti-based bulk metallic glass composite,* Materials Science and Engineering A 720 (2018) 140-144